
**STRUCTURE DEVELOPMENT IN
SILICATE-LAYERED
POLYMER NANOCOMPOSITES**

A Thesis Submitted For The Degree Of Doctor Of Philosophy

by

Julie-Anne Lander

Wolfson Centre for Materials Processing

Brunel University

Uxbridge

Middlesex

January 2002

ABSTRACT

The demands made of materials have resulted in the formation of complex composite structures; one such example of these is nanocomposites. This study is primarily devoted to the preparation and characterisation of nanocomposites. Reactively cast and reactively extruded nanocomposite strategies for the preparation of polyamide-6 composites were compared. The catalyst and activator system selected was based on an industrially successful combination. The extruder screw and barrel configuration used had previously been proven effective for the reactive polymerisation of polyamide-6.

The principal objectives were the investigation of the influence of layered-silicates on both the microstructure and the physical properties of the composites. As well as the analysis of the mechanisms that influence the physical performance of the materials produced.

The characterisation of the filler-matrix microstructure and its effect on physical properties of the composites were investigated using a range of chromatographic, microscopic, thermal and X-ray analytical techniques. Selected mechanical properties were measured using standard test procedures. Therefore results obtained and subsequent trends observed in reaction cast and reaction extruded nanocomposites could be compared and contrasted. The influence of the polymerisation conditions, residual monomer content and the nature of the composite structure produced were considered.

It was observed that the nature of the matrix crystalline structure could be greatly influenced by the material composition, method of preparation and processing technique. The crystal form of the spherulites present appeared to be the key factor in influencing mechanical strength. The treatment of the silicate-layered clay successfully increased the inter-layer spacings, which was further increased by the presence of high shear forces.

ACKNOWLEDGEMENTS

Acknowledgements are difficult because the number of people to whom one feels indebted is so large. Of the many people who have assisted and encouraged this project I firstly offer my sincerest thanks to both of my supervisors: Prof. Peter Hornsby and Dr. Karnik Tarverdi. Both of whom I owe a debt of gratitude for their unceasing supervision and technical support throughout the course of my research.

During my study the EPSRC and Nylacast Ltd. supported me financially.

Thanks also to all the Materials Department technicians, especially Mrs. Tripti Banerjee, Mr. Prakash Dodia, Mr. Les Mellet and Dr. Sue Woodisse. The Staff of the Wolfson Centre also provided valuable assistance, especially Mr. Darren Farmer.

I would particularly like to thank my family and friends for more kinds of support than I can adequately acknowledge, thank you all. And of course to Marc for his unlimited faith and inspiration, which were the best encouragement.

CONTENTS

ABSTRACT	i	
ACKNOWLEDGEMENTS	ii	
CONTENTS	iii	
CHAPTER ONE	INTRODUCTION	
1.1	Introduction	1
1.2	Background	1
1.3	Objectives	4
1.4	Thesis Outline	4
CHAPTER TWO	LITERATURE REVIEW	
2.1	Introduction	6
2.2	Polyamides	6
2.2.1	Polyamide-6	7
2.2.2	Crystalline State	13
2.2.3	Caprolactam	18
2.3	Properties Of Filled Polymer Composites	21
2.3.1	Structure and Property Effects of Fillers	21
2.3.2	Surface Modification of Fillers	23
2.4	Layered Silicates: Clay	25
2.4.1	Structural Considerations	26
2.4.2	Montmorillonite	29
2.4.3	Cation Exchange	34
2.4.4	Clay Fillers	37
2.5	Nanocomposites	39
2.5.1	Nanocomposite Structure	40
2.5.2	Nanocomposite Production	44
2.5.3	Nanocomposite Properties	47
2.5.4	Nanocomposite Characterisation	49
2.6	Polymer Processing	50
2.6.1	Mixing	51
2.6.2	Extrusion	51
2.6.3	Reaction Extruded System	51
2.6.4	Reaction Polymerisation	53

CHAPTER THREE EXPERIMENTAL METHODS AND TECHNIQUES

3.1	Introduction	55
3.2	Material Formulations	55
3.3	Cast System	59
3.3.1	Preparation of Nylon Clay Hybrids	59
3.3.2	Preparation of Composites Using Brabender Apparatus	60
3.3.3	Preparation of Nanocomposites Using Cast Techniques	61
3.4	Extrusion System: Polyamide-6 Composites	63
3.4.1	Preparation of Nanocomposites Using Extrusion Techniques	63
3.5	Sample Preparation	65
3.5.1	Cast Sample Preparation	65
3.5.2	Extruded Sample Preparation	65
3.6	Characterisation of Polyamide-6 Nanocomposites	67
3.7	Chromatographic Methods	68
3.7.1	Residual Monomer Content	68
3.7.2	Gel Permeation Chromatography	71
3.8	Structural Analysis	73
3.8.1	Thermo-gravimetric Analysis	73
3.8.2	Differential Scanning Calorimetry	75
3.8.3	X-ray Diffraction	78
3.9	Microscopic Analysis	81
3.9.1	Scanning Electron Microscopy	81
3.9.2	Transmission Electron Microscopy	84
3.10	Mechanical Properties	87
3.10.1	Charpy Impact Test	87
3.10.2	Tensile Test	89
3.10.3	Flexural Test	90
3.10.4	Dynamic Mechanical Thermal Analysis	91

CHAPTER FOUR RESULTS AND DISCUSSION

4.1	Introduction	93
4.2	Polymerisation of ϵ -Caprolactam and Residual Monomer Content	93
4.2.1	Gas Chromatography: Cast System	94
4.2.2	Gas Chromatography: Reaction Extruded System	95
4.2.3	Molecular Weight and Molecular Weight Distribution: Cast System	97
4.2.4	Molecular Weight and Molecular Weight Distribution: Reaction Extruded System	103
4.3	Structural Analysis	107
4.3.1	Thermo-gravimetric Analysis: Cast System	107
4.3.2	Thermo-gravimetric Analysis: Reaction Extruded System	111
4.3.3	Differential Scanning Calorimetry: Cast System	114
4.3.4	Differential Scanning Calorimetry: Reaction Extruded System	119
4.3.5	X-ray Diffraction: Cast System	121
4.3.6	X-ray Diffraction: Reaction Extruded System	128
4.4	Microscopic Analysis	135
4.4.1	Scanning Electron Microscopy: Cast System	135
4.4.2	Scanning Electron Microscopy: Reaction Extruded System	143
4.4.3	Transmission Electron Microscopy: Reaction Extruded System	146
4.5	Physical Properties	148
4.5.1	Impact Properties: Reaction Extruded System	148
4.5.2	Tensile Properties: Reaction Extruded System	150
4.5.3	Flexural Properties: Reaction Extruded System	152
4.5.4	Dynamic Mechanical Thermal Analysis: Cast System	154
4.5.5	Dynamic Mechanical Thermal Analysis: Reaction Extruded System	157
4.6	Cast System	160
4.6.1	Brabender Series	160
4.6.2	Test Pours	161
4.6.3	Nylon Clay Hybrid	165
4.7	Reaction Extruded System	166

CHAPTER FIVE CONCLUSIONS

5.1	Cast System	168
5.2	Reaction Extruded System	169
5.3	Suggestions for Further Work	170

REFERENCES	172
-------------------	------------

APPENDICES

I	Table Of Materials	184
II	Process Scheme for Screening Tests	185
III	DMTA Raw Data	186
IV	XRD Raw Data	187

CHAPTER ONE

INTRODUCTION

1.1

Introduction

Chapter One provides a general background on silicate-layered polymer nanocomposites. These composites frequently exhibit unexpected hybrid properties synergistically derived from the filler and matrix components. This new class of mineral filled material not only possess above average mechanical strength and heat resistance, but also have enhanced gas barrier properties and increased flame retardancy. The initial concept, and ultimate aims of this research are also incorporated.

1.2

Background

There exists a constant need to improve and enhance the properties of polymers, so that the processability, end product properties and in-service performance may be optimised. This has led to the development of polymer composites, via the addition of fillers, pigments and fibrous reinforcements to name but a few. These polymer blends can be tailor made to suit specific applications; where, for example, attributes such as low moisture absorption, high impact resistance or enhanced flexural modulus may be required. The following table provides a summary of the purpose of some common additives in commercial resins.

Filler Type	Usage	Examples	Limitations
Antioxidant	Protects against oxidation during processing and in service life.	Hindered Phenols (Irganox 1076)	Discolouration High addition levels
Colourant	Dyes in transparent polymers		
Fire Retardant	To reduce or prevent combustion.	Aluminium Phosphorus	High addition levels Toxicity
Foaming Agent	Reduces modulus and strength by making a cellular structure	Copolymer groups of ethylene oxide	
Hardness	Especially in rubbers,	Carbon Black	Cross-linking inhibition
Inert Fillers	Used for cheapness in non-critical products	Chalk in PVC hosepipes.	Contaminants: extraneous minerals in mineral fillers
Lubricant	Prevent adherence to mould/machinery and also reduce melt viscosity.	Hydrocarbon waxes Fatty Acids	Costly to develop specific system
Nucleating Agent	Promotes/ controls spherulite formation	Lithium benzoate Silica Flour	
Plasticiser	Separate adjacent PVC molecules	Organic Esters	
Stiffness	Incorporate stiff strong filler	Glass fibres	Require surface treatment
Toughness	To absorb energy and increase resistance to impact.	Rubber particles	Increase in flexibility Translucent
UV Absorber	Preserves polymers against harmful radiation.	Carbon Black Titanium Dioxide	Dispersion is critical
Wetting Agents	Aid uniform dispersion in polymer matrix, without agglomeration.	Mono- glycerides Di-glycerides	

Table 1.1
Filler types and functions 1-3

When a particulate phase is introduced into a polymer the structure will be affected. The major disadvantage with the addition of fillers is the accompanying decrease in the physical properties observed. The morphology of the filler particles is also known to have an effect on physical properties, for example plate-like particles result in decreased toughness. Certain filler surfaces may even act as nucleators for semi-crystalline polymers, thus altering the amount and type of crystallinity. The high filler loadings in plastic composites leads to the filler-matrix interfacial properties being the major

determinant of composite mechanical properties. Distribution and dispersion of fillers is the key factor affecting microstructure; but controlling processing conditions and polymer surface modification can also result in different microstructures.

To combat the negative effects of inorganic fillers, surface treatments may be used to modify the characteristics of the resultant filler-matrix interface. The chemical nature and amount of surface treatment applied can achieve improved mechanical properties in the resulting composite material and aid the compromised melt processability, by altering the chemical resistance of the bond across the interface. But this is an additional processing step that is specific to the material, and also has associated expenditure.

Current demands made of composites have led to the formation of more complex structures, whereby the inclusion of an additional phase is not sufficient to promote the ideal properties. Various alternative techniques are available, including reactive modification of the polymer - involving the incorporation of functional groups onto the polymer chain, thus promoting adhesion to the particulate phase. Another is reactive processing where the monomer is polymerised in the presence of the filler; so the particulate-filled polymer composite is formed as the polymerisation itself take place. Both of these approaches result in the modification of the interfacial properties between the filler and the matrix. Hence the interest in nanocomposites, which combine both these features; and thus the ability to produce highly, specified polymers, intrinsic to the requirement of the end function.

This project was undertaken with some technical support from Nylacast Ltd. who have commercial interests in the preparation of polyamide-6 parts made by polymerisation and casting of ϵ -caprolactam.

1.3

Objectives

This study is primarily devoted to the preparation and characterisation of nanocomposites using novel techniques, and specifically the following objectives therein:

- 1) Investigation of the influence of nanocomposite layered-silicates (e.g. montmorillonite) on the microstructure and physical properties of polyamide-6 composites.
- 2) To explore and compare alternative methodologies for the preparation of polyamide-6 composites, via cast and reactive extrusion techniques using nanocomposite strategies.
- 3) Characterisation of the filler matrix microstructure and its effect on physical properties of these materials.
- 4) Analysis of the mechanisms influencing physical performance of these materials.
- 5) To apply this knowledge to the preparation of advanced particulate-filled polyamide-6 composites with enhanced physical performance.

1.4

Thesis Outline

This thesis compares and contrast nanocomposites, their formulation and their manufacture. The contents of this study are divided into five chapters, which are broadly outlined below:

Chapter Two presents a comprehensive review of existing literature concerned with silicate-layered polymer nanocomposites. The natures of the individual components, as well as the micro-morphology of the composite are described. Experimental methods of

production are also discussed. Consideration is also given to the effects of flammability.

Chapter Three details the materials and experimental methods used in the production and formulation of polyamide-6 nanocomposites synthesised using cast and extrusion techniques. The practical and theoretical nature of experimental procedures used to characterise structure and properties of the materials prepared are discussed.

Chapter Four describes the comparison between the cast and extruded composites. As well as deliberating the experimental results obtained and subsequent trends observed in the reactively polymerised nanocomposites. The influence of the polymerisation conditions, residual monomer content and the nature of the composite structure produced are discussed, as well as the influence of composite microstructure on mechanical properties observed.

Chapter Five summarises the conclusions reached through this study.

References catalogues the references used through this work.

Appendices are a full directory of materials used and the results data obtained.

CHAPTER TWO

LITERATURE REVIEW

2.1

Introduction

This chapter contains a comprehensive review of the existing literature concerned with silicate-layered polymer nanocomposites. The natures of the individual components, as well as that of the composites produced are described. Experimental methods of production are also submitted. Consideration is also given to the effects of fillers.

2.2

Polyamides

Polyamides were introduced to the market in the late 1930's⁴, emerging as commercial engineering thermoplastics after their remarkable success in the textile field during the Second World War. The large-scale production of polyamide plastics grew mainly from the adaptation of conversion methods and equipment already used for other thermoplastics, together with the availability of relatively cheap raw materials for bulk manufacture of the polymers. The premium properties of the polyamides quickly led to their acceptance and use as high grade engineering plastic materials⁵.

The first polyamide product was sold in 1938 and was a continuous, large diameter filament used as a bristle for toothbrushes. However, moulding powder did not become commercially available until 1941 ⁶. Polyamide-6 occupies a prominent place in the engineering thermoplastics family because of its broad processing temperature range and the relative ease with which the base polymer can be modified to achieve a wide spectrum of properties. As a result there now exists a wide range of applications for polyamide-6 products, including: automotive, electrical, packaging.

2.2.1

Polyamide-6

The Oxford Dictionary of Chemistry ⁷ reports that a polyamide is: a type of polymer produced by the interaction of an amino group of one molecule and a carboxylic group of another molecule to give a protein-like structure. The intermediates for polyamides are dicarboxylic acids diamines, amino acids and lactams. Polyamides are usually identified numerically using the number of carbon atoms in the basic units of the polymer chains. A duplex digit is used when the polyamide is derived from a diamine and a diacid, the first digit of the duplex referring to the diamine ⁵. Nylon is the trade name for the polyamide family of polymers; with polyamide-6 and polyamide-6.6 being the most commonly used. These semi-crystalline synthetic polymers have fibre, film and/or plastic forming properties. All polyamides contain the amide group (—CO—NH—), this link joins the repeating hydrocarbon units of various lengths ⁸. These polyamide chains are linked together by hydrogen bonding, which confers a high degree of crystallinity ⁹. The major disadvantage of hydrogen bonding is the associated affinities for water. Polyamides therefore absorb moisture, accompanied by dimensional changes, reductions in stiffness and increases in toughness, owing to the water reducing the degree of packing of the polyamide molecules in the amorphous regions. Advantages of these polymers are their strength, toughness and rigidity, as well as their abrasion resistance ^{10,11}. They also demonstrate high heat distortion temperatures, but being thermoplastics, exhibit a viscoelastic response under load and soften at elevated temperatures ¹².

There are numerous polyamides, but this study is specifically concerned with polyamide-6, also known as polycaprolactam, Nylon-6, Perlon and various other trade names. It is a synthetic linear polyamide, in which the repeat unit of the chemical structure contains six carbon atoms, one belonging to the recurring amide group ($—CO—NH—$), and five to the $—(CH_2)_5—$ moiety linking the amide groups ¹³, Figure 2.1.

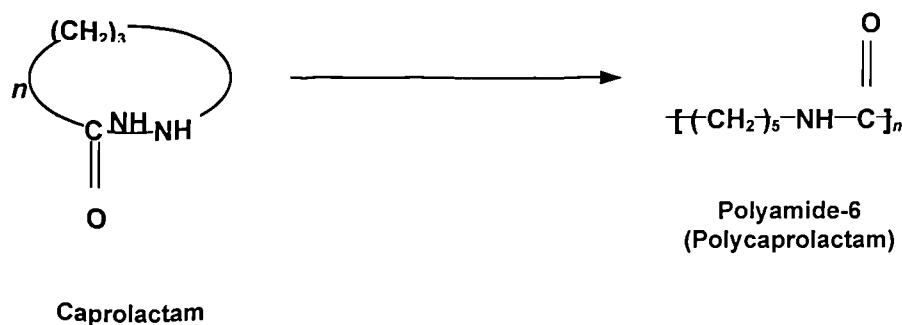


Figure 2.1
Repeat unit for polyamide-6 ¹³

Polyamide-6 is a hygroscopic polymer whose structure is characterised by the functional carbonyl group (CO) and an amine group (NH). The hygroscopic nature of polyamide-6 arises from the extensive hydrogen bonding between the carboxylic and amine groups. The effect of hydrogen bonds in any material allows for water to be attracted by the material, hence the term hygroscopic. A variety of synthetic routes can be used for the production of polyamide-6 and this will be discussed further into the review. Polyamide-6 along with polyamide-6,6 are among the most commonly used nylons, a trade name given to polyamides. The uses of polyamide-6 can vary as discussed earlier, but their fundamental uses are based on their structure.

A variety of methods exist for the polymerisation of polyamides. When an organic acid is heated with an organic amine (Figure 2.2) ¹⁴ condensation polymerisation occurs. Self-condensation of a single monomer containing both functional groups (Figure 2.3) - e.g. the self-condensation of ϵ -caproic acid ⁴, yields polymer. It is also possible to form polyamide-6 by cationic polymerisation, however monomer conversion and attainable molecular weights are not adequate for practical uses; hence this route is not

commercially practised ¹³. Industrial procedures for the manufacture of polyamide-6 involve the polymerisation of caprolactam (Figure 2.4) ¹³.

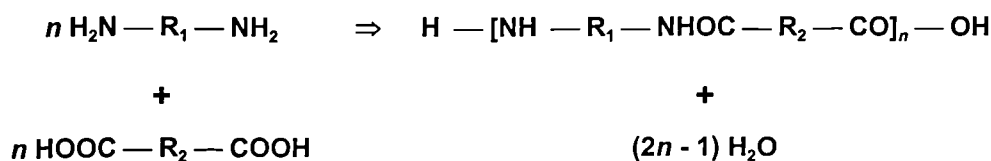


Figure 2.2
Condensation polymerisation between an organic acid and an organic amine ¹⁴

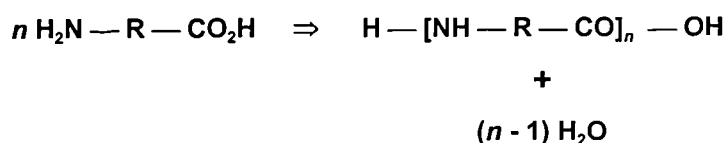


Figure 2.3
Condensation polymerisation, single monomer ¹⁴

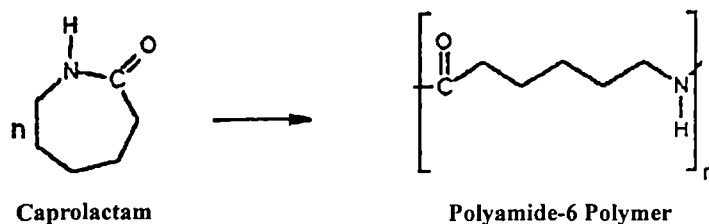


Figure 2.4
Ring-opening polymerisation of ϵ -caprolactam ²⁰

In 1938 Paul Schlack successfully produced high molecular weight polymer via the ring opening polymerisation of caprolactam ¹⁵, despite Carother's ¹⁶ acceptance that "lactam does not polymerise under the conditions of formation of the polyamide either in the presence or absence of catalysts." Although it is not actually known which substances were used in Carother's preliminary experiments. After extensive experimental work using various types of lactam Schlack concluded that caprolactam should be polymerisable at least in the presence of an appropriate initiator. The first such experiment, in which ϵ -aminocaproic acid hydrochloride was used as a catalyst, first as a source for a small amount of water to permit the hydration of end groups, and finally as a chain-length regulator, yielded polyamide-6.

The polymerisation of lactams has been studied in detail by various sources theoretical ^{4,6,13,14,17-19} and industrial ²⁰⁻²². The anionic polymerisation of caprolactam is a base-catalysed reaction. Using suitable initiators, conversion to the equilibrium state can be brought about within minutes, making the process commercial viable ⁵.

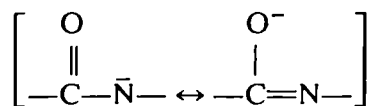


Figure 2.5
Resonance of lactamate ion ¹⁴

Initiation is usually via alkali metals or strong bases and proceeds through initial formation of a lactamate ion, which is stabilised by resonance, Figure 2.5. This anion is needed to facilitate the polymerisation reaction, and is known as the “catalyst”, examples of typical catalysts include sodium caprolactamate and dilactamate. Due to the electrostatic repulsion between the caprolactam molecule and the caprolactam anion, the attack on the carbonyl carbon atom in a molecule of monomer is relatively slow ²⁰. Scission of the $CO-NH$ bond produces a highly reactive terminal $-N^-H$ ion, which rapidly abstracts H^+ from another molecule of monomer ¹⁴. In the initial stages active amino and imide groups are formed, but since amine groups have been shown to inhibit rather than initiate polymerisation, the active initiating group is thus identified as the imide. Polymerisation is therefore considered to be a nucleophilic attack of the caprolactam anion on the carboxyl of the imide group ⁵. The slow normal initiation may be overcome and commercial viability ensured, by using an “activator” to mimic the intermediate species, Figure 2.6.

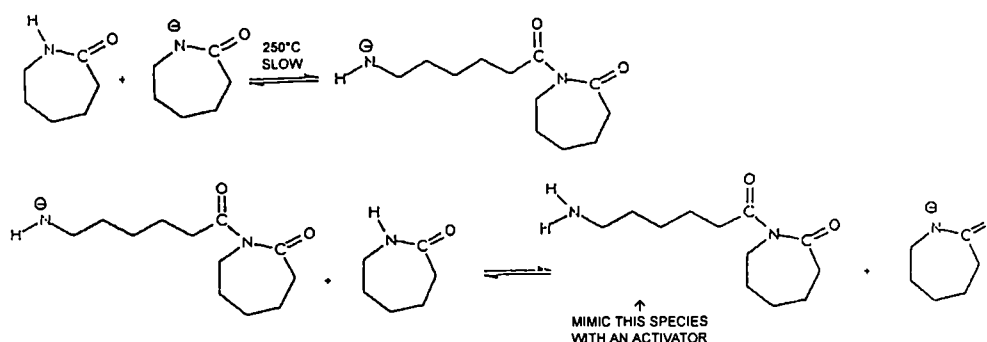


Figure 2.6
Slow reaction to form an intermediate ²⁰

Activated initiation proceeds rapidly, Figure 2.7. It has been shown that in the presence of both a catalyst and an imide initiator, the polymerisation can be carried out between 100°C and 200°C, i.e. below the melting point of the polymer, which is around 225°C.

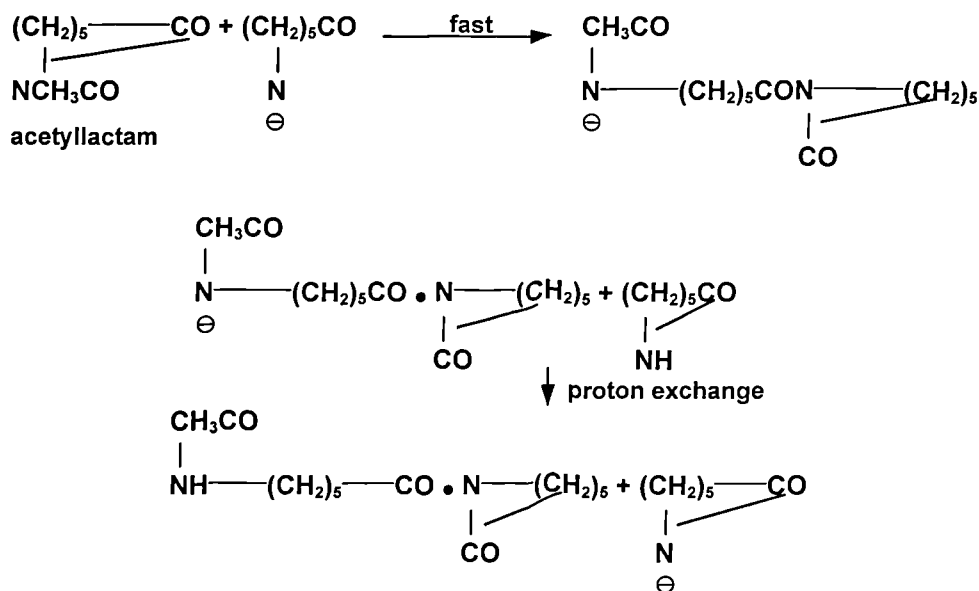


Figure 2.7
Activated initiation⁵

The ring carbonyl carbon atom in the product is much more strongly activated towards nucleophilic attack than that in the monomer due to the second carbonyl group bonded to the ring nitrogen atom. The propagation steps appropriate to the activated initiation are shown in Figure 2.8. The monomeric lactamate ion attacks the ring carbonyl carbon atom of the terminal N-acyllactam causing scission of the $\text{CO} \text{---} \text{N}$ bond to produce a ---N^- ion which abstracts H^+ from a molecule of monomer to form another lactamate ion. It is also possible for the ---N^- ion to attract an N-acyllactam end-group on another propagating chain which leads to the formation of branches. For each propagation step, the configuration of the asymmetric carbon atom on a substituted monomer is retained in the polymer¹⁴. Lactam polymerisation can involve a variety of growing species to which monomer or activated monomer is added. Obviously not all of these active species can co-exist simultaneously. On the other hand, more than one type of propagation reaction can be expected to proceed with a given initiator²³.

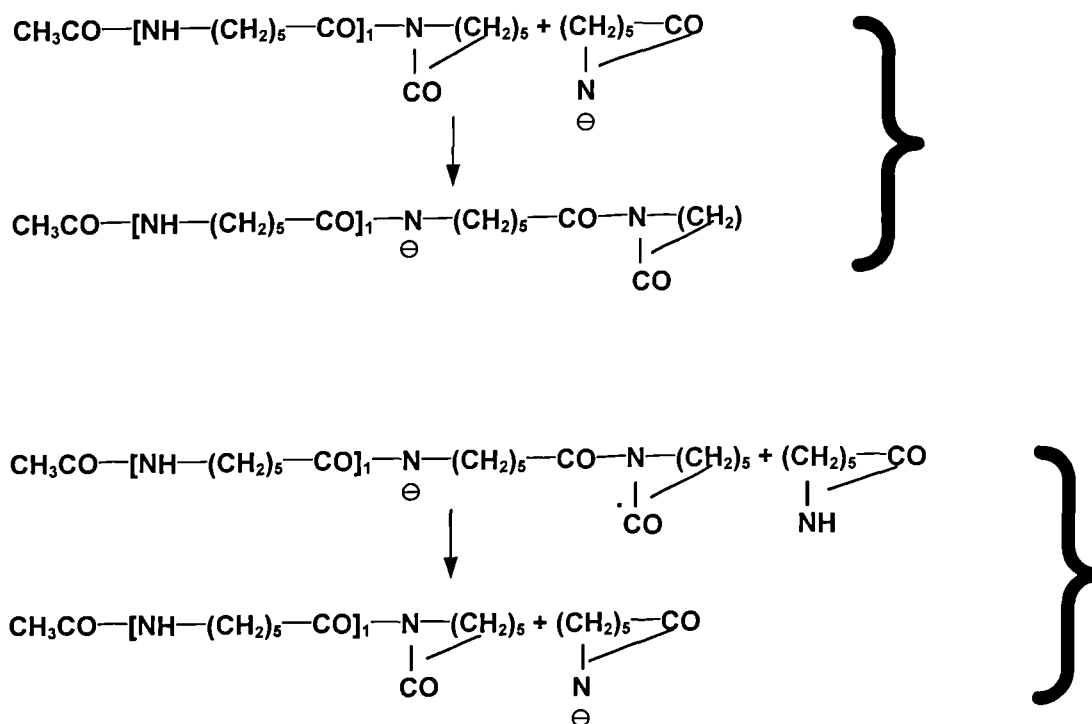


Figure 2.8
Propagation 5

The polymerisation of caprolactam is an exothermic process. The high viscosity and the low heat conductivity result in a considerable rise in temperature in the polymerising mass, and the rate of this increase can be considered a measure of the rate of reaction ⁵. Upon crystallising the high intermolecular attraction, due to the regular spacing of the amide groups, results in the formation of a high strength and high melting point polymer ¹². The characteristics of a particular polyamide-6 depend generally upon a number of functions that pertain to major polymer parameters ¹³:

- (1) Constitution: molecular weight (average), distribution of molecular weights, extent and type of branching, type and density of cross-linking, types and concentration of end-groups, concentration of multi-chain molecules, concentration and sequence distribution of co-monomers.
- (2) Conformation: type and extent of inter-forces and/or intra-forces [Hydrogen bonding (in a solid state), hindrance to internal rotation, solvation phenomena (in solution)].

- (3) Composition: water content, monomer content, concentration and distribution of cyclic oligomers, filler content.
- (4) Crystallinity: degree of crystallinity, composition of the crystalline phase morphology, micro-morphological structure (extended and folded chains), type and extent of super structures (spherulites).
- (5) Orientation: extent of orientation of either or both the polymer chain molecules and crystalline structures and super structures.

Thus for instance, tensile strength, modulus, hardness, abrasion resistance, heat distortion temperature, and thermal conductivity increase as molecular weight, orientation, and crystallinity increase, and as temperature and water content decrease. Impact strength, elongation, creep, and linear thermal expansion increase as water content and molecular weight, and temperature increase and the crystallinity decreases. Electrical properties, such as volume resistivity, dielectric strength, dielectric constant, and loss factor depend mainly on the water content and temperature. The water absorption and thus the water content of polyamide-6 in a given environment depends on the crystallinity of the polymer. As the crystallinity increases the amount of water being absorbed decreases. The hygroscopic nature of this thermoplastic not only affects the glass transition temperature, but also the mechanical properties, the extent of which is dependent on the amount of water absorbed. Whilst the absorption of moisture increases toughness, it does however reduce stiffness and dimensional stability ¹².

2.2.2

Crystalline State

Polyamide-6 can exist in either of two crystalline forms ²⁴, the α -crystal with hydrogen bonds between anti-parallel chains or the γ -crystal with hydrogen bonds between parallel chains. Polymers are composed of a large number of molecular lengths, hence two or more different crystalline phases may well exist in equilibrium with each other. The γ -phase is less stable thermodynamically stable than the α -phase. The α -phase has been characterised as having $\theta = 19.6^\circ$ (α_1) and $\theta = 23.5^\circ$ (α_2), these anti-parallel chains

have a repeat distance in excess of 170nm. For the γ -phase $\theta = 21.3^\circ$, bonding between parallel chains requires a distance of 168nm or less.

As discussed earlier, the structure of polyamide-6 is basically a carbon backbone from which there are a functional carbonyl group (CO) and an amine group (NH). These groups give polyamide-6 its characteristic properties.

The small sized side groups and the lack of any significant branching allow for a high packing efficiency. This coupled with the ability to form hydrogen bonds give a well-ordered sheet nylon, which has extensive secondary bonding inter-linking the polymer sheets.

Polyamides can be classed as being either odd or even, the distinction being determined by how many carbon atoms are in the repeat unit. For example, polyamide-6 is classed as an even, while polyamide-7 is odd. Even polyamides can form 100% hydrogen bonds in a planar arrangement (sheet) provided the adjacent molecules are anti-parallel. Hence adjacent molecules that are parallel will form only 50% of the hydrogen bonds. Odd polyamides can form 100% hydrogen bonds regardless of whether adjacent molecules are parallel or anti-parallel.

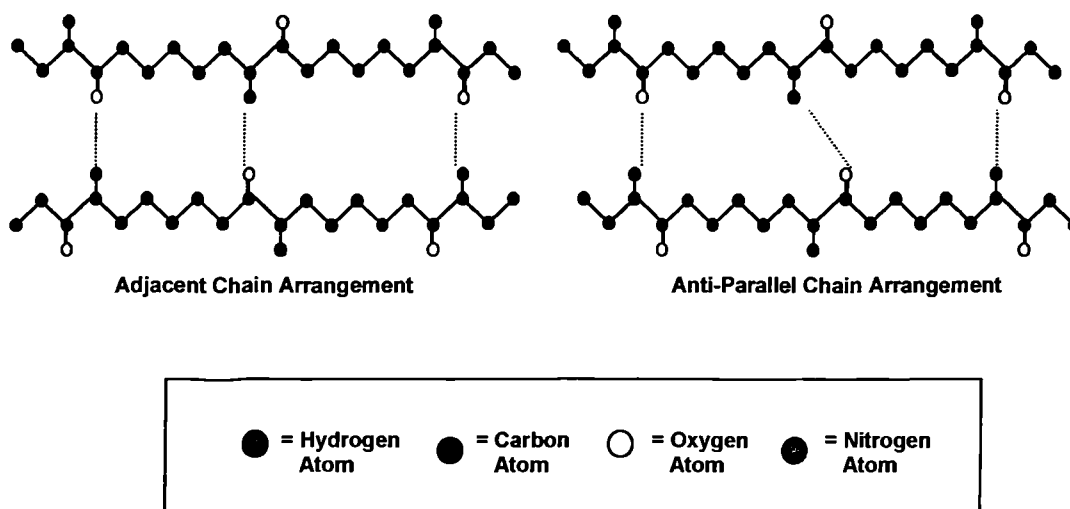


Figure 2.9
*Planar conformation of polyamide-6 chains*¹⁴

Isotactic arrangement of the amide group allows for a more energetically favourable arrangement provided the polarity isn't neutralised by the possibility of poor alignment of adjacent molecules.

Polyamides can be further classified according to their phases by forming either an α -phase or a γ -phase. Polyamides that crystallise to form the α -phase are generally even polymers with less than seven carbon atoms in the repeat unit. The α -phase is a fully extended zigzag arrangement of chains that fold back and forth to produce a sheet. The sheets are stacked upon one another and hydrogen bond is present between the sheets. The sheets are stacked with a progressive displacement of the hydrogen bond by one chain atom. However, a β -phase can be found and this confers a staggered structure. The polyamides that crystallise to form the α -phase are triclinic.

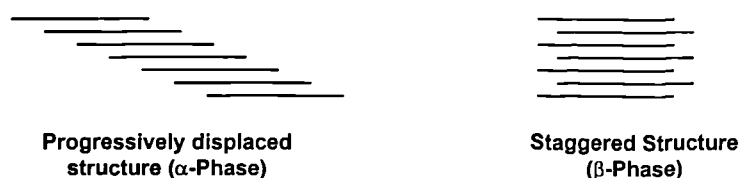


Figure 2.10
Stacking arrangements of Polyamide-6 14

The γ -phase is primarily produced by all even polyamides with more than seven carbon atoms in the repeat unit, as well as the odd and even-odd or odd-even systems. The γ -phase has a 30° tilting of the amide groups with respect to the chain axis. As a result of this there are no co-linear hydrogen bonds between adjacent chains. The cross-section of the γ -phase polyamide indicates that the chains can form the edges of a hexagonal unit cell. However, restrictions imposed by the hydrogen bonding will keep the planar zigzag structure and hence the γ -phase polyamides are termed pseudo-hexagonal. γ -Phase polyamides are usually monoclinic.

The production of either the α - and γ -phases will depend on environmental conditions and/or thermo-mechanical and pressure treatments.

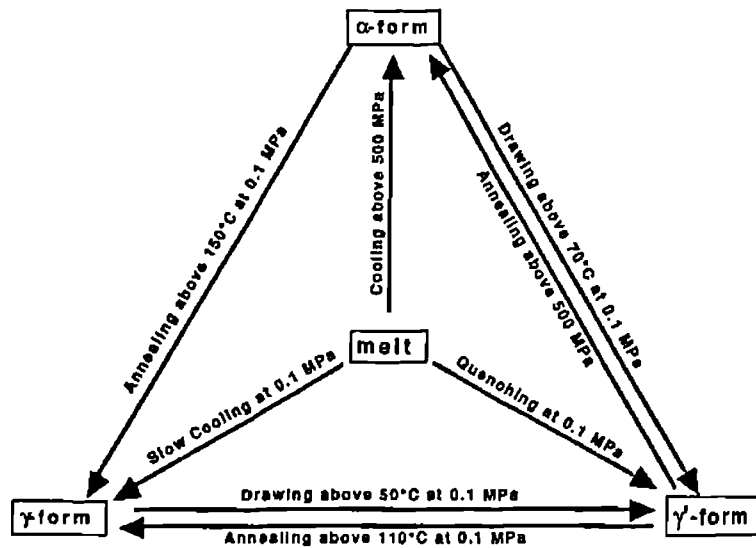


Figure 2.11
Schematic phase transformations of PA-12 under various thermo-mechanical and pressure treatments ¹⁴

Although Figure 2.11 is a schematic for Polyamide-12, the basis for phase production or transformation is principally the same as that for polyamide-6. In short, a history that involves cooling from melt under stress and at a reasonably rapid rate will generally produce a α -phase as will drawing and annealing at high stresses. Slower cooling from melt with less stress and/or annealing will produce a γ -phase. The γ^* -phase in terms of polyamide-6 could be thought to be the less common β -phase.

Polymers that precipitate from dilute solutions form a lamella (plate-like) structure. A lamella structure is regularly shaped with well-defined angles and straight edges that lie in particular crystallographic planes. A lamella structure is typically 10-20nm thick and 10 μ m long. The molecular chains with each platelet fold back and forth on themselves with the folds occurring at the faces. The lamella structure is the proposed model for the crystalline regions of the polymer and it is generally thought that the non-crystalline regions are found at the fold surfaces.

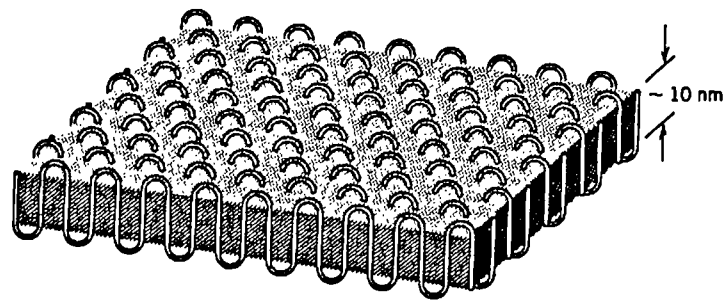


Figure 2.12
Chain folded structure for a plate-shaped polymer crystallite ⁸⁸

Polyamides that precipitate from melt generally form a spherulitic structure. Spherulites are spherical in shape and consist of an aggregate of lamellae (folded crystallites). There is a nucleation site for each spherulite and it is from this point that the lamellae radiate outwards to form the spherulite. Between lamella structures there is a belief that a tie chain molecule forms a link between adjacent lamellae and that this tie chain passes through an amorphous region.

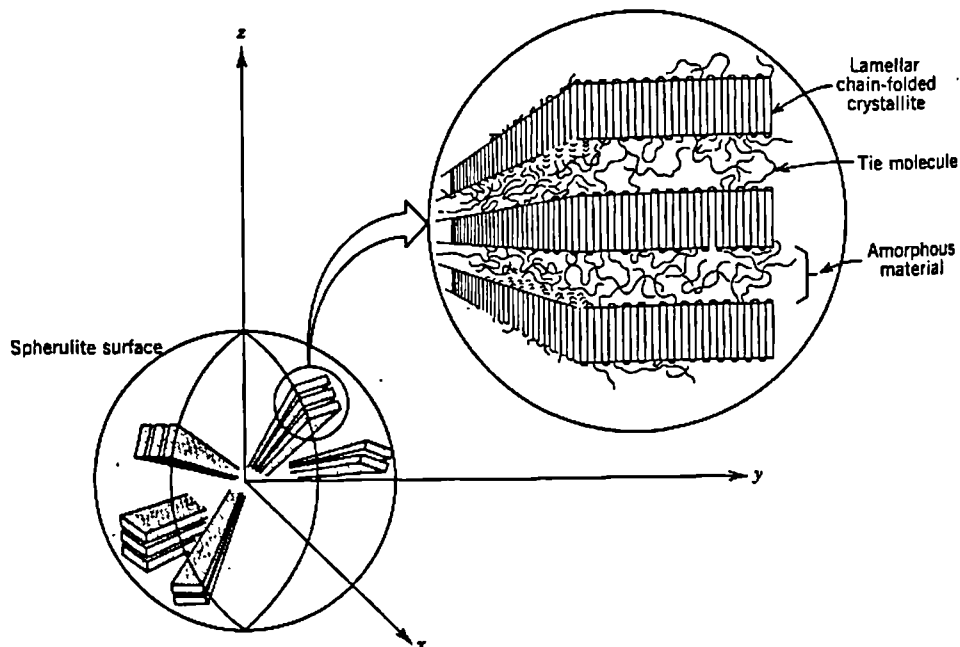


Figure 2.13
Schematic representation of a spherulitic structure ⁸⁸

The size of the spherulites is controlled by impingement on other spherulites, forming what could be thought of as planar boundaries. Prior to impingement the spherulites are spherical in shape. A characteristic Maltese cross is formed within each spherulite and this is attributed to orientation of the lamellae. Ringed lines radiate out from a point and this illustrates how the lamellae radiate out from the nucleation point/site.

Crystalline regions of a polymer are more restricted in their motion than amorphous regions. Therefore a highly crystalline polymer will have better mechanical properties than a less crystalline polymer. Furthermore, highly crystalline polymers show less glassy behaviour when approaching their glass transition temperature. The morphology and structure of the crystalline phase will influence the extent of hydrogen bonding and hence the mechanical properties. Firstly the parallel or anti-parallel arrangement will influence the amount of hydrogen bonding (the influence of hydrogen bonding has been discussed earlier). The phases present (i.e. α or γ) will influence the packing of the structure. The γ -phase produces a 'tighter' packing arrangement than the α -phase, which results in better mechanical properties⁸⁹. Again this is due to the restricted motion of the polymer chains.

2.2.3

Caprolactam

At the turn of the century Otto Wallach synthesised the lactam of ω -aminocaproic acid, caprolactam¹⁵. Lactams are cyclic amides of the type $\text{—}R\text{—}NH\text{—}CO\text{—}$, where R represents a hydrocarbon chain. The different ring sizes and substitution very strongly affect the reactivities of lactams as well as the properties of the resulting polymer. Caprolactam has seven atoms in its hydrocarbon chain, as shown in Figure 2.14.

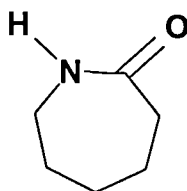


Figure 2.14
Structural formula of ε-caprolactam.

The formal names for ε-caprolactam are: 2-oxohexamethylenimine, 1-azacycloheptan-2-one or cyclohexanone-iso-oxime. It is hygroscopic in nature and the amount of water it absorbs has a major influence on its ability to polymerise. As a chemical intermediate caprolactam is quite important, owing to commercial interest in polyamide-6; however, non-polymer applications for caprolactam do exist, for example in the Netherlands L-lysine it is used as a nutrition additive ²⁵.

Several processes have evolved for the manufacture of caprolactam, including those manufacturing routes developed by Snia Viscosa ²⁶ and BASF ²⁷. Commercially caprolactam is produced from cyclohexane and hydroxylamine via cyclohexanone oxime ²⁸, and by the following routes ^{6, 164}:

- (1) From cyclohexane through cyclohexanone by oxidation, oximation and Beckmann rearrangement.
- (2) From phenol through cyclohexanone by hydrogenation oximation and Beckmann rearrangement.
- (3) From toluene through hexahydrobenzoic acid by oxidation, hydrogenation, nitrosation and rearrangement.
- (4) From cyclohexane by photonitrosation and rearrangement.

The majority of caprolactam produced is derived from cyclohexane. The reaction steps involving getting to cyclohexanone from either cyclohexane or phenol are quite similar and vary primarily in the catalysts and reaction conditions employed.

The earliest process, and still the most widely used, involves the reaction of cyclohexanone with a hydroxyl amine salt to give cyclohexanone oxime which is then treated with concentrated sulphuric acid via the Beckmann rearrangement ⁸. In one application of this process, cyclohexanone is added to an agitated reactor together with an excess of hydroxyl amine salt solution:

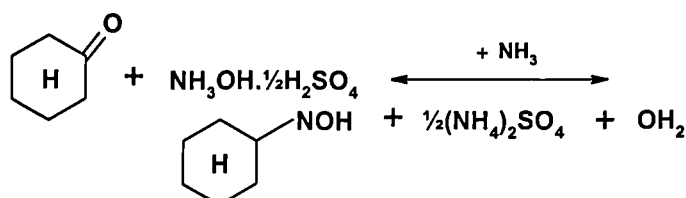


Figure 2.15
Manufacture of caprolactam ⁸

The mixture is cooled to hold the temperature below 50°C. Anhydrous ammonia is then added to the solution to form the oxime, which precipitates as a crystalline solid. Cooling is required to remove the heat of reaction. The reaction product is then filtered in order to recover the wet oxime. The oxime is melted and pumped to an agitated and water-cooled autoclave where it mixes with concentrated sulphuric acid at a temperature 115-140°C. The reaction is vigorous, hence control of: mixing, temperature and ratios of acid to oxime streams is required to carry out the reaction safely. The crude product is cooled below 75°C.

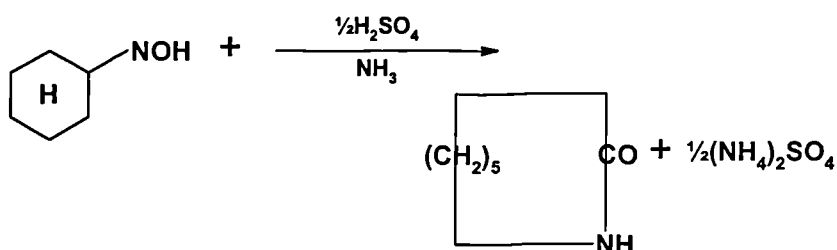


Figure 2.16
Manufacture of caprolactam ⁸

In the final step, the caprolactam-sulphuric acid solution is neutralised with ammonia while being cooled. The crude lactam solution is decanted and refined in a vacuum distillation train. A disadvantage of this process is that the ammonium sulphate in the aqueous solution decanted from the crude lactam must be recovered to make the process economically viable.

2.3

Properties Of Filled Polymer Composites

Fillers have an important role in the property modification of polymers ²⁹⁻³², although account has to be taken of any negative changes that may occur owing to this addition and whether these are tolerable ¹². Effects on composite properties are dependent on filler concentration, particle size and shape, as well as matrix interaction. Other factors that require consideration include: ease of filler handling and any effect the filler may have on processing. Associated with this is the prospect of any special additives or surface treatments that may be required. Finally, and possibly most significantly from an industrial perspective, is the true cost of using the filler and whether it is justifiable in comparison to other alternatives. Fillers are often used to cheapen, but the savings are frequently not as great as anticipated. Two of the main reasons for this are the associated costs of compounding the filler into the polymer and the increase in the volume of product required, due to the increased specific gravity of the filler – although in some cases air may be deliberately introduced in order to reduce density ¹². So even though fillers can be used simply as matrix dilutents, more commonly they are utilised in a functional role, where they impart some special property characteristic to the composite ³⁰.

2.3.1

Structure and Property Effects of Fillers

When a particulate phase is introduced into a polymer the structure will be affected. The major disadvantage with the addition of fillers is the accompanying decrease in the physical properties observed, especially toughness ^{12,30,33}. Toughness is influenced by the extent of filler dispersion; poorly dispersed filler will result in reduced toughness. The morphology of the filler particles is also known to have an effect, for example plate-like particles result in decreased toughness ³⁰. Certain filler surfaces may even act as nucleators for semi-crystalline polymers, thus altering the amount and type of crystallinity ³³. The high filler loadings used in plastic composites leads to the

interfacial properties of the filler-matrix being the major determinant of the composites' mechanical properties ³⁴. Distribution and dispersion of fillers is the key factor affecting microstructure; but controlling processing conditions and polymer surface modification can also result in different microstructures ³⁵.

Rothon ¹² has highlighted the property variations that occur during compounding and moulding operations. Polymer matrices and their filler components might undergo mechanical and chemical degradation, consequently a reduction in molecular weight may be observed. This degradation is directly related to the increased mechanical work and chemical interactions at the interface, along with possible deactivation of stabilisers. Modification of molecular weight and cross-linking are likely to occur due to interference with the curing process in thermoset composites. Polar materials are usually more strongly adsorbed onto particulates than the polymer, resulting in their preferential adsorption. Polymer adsorbed onto the surface of the particulate will form a shell of immobilised material, which may well have different properties to that in the bulk. At high filler loadings the effect from this less mobile polymer becomes increasingly important. The presence of particle surfaces will restrict conformation of the polymer molecules in its vicinity. This strained conformation will result in property variations.

In a well-dispersed composite there will be a close interaction between the filler and the matrix, resulting from the radial compressive stress that develops on cooling. The surface interactions in polymer composites are in part due to the greater thermal expansion of the polymer, twenty to thirty times larger than the mineral filler. These stresses will result in interaction between the two phases being at the very least mechanical, but other forms of interaction will exist dependent on the surface chemistry of the filler and also on the chemistry of the polymer. Wettability of the filler is an indication of compatibility between the two substances. Adhesion at a polymer-filler interface has been shown to exert a considerable influence on the mechanical response, and in this connection, a correlation between acid-base characteristics of filler and polymer and properties has been established ¹².

Fracture in polymer occurs by the breaking of primary (covalent) and/or secondary (van der Waals or hydrogen) bonds, depending on the structure of the polymer³⁶. The degree of interfacial adhesion at the boundary between the polymer matrix and the filler is known to have a critical bearing on the ability of a particulate composite to resist crack propagation, and hence impact behaviour³⁰. There are various forms of composite failure, all dependent of the nature of the interfacial bonding. If the filler-polymer interface is extremely strong (greater than the strength of the matrix) the failure pathway is confined to the matrix and little or no emergence of filler is observed on the fracture surface. If the matrix strength is equivalent to that of the interface, a propagating crack will follow the filler-matrix boundary; unless the filler particle is weak (e.g. an agglomerate), in which case the crack will pass through the particle. With very weak interfacial bonding, the filler and matrix will separate completely; and thus there will be limited filler contribution to overall impact strength. Any modification that improves energy absorption at the interface, will effect a corresponding improvement in the composite toughness.

2.3.2

Surface Modification of Fillers

In order to ameliorate negative effects, inorganic fillers intended for incorporation into plastics and rubbers might be surface treated with organic reagents thereby modifying the characteristics of the resultant filler-matrix interface³⁰. The interaction between the filler and the polymer may be altered by modification of the filler surface. The chemical nature and amount of surface treatment applied can strongly affect mechanical properties, with the method of modification being dependent on the surfaces in question. The objective of coating the filler surface is to achieve improved mechanical properties in the resulting composite materials³⁸. The filler may be pre-coated, or the coating agent may be added in-situ, each system having its own relative merits¹². Reductions in the surface energy of fillers can, via treatments, aid the compromised melt processability and poor mechanical properties³⁷. Coatings can be reactive and act as coupling agents between filler and polymer. More often they alter the energy of interaction so as to improve dispersion and compatibility³⁸, by altering the chemical

resistance of the bond across the interface. Most inorganic fillers have highly polar surfaces that are hydrophilic rather than oleophilic in character, and as such are not readily wetted by organic fluids (hydrocarbon solvents, oils, molten polymers, etc.) that tend to have low/moderate polarity and relatively low surface energies. Mineral fillers can be rendered oleophilic by chemisorption of surface-active agents (fatty acids and unsaturated polymeric acids) ³⁰. The most common functionalities used to produce bonding with the filler surface are acids or acid precursors (for basic or amphoteric fillers) and alkoxy silanes (for fillers with metal hydroxyls present, especially siliceous fillers). Organotitanates and related compounds are also proposed for use with a wide variety of fillers ¹².

When the organic molecule is a simple hydrocarbon, then the coating will generally aid filler incorporation and dispersion, but does not form a strong bond with the polymer matrix. If strong bonding is required, then a further functionality capable of forming a covalent bond with the matrix is also incorporated into the coating molecule. These bifunctional surface treatments are generally known as “coupling agents” because of their ability to chemically couple the filler to the polymer matrix. Modification of the interface between an organic polymer and an inorganic substrate may have beneficial results in composite manufacture, but “coupling agents” should be defined as materials that improve the chemical resistance (especially to water) of the bond across the interface. These coatings form very strong covalent bonds to the filler and then bond to the polymer by a variety of mechanisms ¹². Incorporation of silane coupling agents (e.g. silanes, metal alkoxides, etc.) result in some improvement to the impact and the tensile strength of the composite relative to untreated filler, which is characteristic of enhanced filler-matrix adhesion and improved dispersion ³⁷. Organofunctional silicones are widely applied as coupling agents to improve bonding of organic resins to mineral surfaces ³⁹. Alternatively the matrix may be functionalised, but it is more usual to incorporate an extremely reactive functionality into the coating, such as carboxylic acid or anhydride groups, either during polymerisation or by subsequent reactive modification in the melt state ³⁰. This results in greater surface interaction between the inorganic filler and the organic polymer. Typical of such functionalities are primary amine and azido groups ¹².

Fatty acid derivatives (although not true coupling agents) have been found to be an effective surface treatment for improving toughness, owing to increased filler-matrix adhesion ³⁷. The significant improvement in impact performance subsequently observed is attributed to modification of the polymer deformation mechanism; however, there is an accompanying decline in the flexural and the tensile properties ³⁰. Stearic acid is a widely used fatty acid, being absorbed onto polar surfaces through the carboxyl group, with the hydrocarbon chain perpendicular to the surface. It is often added to aid filler handling during production; it also makes the filler less dusty and helps to reduce moisture absorption. It is generally held that fatty acid treatments in thermoplastics reduce melt viscosity, improve filler dispersion and impact resistance, but decrease the modulus ¹². For example, magnesium hydroxide when coated with sodium stearate has been found to give an increase in the melt flow index and the impact strength of composites ⁴⁰.

2.4

Layered Silicates: Clay

The earth's crust is composed almost entirely of silicates and silica, which constitute the bulk and of soils, clays and sands, the breakdown products of rocks ⁴¹. Clay is undoubtedly the oldest ceramic material ⁴². Whilst the term "clay" itself has no genetic significance, it is used to describe the product of weathering, the result of hydrothermal action, or deposited sediment. These materials are crystalline in nature ⁶⁶ and are hydrous silicates or alumino-silicates. Tending to be natural, earthy, fine-grained materials, which develop plasticity when mixed with a limited amount of water ⁴³.

The majority of the clay minerals are layered silicates or phyllosilicates. The definition of a phyllosilicate is that the tetrahedral sheet must be continuous and the layer structure must be evident in the nature of the interlayer bonding, which should be weaker than the bonding within the layers and give rise to characteristic properties, such as basal cleavage ⁴⁴. All silicates are based on one simple group $[SiO_4]^{4-}$, this group is incapable of independent existence and requires four positively-charged ions or other groups to

neutralise the excess negative charge ⁴⁵. The principal building elements are two-dimensional arrays of silicon-oxygen tetrahedra and two-dimensional arrays of aluminium- or magnesium-oxygen-hydroxyl octahedra. In most clay minerals, such sheets of tetrahedra and octahedra are superimposed in different fashions ⁴⁶.

2.4.1

Structural Considerations

The structural framework is basically composed of layers comprising silica and alumina sheets, joined together in varying proportions and stacked on top of each other in ordered arrangements. Theng discusses this organisation in detail ⁶⁶, which is summarised in Table 2.1. This table is by no means comprehensive, and in fact several classification schemes exist, this particular one follows the recommendations submitted by the Nomenclature Committee of the Clay Minerals Society ⁴⁴.

Type	Group	Series	Species
1:1	Kaolinite	Diocahedral	Kaolinite
	Serpentine	Triocahedral	Halloysite
Antigorite			
Chrysotile			
2:1	Pyrophyllite-talc	Diocahedral	Pyrophyllite
		Triocahedral	Talc
	Smectite	Diocahedral	Montmorillonite
		Triocahedral	Saponite
	Vermiculite	Diocahedral	Vermiculite
		Triocahedral	Vermiculite
	Illite	Diocahedral	Illite
		Triocahedral	Ledikite
	Mica	Diocahedral	Muscovite
		Triocahedral	Phlogopite
	Brittle Mica	Diocahedral	Margarite
		Triocahedral	Clintonite

Table 2.1
Classification scheme for crystalline phyllosilicates or layer silicate minerals ⁶⁶

Each group of minerals is divided into two sub-groups, dioctahedral and trioctahedral, with each containing a number of mineral species. The neutral 2:1 layer structure, shown below, represents the structure of the mineral pyrophyllite ⁴⁶. In this mineral two of the three possible octahedral positions are occupied by trivalent aluminium, hence this structure is called dioctahedral.

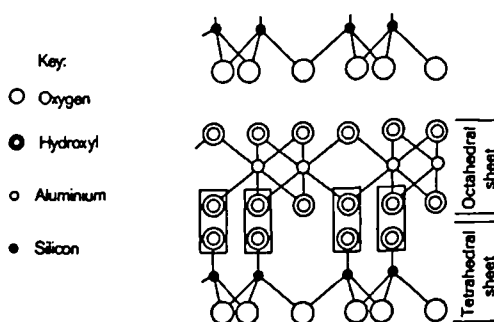


Figure 2.17

*Schematic representation of a silica tetrahedral sheet and an alumina octahedral sheet
The mode of condensation between the two sheets is indicated by the rectangles ⁴⁶*

In the silicon-oxygen sheets, the silicon atoms are co-ordinated with four oxygen atoms. The oxygen atoms are located on the four corners of a regular tetrahedron with the silicon atom in the centre. In the sheet, three of the four oxygen atoms of each tetrahedron are shared by the neighbouring tetrahedra. The fourth oxygen atom of each tetrahedron is pointed downward. The silica-oxygen sheet is called the tetrahedral sheet or the silica sheet.

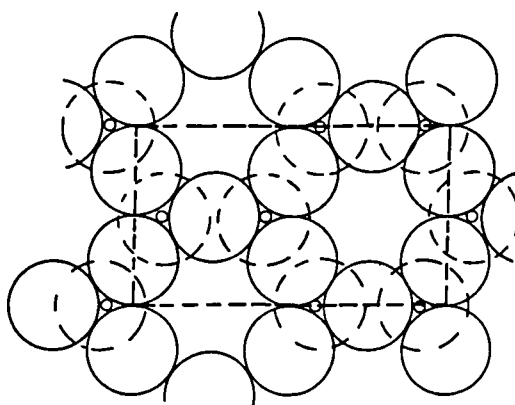


Figure 2.18

*Top view of tetrahedral sheet (dotted line: unit cell area)
Large circles represent oxygen; small circles represent silicon ⁴⁷*

In the aluminium sheet, the aluminium atoms are co-ordinated with six oxygen atoms or OH groups that are located around the aluminium atom with their centres on the six corners of a regular octahedron. The oxygen atoms and hydroxyl groups lie in two parallel planes with aluminium atoms between these planes. The projections of the sheet show that the oxygen atoms and hydroxyl groups form hexagonal close packing. This sheet is called the octahedral sheet or the alumina sheet. According to Pauling, who was the first to elucidate the structure of clay minerals, each plate-like clay particle consists of a stack of parallel layers. Each layer is a combination of tetrahedrally arranged silica sheets and octahedrally arranged alumina or magnesia sheets. 2:1 layer clays, montmorillonite, are built of layers composed of two tetrahedral sheets with one octahedral sheet in between.

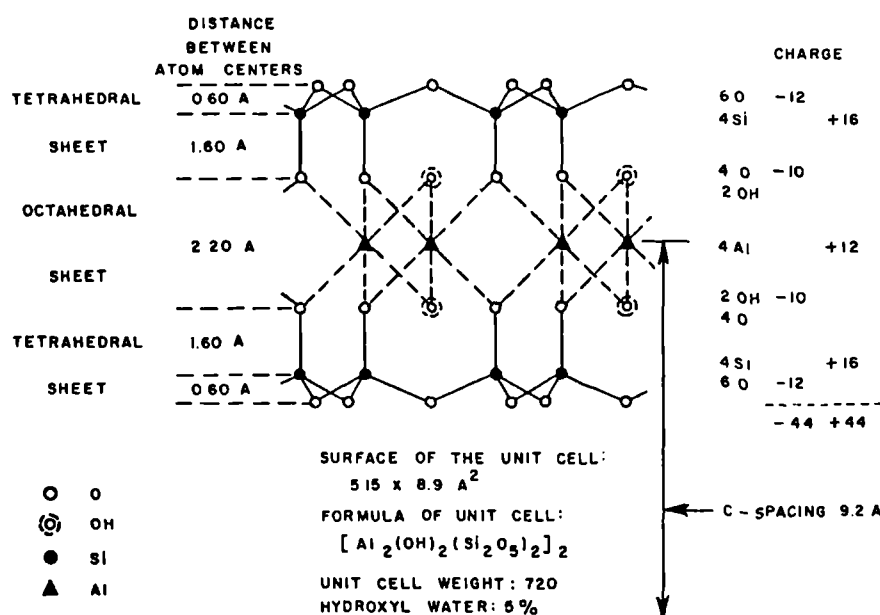


Figure 2.19
Atom arrangement in the unit cell of a 2:1 layer mineral 42

The symmetry of this type structure is basically hexagonal, although, in reality there is some departure from this ideal. Which may be attributed to the opposed rotation of alternate silica tetrahedra, these tetrahedra may also be tilted with respect to the plane of surface oxygen atoms. Factors such as the geometric fit between the larger tetrahedral and the smaller octahedral sheets, as well as the amount and site of isomorphous substitution, and also the nature of the charge balancing cation influence the extent of rotation and tilting.

2.4.2

Montmorillonite

The Smectite ⁴⁷ minerals are a series where: silica, magnesia, alumina, iron oxide and water are the principal components. These layered silicates are often expressed chemically as having the formula: $Al_2O_3 \cdot 4SiO_2 \cdot nH_2O$, but this can be misleading as the aluminium content can be very small, as in the case of hectorite. These minerals all have in common a large endotherm at about 150°C, corresponding to the evolution of inter-layer water and water associated with the exchangeable cations. Inter-layer water is defined as the entire interfacial region between the hydroxyl surface of the clay and bulk liquid water ⁴⁸. The thickness of this adsorbed water layer is variable, ranging from only a fraction of the surface being covered by one molecular layer up to many tens of molecular layers, depending on the water content and nature of the clay. Thus the endotherm correspondingly varies in size and shape. The main decomposition endotherm of the mineral occurs at about 700°C, and there is a final exotherm at about 1000°C. In montmorillonite, owing to the many different substitutions, there is wide variation in their chemical compositions and therefore final products of heating. Adsorbed water is lost at about 105°C from the external surfaces, but a much higher temperature, from 120-300°C, is required to remove the inter-layer water, depending somewhat on the nature of the exchangeable cations. At about 650°C the hydroxyl groups are removed as water, the exact temperature depending on the type of montmorillonite. The initial dehydration products in this case are probably amorphous alumina and silica ⁴⁵.

Montmorillonite is a member of the Smectite mineral grouping, and with out considering lattice substitutions, montmorillonite has the theoretical formula:

$(OH)_4 \cdot Si_8Al_4O_{20} \cdot nH_2O$ and has the theoretical composition:

$$SiO_2 = 66.7\%$$

$$Al_2O_3 = 28.3\%$$

$$H_2O = 5\%$$

As shown in Figure 2.20 the montmorillonite structure is composed of a four-high packing of oxygen and hydroxyl ions co-ordinated about three layers of cations ⁴⁹. The units consist of two silica tetrahedral sheets, with a central alumina octahedral sheet ⁵⁰. In layered crystals, atoms are held together by strong covalent bonds, but between the layers the forces are considerably weaker. In the montmorillonites there is no possibility of hydrogen bonding, since both the outer layers are silica and there are no exposed hydroxyl groups at the surface ⁵¹. Weak van der Waal's forces therefore only hold the montmorillonite sheets together. The inter-layer space can therefore expand considerably to accommodate guest ions or molecules with out destroying the layered structure ⁵². Exchangeable cations are situated between the silica layers and because of the relatively weak bonding are able to diffuse outwards when on contact with water ⁴⁵.

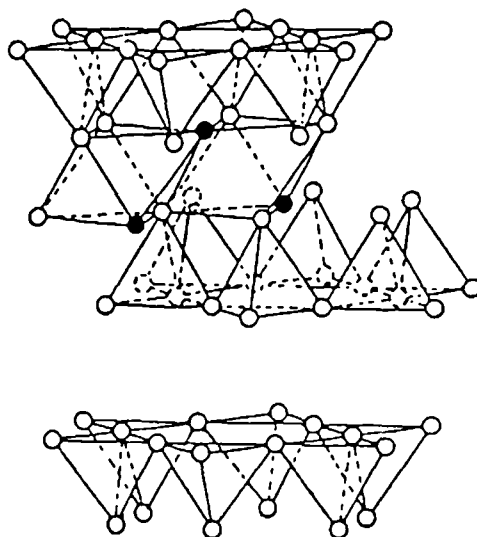


Figure 2.20
Idealised structure of a 2:1 layered silicate ⁹³.

In montmorillonite the individual particles are difficult to discern, the general appearance being that of a fluffy, irregular mass of agglomerated particles. In fact there is no guarantee that the electron micrographs of dry clay particles reflect the size and shape of the particles in the suspended condition. Where individual particles have been found, they appear to be extremely thin – approximately $0.002\mu\text{m}$ in thickness – showing that they approach unit cell size. The average diameters are difficult to assess but are reported to be $0.02\text{-}0.2\mu\text{m}$. It is becoming increasingly clear that the apparent size of montmorillonite particles depends very much on the degree of dispersion

achieved in their preparation; this is influenced, among other things, by the nature of the exchangeable cations ⁴⁵. When montmorillonite powder is added to water and allowed to disperse it will break down into its primary particle, a crystal which is a platelet structure up to 1000nm across and 0.92nm thick ⁵³. This type of particle morphology leads to an extremely large surface area of 800m²g⁻¹.

Montmorillonites exhibit characteristic swelling in certain liquids, particularly water and other polar molecules, glycerol, ethylene glycol and phenols ⁴⁵, for example. These organic molecules enter between the unit layers, causing the lattice to expand ⁴³. This results in a variable basal spacing, which in montmorillonite, may range between about 110nm and 600nm depending on the type and amount of liquid absorbed between the layers. Aliphatic chains may be adsorbed on montmorillonite surfaces with the zigzag of their carbon chain either parallel or perpendicular to the surface ⁵⁴. It has been shown despite the parallel orientation seeming the most probable, because it yields the smallest spacing, in fact only aliphatic compounds with strongly polar groups favour this arrangement. Geometric packing is almost equally effective in both cases. In those molecules, which do not have such polar groups, it is conceivable that the organic-organic interaction may be responsible for the arrangement.

The introduction of polar liquids raises the basal spacing to a constant and characteristic 171nm, which corresponds to a double layer of organic molecules between the montmorillonite layers ^{55,56}. The basal reflections vary with the hydration of the mineral; values from 100nm to 150nm have been reported. The *d*-spacings of around 25nm to 26.4nm are also characteristic of montmorillonites and are not affected by hydration ⁴⁵. This extensive inter-layer expansion results in a large active surface area being exposed, allowing an enormous range, both in number and variety, of guest molecules to be intercalated ⁶⁶. Montmorillonite is capable of intercalating a number of water layers through which basal spacing increases stepwise, resulting in products of a very high aspect ratio. This type of expansion is referred to as intra-crystalline, or simply crystalline swelling, signifying that the gross crystal morphology is preserved.

The choice of montmorillonite as a sorbent of organic compounds is dictated by its large surface area, its high cation exchange capacity, which is largely independent of salt concentration and pH, and the relative ease by which it forms an inter-layer complex with a variety of organic molecules ⁵⁷. The main uses of montmorillonite actually stem from the characteristic expansion that it exhibits. For example it is used to control viscosity, or to impart thixotropy to a variety of liquid polymers ¹². Smectite minerals also have patented applications as catalysts, catalytic supports and sorbents ⁵⁸.

A dry montmorillonite powder swells spontaneously when contacted with water ⁴⁶. The dry clay usually imbibes water and becomes a gel, and it can be stirred up with more water to yield a suspension or sol. The montmorillonite clay first takes up one to four monolayers between the layers. This inter-layer swelling causes, at most, a doubling of the volume of the dry clay. However, the swelling process continues, and an amount of water is imbibed which is many times the volume of the original clay. The additional swelling is a result of the double-layer repulsion between the surfaces of the individual particles, which pushes them apart. This swelling may be called osmotic swelling since the water tends to equalise the high concentration of ions between two particles, which are so close together that their double-layer overlap, and the low concentration of ions far away from the particle surfaces in the bulk solution. Organic anions are adsorbed at the edges of the clay particles. Organic cations, on the contrary, are adsorbed on the negative face surfaces of the clay. This fact is evident from the much larger adsorption capacity of the clay for these cations and also from the increase of the basal spacing of montmorillonite clays after treatment with organic cations. The adsorption of organic cations is usually not limited to an amount equivalent to the cation exchange capacity of the clay. The van der Waals forces linking the hydrocarbon chains of the exchange-adsorbed cations and those of the excess organic molecules physically adsorb the excess of the organic salt. The ionised groups of the physically adsorbed molecules will point towards the water phase. The organic cations and the anions of the ionic groups together will create a more or less diffuse electrical double layer, and the absorption complex now assumes a positive charge.

When montmorillonite clays are contacted with water or water vapour, the water molecules penetrate between the layers ⁴⁶. This so called inter-layer swelling or intra-crystalline swelling of montmorillonite is evident from an increase of the basal spacing of the clays to definite values between 1.3-2.0nm, depending on the type of clay and the type of cation. However minerals such as pyrophyllite and talc do not swell, so why does montmorillonite? Two alternative explanations have been advanced. According to one point of view, the inter-layer cations in montmorillonite become hydrated, and the large hydration energy involved is able to over-come the attractive forces between the layers. Since in the prototype minerals inter-layer cations are absent, there is no cation hydration energy available to separate the layers. Alternatively, it has been proposed that the penetrating water does not hydrate the cations between the layers but becomes adsorbed on the oxygen surfaces by establishing hydrogen bonds. Certain geometric arrangements of the water molecules in the water layers have been proposed which would favour such a bonding.

Provided the particles of a colloidal suspension remain as discrete individual units, Brownian motion and diffusion operate to counteract sedimentation forces. If, however, the particles are caused to gather together into flocs or aggregates, the latter behave as single, large particles, sedimentation occurs and thus the system is flocculated ⁴⁵. When the particle migrates, the water layer, together with the ions in the Stern Layer (The fraction of positive counter-ions that are strongly adsorbed and form a monolayer close to the surface.) move with it. Therefore, the electrical interaction between adjacent particles depends on the potential at the boundary of the immobile water layer, usually known as the zeta potential. The forces between suspended particles, on which viscosity depends, are in turn dependant on the nature of the cation associated with the double layer. Thus flocculating cations (Such as: OH_3^+ , Ca^{2+} and Mg^{2+}) favour the formation of particle links, leading to thixotropic structures and the viscosity of such systems is correspondingly high. If Na^+ , K^+ , Li^+ or NH_4^+ replaces the above, which favour a high zeta potential, the interparticle forces of attraction are outweighed by the electrostatic forces of repulsion and a deflocculated system results. Such a system has low viscosity. Whatever the nature of the original ions their replacement affects flocculation properties; for example the addition of an amine to an aqueous suspension, results in the clay being strongly flocculated.

As a result of isomorphous substitution of certain electropositive elements by such elements of lower valence, the clay crystal carries a net negative charge ^{46,59}. This net negative charge is compensated by cations that are located on the layer surfaces. In the presence of water, these compensating cations have a tendency to diffuse away from the layer surface since their concentration will be smaller in the bulk solution. On the other hand, they are attracted electrostatically to the charged layers. The result of these opposing trends is the creation of an atmospheric distribution of the compensating cations in a diffuse electrical double layer on the exterior layer surfaces of a clay particle. The compensating cations between the layers of the stack are confined to the narrow space between opposite layer surfaces. When a clay is dispersed in water an equilibrium is set up between the osmotic pressure which pulls the sodium ions away from the clay into the bulk of the surrounding liquid and the electrostatic pressure which tends to hold the same ions back at the clay surface. This is known as the electrical double layer.

If the clay platelets approach each other face-to-face then repulsion will occur. If the platelets approach each other edge-to-face then the platelets will be attracted to each other; if sufficient concentration of clay is present then a system of edge-face bonds can be set up in three-dimensions throughout the dispersion. When this occurs all the water present is tied up in the electrical double layers around the clay platelet and the dispersion becomes a gel. The electrostatic attraction between the positively charged edges and negatively charged faces is fragile and may easily be broken by the application of shear. However, when the shear is removed the system of edge-face bonds will reform quickly. This property is known as thixotropy ⁵³.

2.4.3

Cation Exchange

Lattice silicate minerals possess high cation exchange capacities greatly in excess of that attributable to surface area, crystal fracture and edge effects. Confirmatory evidence for this includes ⁶⁰:

- (1) The separation of the montmorillonite layers in contact with a definite pressure of water vapour depends on the cation present.
- (2) If a montmorillonite is saturated with an inorganic cation and dried, the resulting inter-layer separation varies with the cation, and is larger for the cations of larger radius.
- (3) Montmorillonites can be saturated with large organic cations (including proteins), giving large inter-layer separations.

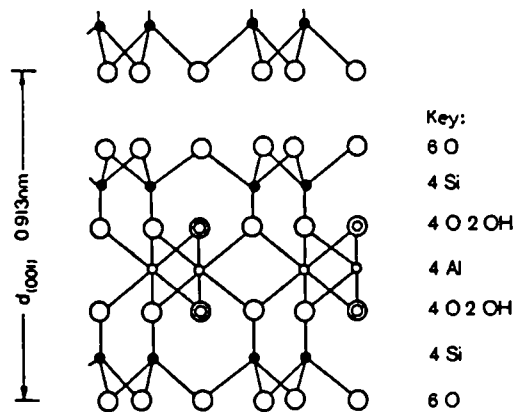


Figure 2.21
The pyrophyllite layer structure viewed along the a-axis.
The basal spacing and layer composition are also indicated ⁶⁶

In the kaolin minerals, the oxygen and hydroxyl valencies at the planar structure are completely satisfied. At the edges, however, there are aluminium, silicon, oxygen and hydroxyl ions that are not satisfied, because the lattice is capable of infinite extension in the *ab* plane. These unsatisfied valencies, or “broken bonds” as they are often called, are satisfied by external ions that do not form part of the structure, but merely act as counter-ions.

The cations are capable of being exchanged for other ions and are one possible cause of cation exchange. In the tetrahedral sheet, tetravalent *Si* is sometimes partly replaced by trivalent *Al*. In the octahedral sheet, there may be replacement of trivalent *Al* by divalent *Mg* without complete filling of the third vacant octahedral position; *Fe*, *Cr*, *Zn*, *Li* and other atoms may also replace *Al* atoms. The small size of these atoms permits them to take the place of the small *Si* and *Al* atoms; therefore the replacement is often referred to as isomorphous substitution ⁴⁶. This isomorphous substitution results in charge deficiencies in the layer lattice. Because this substitution occurs in the

octahedral layer, the resulting positive charge deficiency is relatively delocalised with respect to the inter-lamellar plane. To state categorically that isomorphous substitution in the montmorillonites concerns only the octahedral layer would be misleading. Some tetrahedral replacement does occur, but for most minerals within this class the observed exchange capacity correlates closely with the degree of octahedral substitution ⁶¹.

Cation exchange in the montmorillonites is probably principally due to the external cations balancing the lattice substitutions ⁴⁷. Although the cations may affect some kind of inter-layer bonding they are nevertheless readily exchanged by means of simple reversible diffusion between external solution and inter-lamellar sites. In the disordered kalonites, additional balancing cations are present because of the lattice substitutions, and these additional cations probably account for the greater part of the cation exchange that occurs ⁴². In the stack of layers which form a montmorillonite particle, the exchangeable cations are located on each side of each layer in the stack; hence they are present not only on external surfaces of the particle but also in between the layers ⁴⁶. Their presence causes a slight increase of the basal spacing compared with that of pyrophyllite or slightly higher when the compensating cations are larger. The difference between the basal spacing of pyrophyllite and that of montmorillonite is much less than the diameter of the compensating cations. Apparently these cations are partly sunk in the holes of the tetrahedral sheet.

For any given clay, the maximum amount of any cation that can be taken up is constant and is known as the cation exchange capacity, and has units of milli-equivalents per 100g. In principle, the cation exchange capacity is determined by leaching the clay with a chosen electrolyte, so as to replace all the existing cations with one particular cation. The clay is then filtered, washed free of excess electrolyte (with alcohol rather than water, to avoid hydrolysis) and the amount of chosen cation determined ⁶²⁻⁶⁴. Values for exchange capacity obtained with different monovalent cations agree reasonably. But when comparing monovalent with polyvalent cations discrepancies are found. These have been ascribed to the formation of complex ions of the type — M-OH by polyvalent ions ⁴². It is considered that a monovalent $[Ca - OH]^+$ ion could be attached to every exchange site. So consequent calculation as Ca^{2+} rather than $Ca - OH$, would result in the apparent cation exchange capacity being twice the normal value.

For montmorillonite to have the high exchange capacity (70-150 me/100g) and to explain its peculiar hydration properties, requires a relatively low amount of isomorphous substitution in the basic pyrophyllite, as the stacking of successive layers in montmorillonite is more or less random ⁶⁶. Montmorillonite always differs from the theoretical formula; in fact an infinite variety of substitutions is theoretically possible ⁴⁵ within the lattice of aluminium and possibly phosphorous for silicon in the tetrahedral co-ordination and/or magnesium, iron, zinc, nickel, lithium, etc., for aluminium in the octahedral sheet. Although some internal compensating substitution may occur, the final result of isomorphous replacement in the structure is a layer that carries a permanent negative charge. This positive charge deficiency is balanced by sorption of exchangeable cations which, apart from those associated with external crystal surfaces, are situated between the randomly superposed layers within a crystal ⁵⁷. Another way in which montmorillonite always differs from its theoretical formula, is that the lattice is always unbalanced by these substitutions ⁴³.

2.4.4

Clay Fillers

The efficiency of clay to modify the properties of a polymer is primarily determined by its degree of dispersion in the polymer matrix ³⁶. With the dispersion being dependent on the clay particle size and the hydrophilic nature of the clay surface. The hydrophilic surface nature of the clay layers impedes its homogeneous dispersion in the organic phase. Hence there is need to modify the surface of the clay to render it hydrophobic and/or organophilic prior to blending or compounding with the polymer. Commercially available mineral-filled polyamides, for example polyamides filled with organo-titanium kaolinites have shown significant reductions in water uptake. When a pendent amine group is introduced into the organic coating, the filler becomes even more compatible with the polymer matrix, thus giving improved dimensional stability in situations where there are large fluctuations in relative humidity. Since these materials also have improved tensile and flexural properties, they have proved very useful in the manufacture of such objects as carburettor bodies, fan blades and skate boards ⁶⁵.

Mineral and organic components must form a bond or complex if their union is to have more than a transitory existence. Dissolving a polymer in a suitable solvent and its subsequent addition to dry clay or to clay suspension, involves the adsorption of the organic phase onto the inorganic particles surface with or without the participation of inter-particle bonding. Introducing the polymer in the form of an emulsion, a solid or a melt that is insoluble in the continuous phase results in the principal mode of attachment being adhesion, although this process may be regarded as an extension or amplification of adsorption. Physical (van der Waals) attraction plays a prominent part in the adhesion of the organic to the inorganic, although chemical interactions and bridging of the filler surface are also involved. The prior adsorption of a suitable organic substance over the particles' surfaces or by the covalent addition of simple organics (alcohols, organosilanes, etc.) to the reactive surface groups of the mineral ⁶⁶ may substantially increase the compatibility of the mineral with the organic phase, in terms of wetting and dispersion. Alternatively, polymers may be grafted onto hydroxy groups on the clay surface through coupling agents that contain two reactive groups, one suitable for reaction with the polymer and the other capable of reacting with the clay ³⁶. However, such surface modification processes do not lead to penetration of the polymers between the inter-layers of the clay, which may not be homogeneously dispersed.

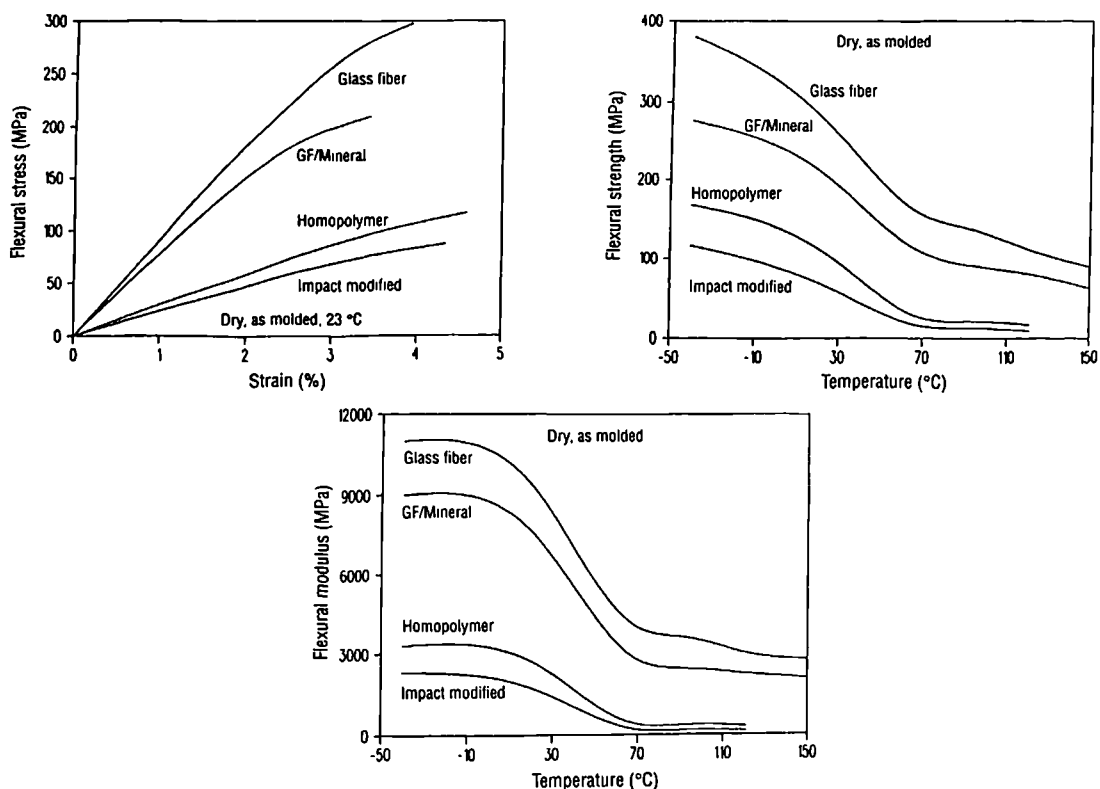


Figure 2.22

Mechanical property effects of fillers on polyamide-6 ⁶

2.5

Nanocomposites

In recent years, organic-inorganic nanometre composites have attracted great interest, since they frequently exhibit unexpected hybrid properties synergistically derived from two components ⁶⁷. There are many organic-inorganic hybrid biomineral materials such as shells, teeth and bones, etc. ⁶⁸.

One proposed method to prepare artificial-inorganic hybrid materials is the sol-gel route, using metal alkoxides and organic molecules ⁶⁹. In this method the inorganic phase is formed by the hydrolysis and condensation of metal oxide precursors while the organic matrix is simultaneously polymerised. By controlling process kinetics, the organic compound becomes intimately associated with the inorganic component ⁷⁰. The size of inorganic building blocks is controllable and the interfacial properties can be improved by introducing covalent bonding between organic and inorganic phases. However, the sol-gel approach is limited by evolution of volatile by-products and shrinkage, when moulded at elevated temperature ⁷¹.

Another method is the intercalation reaction of clay minerals ^{68, 165}. This composite system is based on nano-scale hybrids of organic polymers and inorganic clay minerals ⁶⁷. In these hybrids, negatively charged silicate (clay) minerals and positively charged polymer-ends, are directly ionically bonded. Layered silicates are good candidates for the formation of organic-inorganic nanocomposites due to the chemically stable siloxane surfaces and high surface area, and also owing to the high aspect ratio and high strength ⁹⁴. The clay-organic intercalation refers to the reversible insertion of molecules or compounds (guests) into a layered material (host) without destroying the host ⁷². These compounds can be grouped into two main types ⁶⁸:

- (1) Those that are formed by ion exchange of inter-layer exchangeable cations.
- (2) Those that are formed by absorption of polar organic compounds.

With the synthesis either involving intercalation of a suitable monomer and subsequent polymerisation, or polymer intercalation from solution ⁷³; in both cases the nano-sized organically treated clays, indirectly interact with polymers.

Another hybrid plastic is based on Polyhedral Oligomeric Silsesquioxanes (POSS) ¹⁵⁶; in which the nanostructured chemical molecules directly interact and bond with polymers. They are termed hybrid as a result of their combined inorganic and organic nature and can be viewed as discrete, chemically modified particles of silica having dimensions at the nanometre scale. However, unlike silica or modified clays, each POSS molecule contains covalently bonded reactive functionalities suitable for polymerisation or grafting POSS monomers to polymer chains. Each POSS molecule contains non-reactive organic functionalities for solubility and compatibility of the POSS segments with the various polymer systems.

2.5.1

Nanocomposite Structure

Nanocomposites are a class of mineral filled material ⁷⁴, comprising a polymer matrix containing a uniform dispersion of silicate layers, in the order of molecules within the polymer matrix ⁷⁵. This nano-scale dispersion of the inorganic component typically optimises the mechanical properties of the composite ⁷⁶. As a result of the “nano”-sized dispersion, reinforcement efficiency is realised at low loading levels (3-5%) ⁷⁷, at a small cost in terms of specific gravity and loss of impact strength. The term “Nanocomposite” is used to refer to composites of more than one Gibbsian solid phase where at least one dimension is in the nanometer range 1-20nm ⁵². The solid phases can be amorphous, semi-crystalline, crystalline or combinations thereof. They can be inorganic or organic, or both, and essentially of any composition.

Polymer matrix nanocomposites typically have lateral dimensions ranging between 1-10nm. Owing to these ultra-fine phase dimensions, new and improved properties are exhibited compared to their pure polymer constituent or micro- and macrocomposite counterparts ^{98,78,167}, their properties are potentially superior to fibre reinforced

polymers ¹³⁰. Due to the layer orientation, polymer-silicate nanocomposites exhibit stiffness, strength and dimensional stability in two dimensions ⁹³. As well as increased flame retardancy ¹⁶⁶.

However there are disadvantages with this processing technique. The polymer resin may be moisture sensitive, e.g. polyamide, and thus prone to decreased dimensional stability ⁸⁴. The polymer chains synthesised in the inter-layer space, may not infiltrate sufficiently into the clay mineral, consequently the silicate layers will not be uniformly dispersed in the organic polymer, resulting in a lack of homogeneity ⁸⁵. For uniform dispersion it is necessary to reduce the aspect ratio, and this adversely affects the mechanical strength of the composite ⁸⁴. The critical issue for making nanocomposites with a homogeneous dispersion of the involved phases lies in an understanding of the surface/interface chemistry ⁸⁶. Successful compounding of a nanocomposite material requires that the starting materials must be broken down into nano-particles and dispersed. Insufficient bonding between the inorganic polymer and the organic matrix could result in a brittle composite ⁷⁵.

In general, polymer-clay composites can be divided into three categories: conventional composites, intercalated nanocomposites and exfoliated nanocomposites ^{80,92,105,106}. In a conventional composite, the clay tactoids exist in their original aggregated state with no intercalation of the polymer matrix into the clay. Insertion of polymer into the clay structure occurs in a crystallographically regular fashion within an intercalated nanocomposite, regardless of the clay-to-polymer ratio. In a delaminated (exfoliated) nanocomposite the silicate layers are exfoliated and uniformly dispersed in a continuous polymer matrix; although this system is less ordered than the intercalated structure.

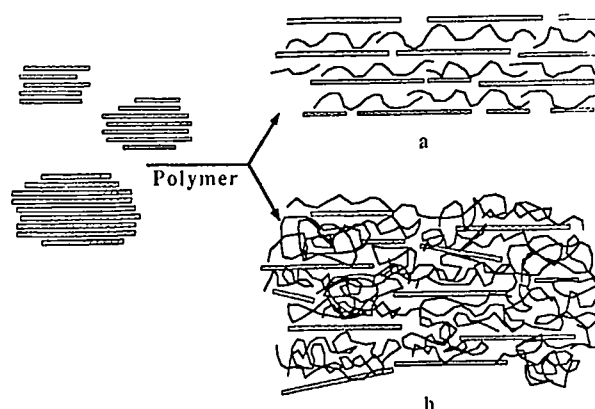


Figure 2.23

*Schematic of composite structures obtained using layered silicates (Indicated by rectangular bars)
(a) intercalated hybrids, (b) delaminated hybrids*⁹³

Intercalation refers to a composite in which a single extended polymer chain is inserted between the host layers resulting in a well-ordered multi-layer structure, with alternating polymer/inorganic host layers and a repeat distance of a few nanometers. In contrast, in an exfoliated nanocomposite the individual 100nm thick clay layers are separated in a continuous polymer matrix by average distances that depend on loading. Usually, the clay content of exfoliated clay composites is much lower than that of an intercalated nanocomposite. Consequently, an exfoliated nanocomposite has a monolithic structure with properties related primarily to those of the starting polymer. In the delaminated structure, silicate layers (1nm) thick are exfoliated and dispersed in a continuous polymer matrix. Layer exfoliation maximises interfacial contact between the organic and inorganic phases⁹⁴. Consequently delaminated nanocomposites offer measurable improvement in a variety of physical properties⁹⁵, and can attain degrees of stiffness, strength and barrier properties with far less ceramic content than are used in conventionally filled polymer composites⁹⁶. The tensile properties improve with increasing degree of exfoliation of the nano-layers⁹⁷; in general the higher the degree of delamination in polymer-clay nanocomposites, the greater the enhancement of these properties. Exfoliated nanocomposites show greater phases homogeneity than intercalated nanocomposites, this structural distinction is the primary reason the exfoliated state is effective in improving the performance properties of clay composite materials. Intercalated versions offer reduced flammability benefits, but with less improvement in physical properties⁹⁵.

A third type of nanocomposite structure is possible, although it is not as well documented as the intercalated and delaminated structures. This type of structure is referred to as end-tethered, and two types have been produced ⁸³:

- (1) End of the polymer attached to the outside of the silicate sheet.
- (2) End of the polymer attached to an exfoliated layer of the silicate.

The second type is similar to a delaminated structure with polymer surrounding exfoliated layers of silicate.



Figure 2.24
Possible structure of end-tethered ⁸³

Although at present there is no agreement as to the preferred structure and it is also probable that more than one type of structure will be present within a composite system. Hybrid formation is dependent on a number of factors, including optimal interlayer structure for the organically modified layered silicate, with respect to the number per host area and size of the alkylammonium chains ¹⁰; the presence of polar interactions between the modified silicate and the polymer. The interlayer structure of the silicate should be optimised to maximise the configurational freedom of the functionalising chains upon layer separation, while maximising potential surface interaction sites.

Various polymer-clay hybrids have been reported for a range of polymers, with varying degrees of polarity and crystallinity ⁹⁸, such as: poly(vinyl alcohol) ⁹⁹, high density polyethylene ¹⁰⁰, poly(ϵ -caprolactone) ¹⁰¹, polyimide, epoxy resin ¹⁰², polystyrene, acryl-amide ¹⁰³, acrylic polymer ¹⁰⁴, etc. The synthesis method is general and broadly applicable to a range of commodity polymers, from essentially nonpolar polymers to strongly polar polymers. Nanocomposites can be produced using currently available techniques such as extrusion, lowering the barrier to commercialisation ¹⁰⁵; and are adaptable to thin transparent films ¹⁰⁶, fibres and monoliths ¹⁰⁸.

2.5.2

Nanocomposite Production

Methods for the incorporation of layered silicates into a polymer can be divided as follows: by addition of a modified silicate either during the polymerisation, or to a solvent-swollen polymer or to the polymer melt. Another method has been developed to prepare the layered-silicate by polymerising silicate precursors in the presence of a polymer.

Polyamide clay hybrids are molecular composites comprising a polyamide-6 resin containing uniformly dispersed silicate layers of montmorillonite ^{81,107}. These are ionically bonded and uniformly mixed with each other. Layer silicates with a single layers thickness of about 1nm, are held together by exchangeable cations. During cation exchange, layer silicates can be swollen or completely defoliated by replacing the inorganic cations e.g. Na^+ , K^+ or Ca^{2+} with organic cations, preferably $R-NH_3^+$ groups ¹⁰⁸. These composite materials are produced via three stages ⁸⁴: contacting, mixing and polymerisation. In the contacting step, the clay mineral is brought into contact with a swelling agent in a dispersion medium such as water. This complex is dried to remove the dispersion medium and pulverised, after which it is mixed with a monomer in the mixing step. The resulting mixture is then heated to polymerise the monomer in the mixture; hence the layered-silicate is ultimately dispersed in the polyamide resin.

Synthesis of polyamide-6 silicate nanocomposites is carried out by the ring opening polymerisation of the ϵ -caprolactam, in the presence of cation-exchanged montmorillonite ¹⁰⁷. Natural sodium-montmorillonite is hydrophilic and therefore not compatible with most organic molecules, however it may be converted from the hydrophilic to the organophilic state, by simply exposing the parent water-rich intercalate (when the interlamellar sodium cation is hydrated) to an appropriate organic reagents ¹⁰⁹. Yielding an organophilic montmorillonite ⁶⁸, capable of intercalating organic molecules between adjacent planar silicates ¹¹⁰. In contrast to pristine silicates, organically modified silicates contain alkylammonium cations ¹¹¹. As a negative charge occurs in the silicate layer, the cation head group of the alkylammonium

molecule will preferentially reside at the layer surface and the aliphatic tail will radiate away from the surface. The presence of these aliphatic chains in the silicate layers renders the originally hydrophilic silicate organophilic ¹¹². The role of alkylammonium cations in the organosilicates is to lower the surface energy of the inorganic host and improve the wetting characteristics of the polymer. Additionally the alkylammonium cations can provide functional groups that can react with the polymer or initiate polymerisation of monomer to improve the strength of the interface between the inorganic phase and the polymer ¹⁰⁵.

Depending upon the precise chemical nature of the cation, a variety of polymers, both polar and nonpolar, can be intercalated into the inter-layer region ⁸². Infra-red spectroscopy provides compelling evidence that adsorbed polar organics, at least short-chain compounds, interact with the exchangeable cations rather than with the silicate surface. Uncharged organic molecules, like those of water, are evidently either directly co-ordinated to the cation, or indirectly linked to the cation by means of (bridging) water molecules. What is important to appreciate here is that polar organic compounds must successfully compete with water for essentially the same ligand positions or sites around the exchangeable cation, for the adsorption process is largely dependent on the polarising power of the cation ⁵⁷.

It has been found that montmorillonite can be cation exchanged for 12-aminolauric acid (12-aminododecanoic)⁷⁹. The protonated amino-acid derivative promotes delamination/dispersion of the host layers ⁷⁷. The ability to delaminate and disperse the layered silicate in a medium is related to a number of factors, including the cation exchange capacity of the silicate, the polarity of the medium and the chemical nature of the inter-layer cations. The length of the silicate layers also has an effect on the modulus and heat distortion temperature of the nanocomposite ⁷⁵. Increasing the spacing between the layers allows the insertion and ionic attachment of an organic molecule. This molecule permits the platelet to react with functional groups within the polymer.

Caprolactam can be polymerised in the inter-layers of montmorillonite during polymerisation or compounding. The carboxyl end groups of the 12-aminolauric acid, contained within the 12-montmorillonite, initiate polymerisation of ϵ -caprolactam ⁷⁹. The —COOH group catalyses the ring opening polymerisation; this is the reason for choosing ammonium cations of ω -amino acids ⁶⁸. During heating of this mixture, the organic acid group initiates ring-opening polymerisation of the heterocyclic monomer by nucleophilic attack on the ϵ -caprolactone carbonyl. The consequence of this reaction is that the resulting poly(ϵ -caprolactam) is ionically bound to the silicate layers through the protonated amine terminus of the polymer chains ⁷⁷.

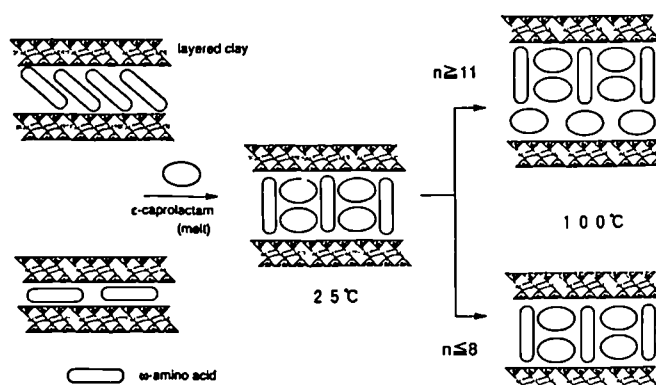


Figure 2.25

Schematic diagram of intercalation of ϵ -caprolactam ⁶⁸

This intercalation is accompanied by displacement of water molecules, dispersed between the clay platelets, by polymer molecules. The polymers will be sorbed between the layers spacing, thereby substantially increasing the inter-layer spacing between adjacent silicate layers. The treated intercalated phyllosilicates, can then be exfoliated by sorption of polymers that have carbonyl, hydroxyl, amine, amide and/or ether functionalities or aromatic rings. This provides metal cation chelate-type bonding between two functional groups of one or two intercalant polymer molecules and the metal cations bonded to the inner surfaces of the phyllosilicate platelets. In principle, such intercalated phyllosilicates can easily be exfoliated into individual phyllosilicate platelets before or during mixing with a thermoplastic or thermosetting matrix polymer composite material. The driving force for this swelling is concluded to be a combination of the polymerisation energy of ϵ -caprolactam and the attractive force between the ϵ -caprolactam and interlayer cation ¹¹³.

2.5.3

Nanocomposite Properties

These composites generally possess high mechanical strength ^{78,157,162} and excellent heat distortion resistance ⁷⁹, as well as self-extinguishing characteristics ^{130,134,135}. The thermal and rheological properties are likewise improved significantly by nanocomposite formation ⁸⁰. Outstanding diffusion barrier properties are exhibited without requiring a multi-polymer layered design, thus allowing for recycling ¹³⁰. The nano-size of the filler is much lower than the wavelength of visible light, therefore the particles do not scatter light and the filled sample should retain transparency ^{29,81}. Other attributes include increased solvent resistance ⁷⁷, reduced gas permeability, enhanced ionic conductivity and increased swelling resistance ⁸². Montmorillonite, at an addition level of 6.5 wt%, has also been shown to serve as a screen to block the penetration of UV light into nanocomposites, and therefore improves weatherability ⁷⁸.

The overall properties of nanocomposite are determined by the parent composition ⁹⁷, the composite phase morphology ¹⁰⁶ and depend greatly on the distribution, arrangement and interfacial bonding between the silicate layers and the polymer ⁷⁷. Their unusual properties profile is due to a combination of factors: the highly anisotropic platelet structure of montmorillonite clay, the high aspect ratio (≈ 100 -1000) of the platelets ⁸³, and the molecular bonds formed between the platelets and the polymer during compounding ⁷⁴. Fillers having a particle size in the nanometer range have an extremely large surface per unit volume and may have considerably stronger interaction with the matrix ²⁹.

Nanocomposites demonstrate a significant increase in thermal stability ¹¹⁴, with the heat distortion temperature increasing from 65°C to 152°C. The fire retardant properties improve ¹¹⁵, with the cone calorimeter data showing that the peak heat release rate, the most important parameter for predicting fire hazard, was reduced by 63% in a polyamide-6 clay-nanocomposite containing a clay mass fraction of only 5% ¹¹⁵. The mechanism for the fire retardancy of these composites is considered to be due to the structure of the char formed during combustion, which enables the char to thermally insulate the polymer and inhibit the formation and escape of volatiles ⁸⁷.

This increased fire resistance is not achieved at the expense of compromising other physical properties ¹¹⁶, the mechanical properties displayed improvements compared with pure polyamide-6 ¹¹⁷. With the nanocomposite exhibiting 40% higher tensile strength, 68% greater tensile modulus, 60% higher flexural strength, 126% increased flexural modulus and comparable impact strength.

Properties	Composite Type			
	Temp.	Nanocomposite (Exfoliated)	Microcomposite (Tactoids)	Polyamide-6
wt % Clay	A 23°C	4.2	5.0	0
	B 23°C	4.7	-	0
	B 120°C	4.7	-	0
Tensile Strength (MPa)	A 23°C	107	61	69
	B 23°C	97	-	69
	B 120°C	32	-	27
Tensile Modulus (GPa)	A 23°C	2.1	1.0	1.1
	B 23°C	1.9	-	1.1
	B 120°C	0.6	-	0.2
Flexural Strength (MPa)	B 23°C	143	-	89
	B 120°C	34	-	13
Flexural Modulus (GPa)	B 23°C	4.3	-	1.9
	B 120°C	1.2	-	0.3
Charpy Impact Strength (kJ/M ₂)	A 23°C	2.8	2.2	2.3
	B 23°C	6.1	-	6.2
HDT (°C @ 18.5 kg/cm ²)	A	145	89	65
	B	152	-	65

Table 2.2

Mechanical and thermal properties of polyamide-6 composites, A ¹³² & B ⁷⁹

As can be seen from the table the reported results are relatively consistent, with the biggest discrepancies being between the impact results. However the very nature of this test is dependent on the largest flaw within the material, so caution should be taken in interpretation of this particular difference. In general an improvement in properties is observed between the nanocomposite and the polyamide-6. The difference between the properties of the polyamide-6 and the microcomposite are negligible. Inferring that the exfoliation of the clay leads to improved physical properties.

2.5.4

Nanocomposite Characterisation

Methods have been described for quantitative infrared spectrophotometric techniques that can be used to determine free caprolactam in polyamide-6 ^{97,131}. However, these methods proved lengthy and time consuming ¹³⁸, owing to the extraction of the aqueous concentrate with carbon tetrachloride prior to infrared spectrophotometric determination. A more rapid method based on gas chromatography for the determination of residual caprolactam has been proposed ¹³³. This method uses an internal standard for calibration and measurement of the elutant. For accurate determination of the residual monomer content in this study, a modified gas chromatography technique can be used which involves only distilled water as the internal standard ¹³⁸.

The most commonly used technique for the structural characterisation of nanocomposites is X-Ray Diffraction ⁶⁷. This technique allows for characterisation of the polyamide crystal structure. It also provides a primary indication as to whether intercalation or delamination has occurred; both these processes changes the dimensions of the gaps between the silicate layers, so an increase in layer distance suggests that a nanocomposite has formed. Reflection in the low angle region indicates the *d*-spacing (basal spacing) of ordered intercalated and ordered delaminated nanocomposites, disordered delaminated nanocomposites show no peaks in this region due to the loss of structural registry and the fact that the *d*-spacing typically exceeds 10nm ¹³⁴. This initial indication, however, needs to be confirmed with a technique such as

Transmission Electron Microscopy ^{67,93}. When a nanocomposite has formed the intersections of the silicate sheets may be observed as dark lines on the micrograph.

Differential Scanning Calorimetry has been used to ascertain the latent heat of fusion and the melting point of nanocomposites; dynamic viscoelastic properties have been measured to calculate the storage modulus and loss modulus ⁷⁹. Mechanical properties are also of interest namely: tensile, flexural, Charpy impact and Izod impact properties. All tested in accordance with the relevant ASTM standard. Other experimental techniques of interest are those which demonstrate the improved thermal stability of nanocomposites ¹³⁵.

2.6

Polymer Processing

Chemical and physical processes are attracting increasing attention from plastics processors ¹¹⁸. There are two main reasons for this: firstly more and more processors are recognising that the quality of their products is highly dependant upon physical processes (cooling, temperature control, blending, etc.), and secondly that new physical and chemical treatment methods of are being developed, which bring improvements in quality and hence, virtually inevitably, greater profitability in production. Melt compounding is a convenient, economical and familiar process for the production of inter-chain copolymer ¹¹⁹. But it is not the only commercially viable process available. In order to reduce production times and thus costs, the trend is moving towards in-situ processing; whereby the final shape and molecular structure are achieved simultaneously ¹²⁰.

2.6.1

Mixing

In polymer processing, mixing significantly affects materials properties, as intimate mixing at a microscopic level implies better dispersion within the system, thus affecting the processability and hence cost. Mixing can be defined as a process to reduce the non-uniformity of a composition, resulting in a reduction of the concentration gradients or temperature gradients. Two distinct phenomena are involved, dispersion and blending. The basic mechanism of mixing is to induce physical motion of the ingredients ¹²¹.

2.6.2

Extrusion

Mixing in polymer processing is often performed in a continuous mode, such as extrusion. To extrude means to push or force out, material is extruded when it is pushed through an opening ¹²². In a typical extrusion operation the materials to be processed are fed through a hopper into the heated barrel, through which a screw mechanism forces heated thermoplastic through a die opening to produce solid shapes, film, etc.¹²³. Different models of extruders are used in the plastics processing industry, primarily as continuous machines for the compounding and processing of plastics ¹²⁴. The main distinction between the various extruders is their mode of operation: continuous or discontinuous. The latter type extruder delivers polymer in an intermittent fashion and, therefore, is ideally suited for batch type processes, such as injection moulding.

2.6.3

Reaction Extruded System

Reaction extruded system, also termed reactive processing or reactive compounding, refers to the performance of chemical reactions during extrusion processing of polymers through mixing in an extruder ¹²⁵. In this case the extrusion device used is also a

chemical reactor instead of only a processing aid. In this process liquids or low melting point monomers are rapidly converted into polymers, preferentially by an addition process. The extruder may be considered to be a horizontal reactor with one or two internal screws for conveying the reactant polymer or monomer ¹²³.

Polymer processes, which may be candidates for continuous reactions in an extruder, can be classified primarily by their energy and residence time requirements, along with the nature of the starting feeds and of the end products. This system is applicable to a wide range of temperatures and provides excellent dispersive and distributive mixing. The ease of melt feed preparation lends itself to continuous processing. Hence a key advantage of an extrusion device as a reactor is the combination of several chemical process operations into one piece of equipment with accompanying high space-time yields of product ¹²⁵.

Melt phase chemical reactions carried out in the extruder configuration have been studied and used commercially for many years. Other techniques are available in order to produce intimately mixed composites, for example methods such as compatibilisation, dynamic vulcanisation, reactive extrusion, etc. These have been proposed with a view towards enhancing the manner in which resin composites may be blended with one another so as to achieve desired property modifications ¹²⁶. The extruders which are available for continuous reactive extrusion processes differ in the features employed to bring about the desired processes ends, this ability to manipulate their format enables the technique to be adapted to each individual reaction. This is in contrast to solution reactions where the same stirred tank reactor can be used for a wide range of chemistries. The reasons for this difference lie in the comparative advantages and limitations of the extruder as a chemical reactor ¹²⁷. The limitations of this technique to broader applications of extruder processing are attributed to the difficulty in handling large heats of reaction and the high costs incurred due to long reaction times.

2.6.4

Reaction Polymerisation

Polymerisation of ϵ -caprolactam in the presence of alkaline catalysts can yield a high molecular weight polymer in a few minutes, whereas preparation by hydrolytic polymerisation may require a reaction period of several hours. The combined reactive polymerisation of ϵ -caprolactam together with the forming of the resulting polyamide-6 into a semi-finished product has obvious economic and technical benefits. The relatively low melting point of caprolactam, combined with the fact that when molten it is a very powerful solvent, enables the reaction polymerisation of polyamide-6 to be conducted in extruders and reaction injection moulding machines. In fact the polymerisation time at 150°C, has been shown to be less than 90 seconds ¹²⁸, using an appropriate catalyst and activator system together with optimised screw profile and operating conditions. The benefits of the anionic polymerisation route are the rapid rate at which the reaction will occur and the high molecular weights that can be achieved ¹⁶³. Processes for producing polyamides by continuous activated anionic polymerisation have been patented ¹²⁹.

The use of co-rotating, tightly intermeshing twin-screw extruders for high-speed polymerisation makes it necessary to consider a few requirements that this type of polymerisation places on the equipment and the process ¹¹⁸. The extruder must be capable of transporting and discharging the fluid caprolactam melt and the polymerisation polyamide melt which has a viscosity of an order of magnitude higher.

During melting of the monomer and its ingredients, all components must be thoroughly mixed to prevent sporadic starting of the reaction that would lead to a non-uniform end product. At the same time, the material must be brought to the reaction temperature as fast as possible to prevent premature oxidative degradation of the additives. During the course of polymerisation, the material may be subjected to only low stresses. This will prevent the occurrence of mechanical and thermal stresses, which would lead to low molecular weight products. Accurate zone temperature programming adapted to the course of the reaction requires good heat separation between individual barrel zones. To prevent residual monomers from causing foaming of the melt discharge, unreacted

caprolactam must be removed by degassing; this can cause major problems. Because of the high molecular weight, the melt in the extruder will be heated above the boiling point of caprolactam.

In the reaction polymerisation of polyamide-6, caprolactam is converted to the polymer. Two components aid this process: a catalyst and an activator. One component is a solution of the catalyst in caprolactam; the catalyst for the polymerisation tends to be a caprolactamate anion. However, as the selection of catalysts is critical a combination of catalysts may be used in order to achieve the reaction rates required. As an activator or co-catalyst acylated lactams, reaction products of diisocyanates with caprolactam and reaction products of isocyanate terminated prepolymers with caprolactam are used. Such components can provide short reaction times which make it possible to polymerise the lactam with out unduly long polymerisation times. The catalyst and activator are each incorporated into separate streams to give the required reaction control.

After a short induction time, the anionic polymerisation proceeds rapidly at a reaction temperature of approximately 200°C; and is therefore ideally suited to continuous processing in an extruder, where the residence time may be in the order of minutes, and the thermal homogeneity of the reactants can be closely controlled ¹²⁷. The molecular weights obtained by this method are generally higher than in commercial polyamide-6 materials formed by hydrolytic polymerisation, with both the molecular mass and the residual monomer level being strongly influenced the by screw speed. Superior impact and elongational properties are exhibited, but lower tensile strength and flexural modulus properties are observed. It is probable that these differences in mechanical behaviour arise from the variations in the molecular weight and the crystallinity associated with the different synthesis processes. The mechanical properties of polyamide-6 are very sensitive to the reactive processing conditions employed, including: materials formulation, extruder screw profile, temperature and screw speed (different screw speeds yield different molecular weights, molecular weight distribution and residual monomer content) ¹²⁸.

CHAPTER THREE

EXPERIMENTAL METHODS AND TECHNIQUES

3.1

Introduction

The materials and experimental methods used in the production and formulation of the cast and extrusion systems are detailed, together with experimental methods used in the production and formulation of the polyamide-6. Polyamide-6 nanocomposites were synthesised using reactive casting techniques and using reactive extrusion techniques, involving the anionic polymerisation of ϵ -caprolactam in the presence and absence of modified clay. The polymerisation conditions, residual monomer content and the nature of the structure produced are discussed with respect to subsequent variations in the processing methodology.

3.2

Material Formulations

The origin of materials used in this study are given in Appendix 1. Table 3.1 details the compositions of various cast systems. This list is not exclusive, as many other mixtures were trialed at varying temperatures and compositions, but only those that yielded results of significance have been included. In the table (MG) refers to clay which was exchanged using the method as detailed by Messersmith et al ⁷⁷, (AU) refers to clay which was exchanged using the method as detailed by Usuki et al ¹⁵³, and (U) refers to clay which was used in its as received, untreated state.

Name	Detail	Activator (%)	Catalyst (%)	Clay (%)	ϵ -Caprolactam (%)	Other (%)
C-PA6	Cast Polyamide-6 (Standard)	2	2	-	96	-
B-PA6	BASF Polyamide-6	-	-	-	-	100 Polyamide-6
C001	Cast sample 01	2	5	4 (AU)	89	-
C002	Cast sample 02	2	5	2 (MG)	90	1 Antifoam
C003	Cast sample 03	2	5	0	92	1 Antifoam
C004	Cast sample 04	1	3	1 (U)	95	-
C005	Cast sample 05	2	5	4 (U)	89	-
C006	Cast sample 06	1	3	1 (AU)	95	-
C007	Cast sample 07	2	5	0	93	-
C008	Cast sample 08	2	5	1 (AU)	92	-
C009	Cast sample 09	2	5	1 (AU)	92	Addition at ten minute intervals
C010	Cast sample 10	2	5	2 (AU)	91	Addition at ten minute intervals
C011	Cast sample 11	2	5	2 (AU)	91	Simultaneous addition
C020	Cast sample 20	1.4	1.7	2 Cloisite®25A	93.9	1 Antifoam
C021	Cast sample 21	1.4	1.7	2 Cloisite®30B	93.9	1 Antifoam
C022	Cast sample 22	1.4	1.7	2 Cloisite®15A	93.9	1 Antifoam
C024	Cast sample 24	4	2	4 (Montmorillonite)	90	-
C028	Cast sample 28	2	2	4 (Montmorillonite)	92	-
C029	Cast sample 29	2	2	2 (Montmorillonite)	94	-
C029IM	Cast Sample 29 (Injection Moulded)	2	2	2 (Montmorillonite)	94	-
NCH	Nylon Clay Hybrid	-	-	5 (Montmorillonite)	84	11 6-amino caproic acid
C-PA6	Cast Polyamide-6 (Standard)	2	2	-	96	-
B-PA6	BASF Polyamide-6	-	-	-	-	100 Polyamide-6

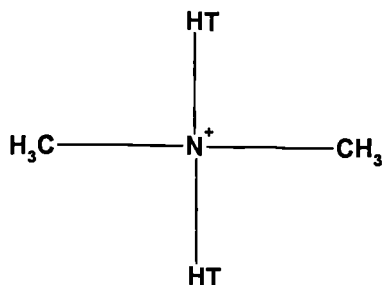
B-PA6(U)	BASF Polyamide 6 (Untreated)	-	-	4	96	-
B-PA6(T)	BASF Polyamide 6 (Treated)	-	-	4	96	-
J-PA6	Reactive Extruded Polyamide	3	4	-	93	-
J-PA6(U)	Reactive Extruded Polyamide (Untreated)	3	4	4	89	-
J-PA6(T)	Reactive Extruded Polyamide (Treated)	3	4	4	89	-
UBE	Ube	-	-	2	-	-

Key	
AR	As Received
CM	Compression Moulded
IM	Injection Moulded
(U)	Untreated
(T)	Treated
B	BASF Series
J	JAL Reaction Extruded Series
C	Cast Series

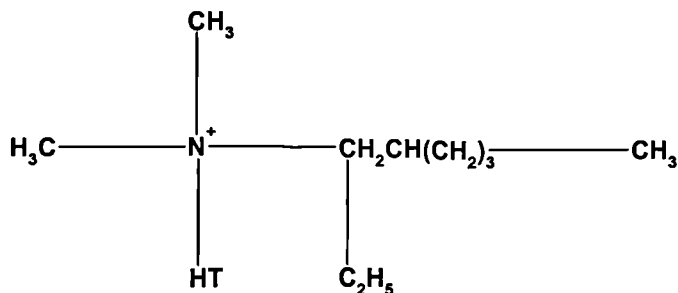
Table 3.1
Sample Classification Table

The structure of the organic chain used to modify the surface of the clay is detailed in Figure 3.1. Where HT = hydrogenated tallow ($\approx 65\%$ C18, $\approx 30\%$ C16, $\approx 5\%$ C14).

Cloisite®15A
(Dimethyl, dihydrogenated tallow, quaternary ammonium chloride)



Cloisite® 25A
(Dimethyl, hydrogenated tallow, 2-ethylhexyl, quaternary ammonium methylsulphate)



Cloisite® 30B
(Methyl, tallow, bis-2-hydroxyethyl, quaternary ammonium chloride)

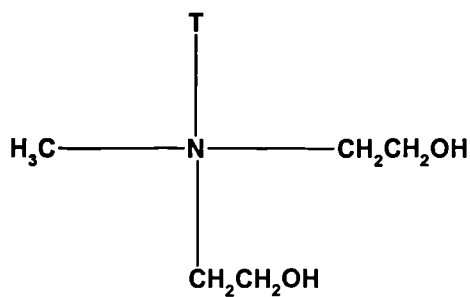


Figure 3.1
Structure of the Cloisite® clays

3.3

Cast System

A series of cast composites were formulated, using a variety of preparation techniques. Polyamide-6 was processed in the presence of both treated and untreated clay. All of these systems were compared with a control system containing only cast polyamide-6.

3.3.1

Preparation Of Nylon Clay Hybrids

Usuki describes the production of a polyamide-6 clay hybrid (NCH) ¹⁵³. This method of production essentially involves two stages: firstly the cation exchange of the montmorillonite clay, followed by the synthesis of the hybrid. This experiment was used as a starting point, so was closely replicated. The theory being that it would provide a worked example of a nanocomposite system with which new materials could be compared.

For the cation exchange of montmorillonite, 10g of montmorillonite was dispersed in 1000ml of hot water – the clay was added slowly in order to reduce agglomeration. The solution was mixed with a magnetic stirrer for approximately 15 minutes to ensure thorough dispersion. 200ml of water was heated to 80°C and to this was added 24mmol of 12-aminododecanoic acid and 2.4ml of concentrated hydrochloric acid. This hot solution was combined with the clay dispersion and stirred vigorously for approximately 30 minutes. The product, 12-montmorillonite, was filtered and washed three times with 1000ml of hot water. It was then dried in a vacuum oven at 90°C overnight.

For the synthesis of the NCH, 12-montmorillonite and ϵ -caprolactam were mixed using a pestle and mortar. The reaction vessel was a three-necked separable flask coupled with a mechanical stirrer and a nitrogen atmosphere. In this vessel were placed 509g of ϵ -caprolactam, 29.7g of 12-montmorillonite and 66g of 6-aminocaproic acid. The

reactants were heated using an oil bath on a hot plate, at 100°C for 30 minutes, followed by heating at 180-185°C for approximately 210 minutes, to polymerise the ϵ -caprolactam using 12-montmorillonite and the 6-aminocaproic acid – added to expedite ring opening.

After this ensued the products were mechanically crushed and washed with 2000ml of water at 80°C. Subsequently they were centrifuged and dried in an oven at 80°C.

3.3.2

Preparation Of Composites Using Brabender Apparatus

A Brabender Plasti-corder PLE 330 was used for composite preparation by reaction blending of ϵ -caprolactam and a specific catalyst and activator system. The combination of catalyst and activator were selected on the basis that they had previously been industrially proven to be effective. This processing technique was used, as it would enable small batches of reactively cast materials to be produced in the presence and absence of clay.

Weighed samples were placed in a plastic bag and blended to evenly disperse the contents. To 250g of ϵ -caprolactam 1.4wt% catalyst and 1.7wt% activator were added. If clay was to be included in the formulation 4wt% was used. The temperatures used ranged between 125-155°C.

Samples were withdrawn from the reservoir at 5 minute intervals for a total of 20 minutes, in order to permit analysis. Initial samples quality was highly variable; hence the apparatus was modified to incorporate a nitrogen blanket in order to reduce the effects of atmospheric moisture.

3.3.3

Preparation of Nanocomposites Using Casting Techniques

The treatment of the clay was refined to include the procedure described in Mather's paper ¹⁵⁵, followed by the Usuki treatment. Thus forming the procedure for the cation exchange of clays. The system of test pours was taken from the standard "Process Scheme for Screening Tests", courtesy of Nylacast Ltd. Upon successful completion of the small-scale test pours, a factory trial was then carried out.

Two methods of exchanging the montmorillonite clays were used. The first method was clay that was exchanged using the method as detailed in the Usuki et al paper ¹⁵³, and referred to as (AU). The second method, referred to as (MG), was exchanged using the method as detailed in the Mesersmith et al Paper ¹⁵⁴.

For the (AU) method the clay was first treated with cold dilute hydrochloric acid to dissolve free carbonates, and then was then leached with 500ml *N* sodium chloride solution, for about an hour, to replace the exchangeable ions. After which time it was filtered and washed, followed by drying at 90°C.

This clay was then cation exchanged. 10g of montmorillonite were dispersed in 1000ml of hot water – the clay was added slowly in order to reduce agglomeration. The solution was stirred with a magnetic stirrer for approximately 15 minutes to ensure thorough dispersion. 200ml of water was heated to 80°C and to this was added 24 mmol of 12-aminododecanoic acid and 2.4ml of concentrated hydrochloric acid. This hot solution was combined with the clay dispersion and stirred vigorously for approximately 30 minutes. The product, 12-montmorillonite, was filtrated and washed three times with 1000ml of hot water. The pH was monitored to ensure that excess chloride ions had been removed. The clay was then dried in a vacuum oven at 90°C over-night ¹⁵³.

With the (MG) method 10g of montmorillonite clay was stirred in 175ml of deionised water at room temperature overnight. A separate solution of 5g 12-aminododecanoic acid and 5.85g concentrated HCl in 50mL deionised water was heated to 85°C to yield a clear yellow solution. The protonated amino acid solution was added at a rate of

approximately 10ml/min with vigorous stirring to the montmorillonite solution suspension kept at 85°C for 12-hours. The modified silicate was recovered by filtering the solution in a Buchner funnel followed by repeated washings of the filter cake with 85°C deionised water to remove any excess of ammonium ions. The final product was dried in a vacuum oven at 90°C over-night ¹⁵⁵.

An oven was preheated to 170°C. A 125cc glass bottle complete with Bakelite cap and a 100mm x 25mm soda glass flat bottomed specimen tube were placed into the oven. 50g of flaked caprolactam were added to the glass bottle, the caprolactam was allowed to melt. After which the required amount of catalyst D was added, stirred and the jar returned to the oven for 5 minutes. Then the required amount of activator B was added to the jar and stirred. Immediately the contents were poured into the glass vial and returned to the oven in a stable, upright position. If clay was to be added, after the addition of activator B the mixture was stirred and the jar returned to the oven for 5 minutes. Then the required amount of treated clay was added to the jar and stirred. Immediately the content was then poured into the glass vial and returned to the oven in a stable, upright position.

Upon successful polymerisation of the small-scale test pours, the process was scaled up to a three-kilogram factory trial. A churn, pouring spout and a casting case were heated in an oven to 130°C. The ϵ -caprolactam was placed in the churn and the anti-foaming agent (stearic acid) was added. The churn was placed back into the oven and once again heated to 130°C. This was followed by the addition of the clay, whence it was then returned to the oven again, and heated to 135°C. The catalyst was added and the sample mixed for 30 seconds to allow dispersal of the catalyst. The activator was added and the sample mixed for a further 30 seconds to allow dispersal of the activator. The mixture was then poured into the casting case, via the pouring spout, and returned to the oven. A thermocouple was inserted and the reaction progress monitored.

3.4

Reaction Extruded System: Polyamide-6 Composites

A series of extruded composites were formulated. A control system containing a high molecular weight polyamide-6 was processed without clay, and in the presence of both treated and untreated clay. A commercially available nanocomposite was also extruded. Both of these systems were compared with a reactive extruded approach combining ϵ -caprolactam with an appropriate activator and catalyst processed with out clay, and in the presence of both treated and untreated clay.

3.4.1

Preparation of Nanocomposites Using Extrusion Techniques

A commercially available polyamide-6 was used as a control, in order to enable comparisons between the various systems. It was processed as a pure material, as well as in formulations containing 4wt% untreated or treated clay, as required.

The raw material feedstock composition for the reactive polymerisation of polyamide-6 consisted of 2kg ϵ -caprolactam, 4% by weight of the monomer of the catalyst (sodium caprolactamate) and 5% by weight of the monomer of the activator (caprolactam blocked diisocyanate in caprolactam, hexamethylene-1,6-diisocyanate). In the formulations that included clay the content was 4wt%.

The UBE material was used as supplied, again in 2kg, with no further additions or modifications. The Manufacturer's material information stated that the clay content was 2%.

The two kilogram batches of solid feedstock were accurately weighed and thoroughly tumble mixed before being introduced, by-hand, into the feed port of the twin-screw extruder at a steady rate.

Polymerisation and extrusion were undertaken in a 40mm screw diameter, TS 40 – Betol Machinery Ltd., intermeshing co-rotating twin-screw extruder. The extruder was assembled with five barrels, having a 25:1 Length to Diameter ratio. The screw profile was designed initially to have screw sections for feeding the ingredients through, after which there was a semi-compression zone for mixing and melting the materials prior to the compression zone where kneading elements were also used to maintain pressure for complete polymerisation. After the compression zone a semi-compression zone was added to prevent excess back-pressure and finally a metering zone was included to condition and steady the polymerised extrudate through the die. The polymer was die-formed into a 4mm diameter rod and quenched in water at 23°C.

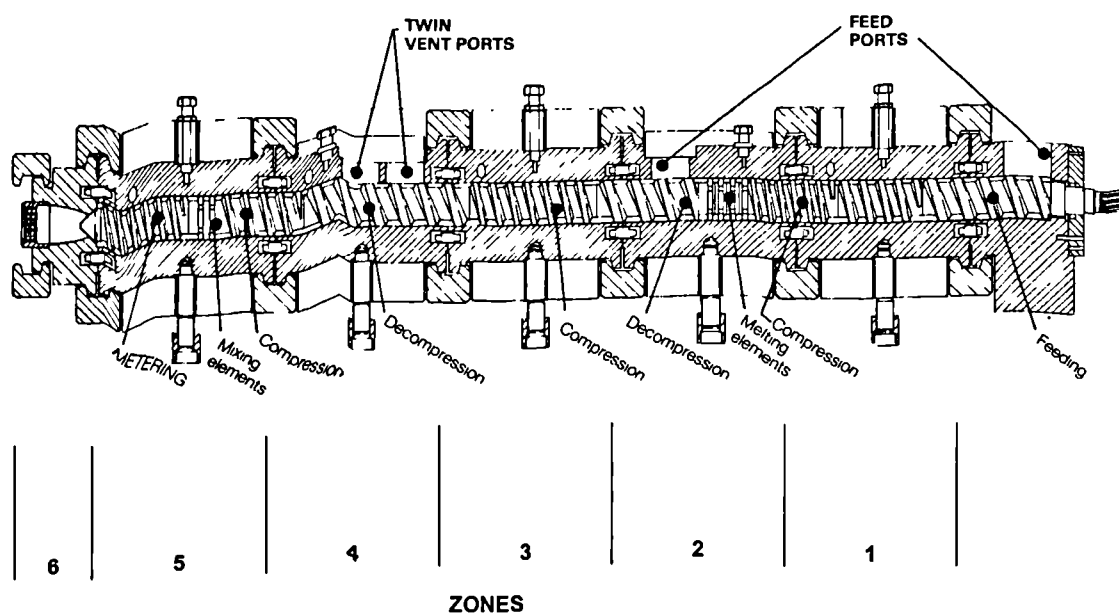


Figure 3.2
Extruder screw profile and barrel zones 151

The temperature profiles along the length of the extruder were set according to the functional requirements of the particular zones. Hence, as the caprolactam monomer melts and polymerises to polyamide-6, the temperature conditions must accommodate the changing rheology of the material. The barrel temperature profile, as shown in Figure 3.2, was used for reactive extrusion procedures at an extruder screw speed of 150rpm.

3.5

Sample Preparation

Prior to testing the samples were prepared as detailed in the following sections. All processed materials were stored in a desiccator until required for sample preparation, and post sample preparation they were returned to the desiccator until required, in order to prevent excess absorption of atmospheric moisture.

3.5.1

Cast Sample Preparation

Test specimens were prepared by CNC milling to the required size as detailed in the appropriate ASTM standard. Immediately after casting the samples were kept in a desiccator, and post machining they were returned to the desiccator until required, in order to prevent excess absorption of atmospheric moisture.

3.5.2

Extruded Sample Preparation

Test specimens were prepared by injection moulding in accordance with procedures stated in BS EN ISO 1874-2 (1996) "Plastics - Polyamide Moulding and Extrusion Materials. Part 2. Preparation of Test Specimens and Determination of Properties." All materials were dried in a vacuum oven at 90°C for at least 24 hours prior to injection moulding. A Mannesmann-Demag injection-moulding machine with a NC III control system (150 Ton clamp force) was used with a single gated, single cavity mould for the production of 4 x 10 x 115mm test specimens. Immediately after moulding the samples were kept in a desiccator until required, in order to prevent excess absorption of atmospheric moisture.

Injection pressure was set at 115bar, which is the maximum setting. However, the actual pressure of injection will be that needed to inject the dose required within the time specified. The moulding conditions were:

Temperature at Nozzle:	200°C
Temperature at Front of Screw:	190°C
Temperature at Middle of Screw:	185°C
Temperature at Rear of Screw:	180°C
Temperature at Intake:	60°C
Mould Temperature:	40°C
Total Cycle Time:	40s
Mould Closed Time	1.5s
Carriage Forward	7s
Injection Time	1s
Hold Time	15s
Dosing Time	4s
Cooling Time	10s
Mould Open Time	1.5s

The formula for calculating the locking force is defined as the area of the moulding multiplied by the stiffness factor ¹⁵², which is dependent on the material:

$$(4 \times 10 \times 115) \times 0.3 = 1.380 \text{ Ton}$$

Hence the clamping pressure used was 1.4 Ton.

3.6

Characterisation of Polyamide-6 nanocomposites

This section describes the characterisation techniques used to assess the structure and properties of the composites, the practical and theoretical nature of experimental procedures used to characterise the structure and properties of the materials prepared.

Chromatographic methods, structural and microscopic analysis only requires a few milligrams of each material. Samples were sectioned in such a way as to reduce any possible variations within the material. Samples were tested in the “as-received” state, which for industrial samples meant pellets of material were randomly selected. Whereas for extruded samples this means after the initial extrusion process. After samples had been injection moulded, post initial processing, sections were taken from the test-bars as illustrated in Figure 3.3. After samples had been cast, thin slices were cut approximately half way along the cast tube and sectioned as illustrated in Figure 3.4. This figure also illustrates how samples were sectioned from the plaque after they had been compression moulded, post initial processing.



Figure 3.3

Schematic detailing injection moulded sample sections

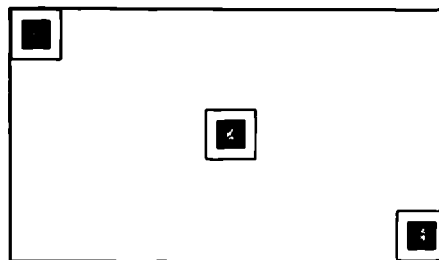


Figure 3.4

Schematic detailing compression moulded and cast samples sections

Prior to testing all materials were stored in a desiccator, at approximately 50% relative humidity for at least 48 hour, in order to minimise any moisture sensitivity.

The materials and experimental methods used in the production and formulation of polyamide-6 are detailed. Polyamide-6 nanocomposites were synthesised using reactive extrusion techniques, including the novel activated anionic polymerisation of ϵ -caprolactam in a twin-screw extruder in the presence of clay. The polymerisation conditions, residual monomer content and the nature of the structure produced are discussed with respect to subsequent alteration in the processing methodology.

3.7

Chromatographic Methods

This section details the use of chromatographic methods in order to ascertain residual monomer content and molecular weight distribution. Small sample sizes are used in these techniques, so it was necessary in each case to perform multiple-experiments to establish consistency.

3.7.1

Residual Monomer Content

Gas chromatography was used to estimate the residual monomer content of samples produced and obtained commercially, in order to allow comparison between polymerisation methods.

Gas chromatography is typically used for the separation of thermally stable and volatile organic and inorganic compounds ¹³⁷. It consists of several basic modules joined together, as shown in Figure 3.5, that:

- Provide a constant flow of carrier (mobile phase) gas.
- Permit the introduction of sample vapours into the following gas stream.
- Contain the appropriate length of stationary phase.
- Maintain the column at the appropriate temperature.
- Detect the sample components as they elute from the column.
- Provide a signal proportional in magnitude to the amount of each component.

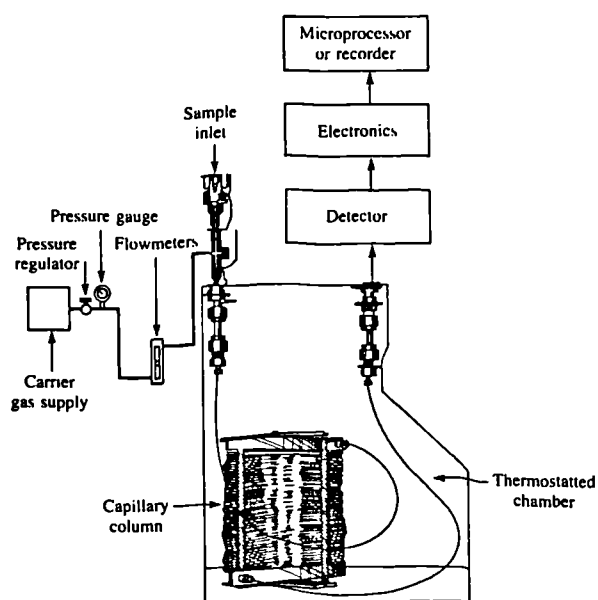


Figure 3.5
Schematic of a gas chromatograph ¹³⁷

Gas chromatography analyses were made using a single column flame ionisation detector unit attached to a Pye Unicam PU 4500 chromatograph. The stationary phase was 10% Apiezon L, 80-100 mesh, the column length was 1m, with a 5mm outside diameter, packed with diatomite. The instrument settings were as follows:

Solvent:	Distilled water
Injection:	1 μ l
Range:	10 ²
Flow-rate, H ₂ :	15psi
Flow-rate, Air:	10psi
Injector Temperature:	200°C
Detector Temperature:	200°C
Column Temperature:	210°C

The chart recorder was a Kipp & Zonen flatbed, with a chart speed of 5 mm/min and a range of 20mV.

Monomer residue remaining in the polymerised samples was calculated from a calibration curve of eluant peak areas as a function of monomer content. Known aqueous caprolactam solutions were vaporised and the corresponding eluant peak areas obtained. This data was used to construct a calibration curve.

Approximately 0.06g of each polymer sample was placed in 5ml of distilled water. The samples were placed in an ultrasonic bath for five hours, to enable monomer extraction. Injecting the samples and correlating the obtained elution data, in terms of peak area, to the corresponding caprolactam concentration, established residual monomer content. In order to establish that monomer extraction was complete the experiment was repeated in its entirety three times at twenty-four hour intervals.

3.7.2

Gel Permeation Chromatography

Gel Permeation Chromatography (GPC) was used to compare the molecular weight and the molecular weight distribution of samples. Gel permeation chromatography is a non-interactive mode of separation ^{137,138}. The particles of the column packing have various pore sizes and pore networks, so that solute molecules are retained or excluded on a shape and size basis. Although, strictly speaking, GPC is not based on molecular weight, it was used for the determination of the molecular mass distribution of samples prepared.

This exclusion chromatography technique involves a dilute solution of the sample being injected into a column of porous gel beads. As the sample passes through the column, the solute molecules are sorted. Very large molecules cannot enter many of the pores and also penetrate less into the comparative open regions of the packing. Thus excluded, these will be eluted first; whereas smaller molecules will diffuse into more of the accessible pores, their increased retention resulting in delayed elution. Between these two extremes, the intermediate-sized molecules can penetrate some passages but not others and, consequently, suffer retardation in their progress down the column.

Analysis of the eluted solution via differential refractometry or spectrophotometric detectors details distribution of the sample molecular weights. Using low-angle laser light scattering (LALLS) it is possible to determine absolute molecular weight directly. Although polymer molecules with different molecular weights may elute simultaneously, skewing the molecular weight distributions generated with conventional detectors, the LALLS detector gives correct results because it responds to analyte molecular weight, not just concentration.

This work was undertaken at RAPRA Technology Ltd. ¹³⁹, with data capture and subsequent data handling carried out using Polymer Laboratories Ltd. "Caliber" software. A single solution of sample was prepared by adding 15ml in the case of Cast samples and 10ml for Extruded samples, of solvent to 30mg of sample. Followed by heating at 120°C for one hour the case of Cast samples and for Extruded samples at

100°C for one hour. The solutions were thoroughly mixed and prior to the chromatography solutions were filtered through a glass fibre pre-filter and a 0.2 μ PTFE membrane. The conditions used were as follows:

Instrument:	Polymer Laboratories GPC-210
Columns:	PL gel 2x mixed bed-B, 30cm, 10 μ m
Solvent:	1,3-cresol, with 0.1% (w/v) antioxidant
Flow-rate:	1.0ml/min (nominal)
Temperature:	120°C (nominal)
Detector:	Refractive Index
Minimum Sample Number:	3

The detector response for polyamides is weak, and thus the quality of GPC results obtained normally are much poorer than for other polymer types. Therefore, triplicate runs are carried out instead of the usual duplicate runs to try and compensate for poorer repeatability. The long-term reproducibility of a particular GPC system may not be that reliable, hence a standard material was supplied for testing, as a control. The GPC system used for this work was calibrated with polystyrene but a mathematical correction has been applied to express the results as for polyamide 6.6. Literature values of Mark-Houwink parameters have been used in this correction but the applicability of the values used is open to question. There could be a considerable difference between these polyamide-6 equivalents and the actual molecular masses of the samples. Hence the results are best considered in a simple comparative manner, with the emphasis being placed on any observed differences between samples and not simply on the numerical values of the results themselves.

3.8

Structural Analysis

The materials were analysed in order to ascertain information about their structures. Thermogravimetric Analysis was used to quantify the inorganic content of the sample. Differential Scanning Calorimetry and X-ray Diffraction were used to give an indication of polymer crystal types and sizes. X-ray Diffraction also provides information on interlayer distance within the layered silicate itself.

3.8.1

Thermo-Gravimetric Analysis

Thermo-Gravimetric Analysis (TGA), because of high temperature ability, was used to ascertain the weight of clay present, once the polymer had been totally degraded. It also provided information on clay particle degradation.

TGA provides a quantitative measurement of any weight changes associated with thermally induced transitions ¹³⁷. Therefore, TGA will record the loss in weight, usually as a percentage, as a function of either temperature or time. The thermally induced transitions associated with TGA correspond to dehydration or decomposition of the sample when operating under isothermal conditions. Thermo-gravimetric curves are characteristic of a given compound or material due to the unique sequence of physical transitions and chemical reactions that occur over definite temperature ranges. Hence, TGA could be used to give information relating to the composition or the identification of a material/sample.

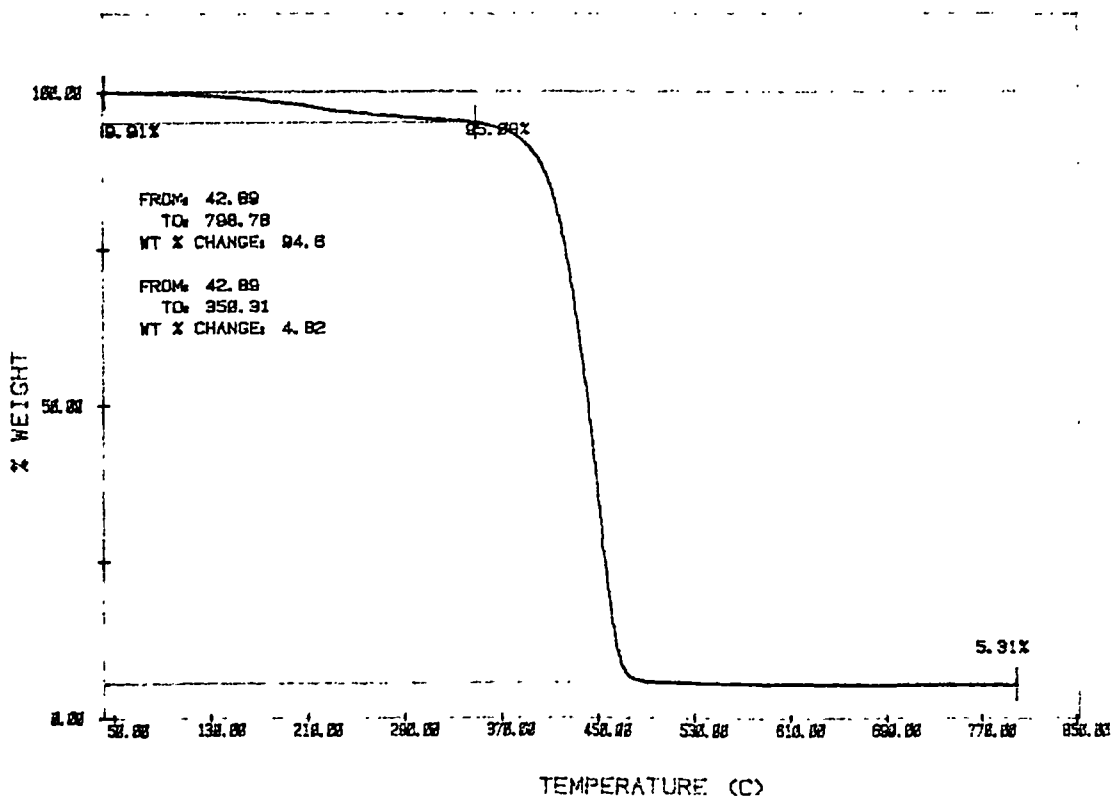


Figure 3.6
Thermogram of B-PA6(T)

TGA involves a constant measuring of the sample weight as the temperature is increased. Samples are placed in a crucible or shallow dish that is positioned in a furnace and attached to an automatic recording balance. The change in sample weight is measured through an electromagnetic servo system, which is linked, to a reference crucible/shallow dish. Any deviation in position of the sample crucible/dish in relation to the reference is recorded and corresponds to a weight change.

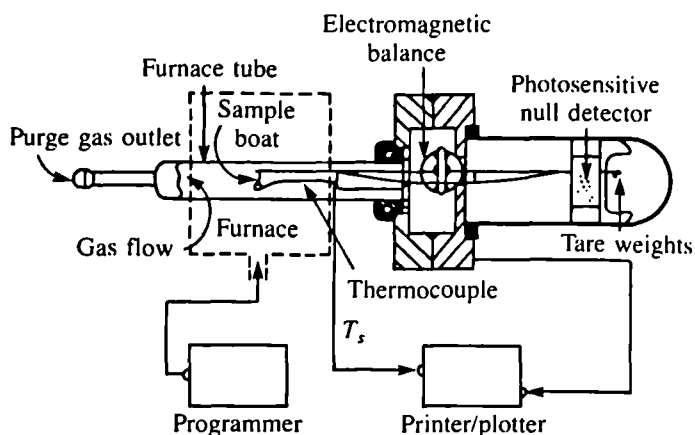


Figure 3.7
Schematic of a thermo-gravimetric analyser 137

Typically sample sizes were between 5-10mg. The samples were placed in platinum pans, and subjected to a controlled heating program. The TGA samples were analysed under the following conditions:

Instrument:	Perkin-Elmer TGS2
Inert Gas:	Nitrogen
Gas Flow-rate:	50cc/min
Heating Range:	40°C to 850°C
Heating Rate:	10°C/min
Cooling Range:	850°C to 40°C
Cooling Rate:	320°C/min
Minimum Sample Number:	3

3.8.2

Differential Scanning Calorimetry

Differential Scanning Calorimetry (DSC) has been used in this investigation to measure the degree of crystallinity, crystallinity temperatures and the melting points of the study materials. This technique was used to confirm that after reactive polymerisation a

polyamide has been produced, and to provide an initial indication of residual monomer content.

The technique involves subjecting a sample and a reference to a precise temperature change programmed by the user ¹⁴⁰. The apparatus contains two holders, one that has the sample (T_s), the other the reference (T_r). The DSC holds $T_s = T_r$ at all times, whatever the programme conditions: heating, isothermal or cooling. When a thermal transition occurs, i.e. the emission or absorption of heat, this corresponds to a chemical or physical change. Because the energy transferred, to maintain $T_s = T_r$, is exactly equivalent in magnitude to the energy absorbed or evolved in the transition, the balancing energy yields a direct calorimetric measurement of the transition energy.

If there is an endothermic reaction in the sample, the DSC, supplies more power to the sample holder. This is so that the temperature does not lag behind T_r . If there is an exothermic reaction then the opposite is true. Therefore the following equation shows the heating/cooling pattern:

$$\frac{dQ}{dT} = m C_p \frac{dT}{dt}$$

Where:

$\frac{dQ}{dt}$ is the power
 m is the mass
 t is the time
 T is the temperature
 C_p is the capacity
 $\frac{dT}{dt}$ is the heating rate

In Figure 3.8 the sample and reference pans can be seen on a raised platform on the thermoelectric (constantan) disc through which the heat is transferred. The difference in heat flow to the sample and reference is monitored by the chromel/constantan thermocouples. This difference is equal to and indicated by ΔH , the enthalpy change. The DSC technique is able to provide melting, re-crystallisation and glass-transition

temperature analysis, and can qualitatively show the difference in the amount of crystallinity of two or more superimposed samples. The system is run with inert gas to prevent reactions with the gas atmosphere, either nitrogen or argon.

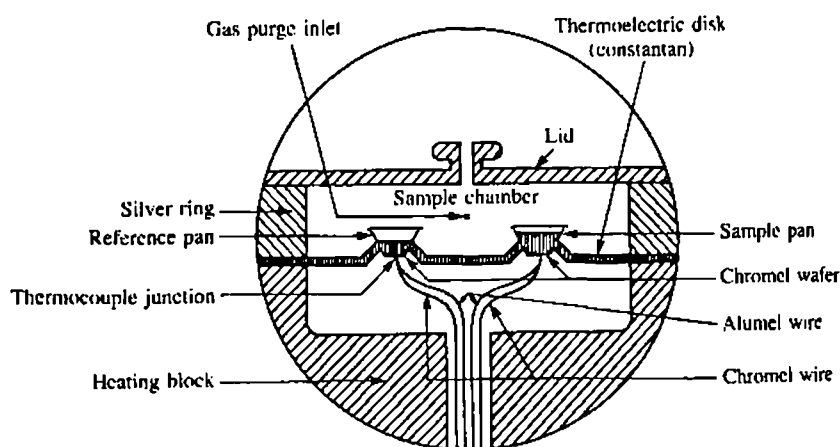


Figure 3.8
Schematic showing the internal DSC 137

The primary means of transferring heat to the sample is the constantan disk; therefore thin flat samples that have good contact with the base of the holder are required. Typically sample sizes were between 5-10mg. Through out the temperature cycle these samples were held in sealed aluminium pans. The DSC samples were analysed under the following conditions:

Instrument:	Perkin-Elmer 7 Series
Inert Gas:	Nitrogen
Gas Flow rate:	5 Bars
Heating Range:	40°C to 250°C
Heating Rate:	10°C/min
Holding Time:	2 minutes, at 250°C
Cooling Range:	250°C to 40°C
Cooling Rate:	10°C/min
Minimum Sample Number:	3

3.8.3

X-Ray Diffraction

X-ray Diffraction (XRD) was used during the course of this investigation to monitor the movement of clay layers. It provides a primary indication of the layer separation caused by processing and treatments.

XRD is a physical technique used in the characterisation of crystalline materials ^{137,141}, and to determine their crystal structures. X-rays are electromagnetic radiation that has a wavelength of approximately 1\AA , typically produced by high-energy collisions of charged particles with matter. The energy released in this transition appears as X-radiation. The transition energies have fixed values, resulting in a characteristic spectrum of X-rays. A simplistic diagram of an X-ray diffractometer is shown in Figure 3.9.

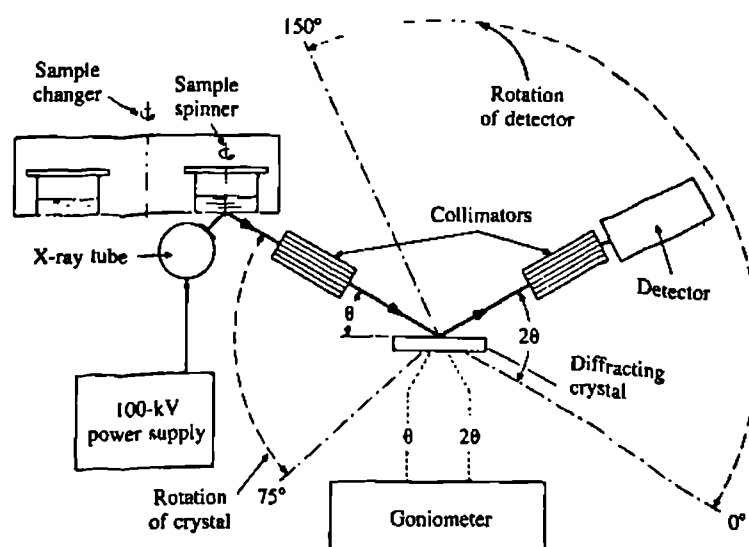


Figure 3.9
Schematic showing an X-ray diffractometer ¹³⁷

Crystalline materials, regarded as being built of layers of planes, scatter the X-rays in unique diffraction patterns, producing a “fingerprint” of its atomic and molecular structure. Therefore when a monochromatic X-ray beam strikes them, some of the

X-rays are reflected, such that the angle of incidence equals the angle of reflection. (Figure 3.10) the rest are transmitted and subsequently reflected by succeeding planes.

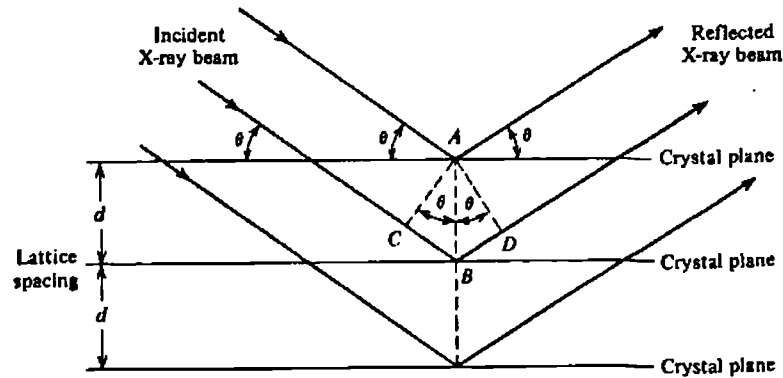


Figure 3.10
Diffraction of X-rays from a set of crystal planes 137

If two X-ray beams, 1 and 2, are reflected from the adjacent planes, A and B , within the crystal; the ray diffracted by the second plane travels the additional distance of \overline{CBD} in comparison the first diffracted beam at the surface plane. Angles CAB and BAD are both equal to θ . The d -spacing, the perpendicular distance between pairs of adjacent planes, is related to the angle of incidence, or the Bragg angle, and to the distance \overline{AB} by:

$$\overline{CB} = \overline{BD} = \overline{AB} \sin \theta$$

And:

$$\overline{CBD} = 2 \overline{AB} \sin \theta$$

Where \overline{AB} is the interplanar spacing d :

$$\overline{CBD} = 2 d \sin \theta$$

To observe a beam in the direction of the diffracted rays, \overline{CBD} must be some multiple of the wavelength of the X-rays so that the diffracted rays are in phase:

$$\overline{CBD} = n \quad (\text{where } n \text{ is an integer})$$

Thus the condition for the diffraction of a beam of X-rays from a crystal is given by:

$$n \lambda = 2 d \sin \theta$$

Which is known as the Bragg equation.

It is only when Bragg's Law is satisfied, that the reflected beams are in phase and interfere constructively. At angles of incidence other than Bragg's angle the reflected beams are out of phase and destructive interference occurs, therefore Bragg's Law imposes stringent conditions on the angles at which reflection may occur.

The d -spacings and their intensities are the most important features of a diffraction pattern. The d -spacings are governed by the values of the unit cell parameters (a , b , c). The intensities provide information on the types of atoms present in the sample. (Intensities are recorded relative to the intensity of the strongest line of the pattern, which is arbitrarily assigned 100.) For a particular substance, the line positions are essentially fixed and are characteristic of that substance. Intensities may vary somewhat from sample to sample depending on the method of sample preparation and instrument conditions.

The samples were rotated around a fixed axis during diffraction runs; analysis over the 2θ range was at room temperature, 23°C. This technique was used to characterise both the glassy amorphous phase and ordered crystalline phases of the polyamide-6; as well as to ascertain an indication of the separation caused by processing and treatments to the clay layers. Analysis of samples by XRD requires a flat surface off which the X-ray beam can be diffracted. The flat surfaces produced by injection moulding were suitable for this process and were sectioned perpendicular to the flow direction. The cast samples owing to the sectioning process had uneven surfaces and therefore had to be lightly finished using silicon-carbide paper. The commercial specimens were hot-pressed from the as-received states into thin films, in order to provide a suitable diffraction surface. Powdered samples are ideal for XRD as they consist of randomly orientated crystals, were packed into shallow stubs, levelled and held in place with PVC (amorphous) cling film.

The power supplied to the X-ray tube was 36kV and 26mA, the machine set-up was as detailed below:

Instrument:	Phillips 1050 Goniometer
Radiation Source:	Nickel filtered copper K_{α}
Diffraction Angles (2θ):	3° to 50°
Step Size:	0.021°
Scan Speed:	$0.02^{\circ}/\text{sec}$
Slit Size:	1° Divergence slit
Minimum Sample Number:	3

3.9

Microscopic Analysis

This section will discuss the Scanning Electron Microscope and Transmission Electron microscope. These techniques are particularly useful for examining the surfaces of materials and have analytical techniques associated with their use.

3.9.1

Scanning Electron Microscopy

Scanning Electron Microscopy (SEM) was used to obtain an initial indication of clay dispersion through out the sample. Microprobe analysis was used to confirm the constituents of any agglomerates made visible through this technique.

To achieve a successful result using a SEM, it is necessary to consider several factors, including: resolution, operating conditions, sample preparation, depth of field/focus, etc. ¹⁴²⁻¹⁴⁴ Resolution is probably the most important consideration, as it is the whole basis of electron microscopy. The increase in resolution is gained by the use of electrons. The resolution is inversely proportional to the electron wavelength used. The wavelength of electrons is a function of their kinetic energy, the higher their kinetic

energy (kV) the shorter their wavelength. The wavelength of electrons can be estimated by the following expression:

$$\lambda = \frac{12.3}{\sqrt{kV}}$$

The SEM is comprised of an evacuated column containing an electron gun, electromagnetic lenses, apertures, electron detector, specimen stage and may contain other detectors, such as, the X-ray spectrometer. In a modern SEM all of the control functions with the exception of the aperture changing are performed electronically. The control column contains all of the control electronics, the camera record tubes, and viewing displays, both of which are cathode ray tubes.

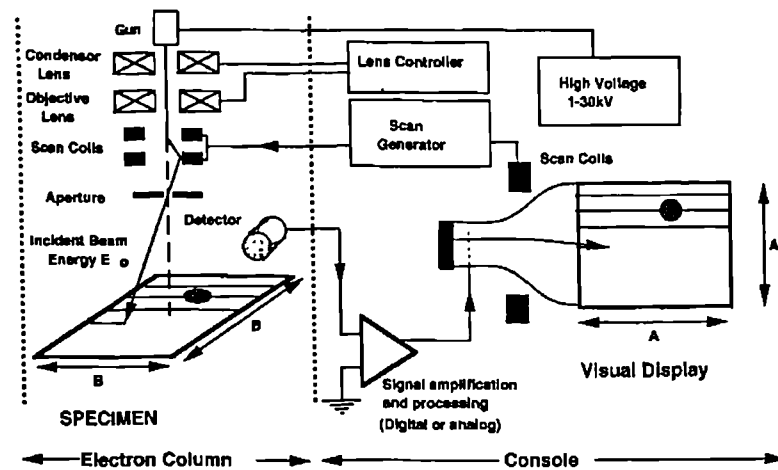


Figure 3.11
Basic components of the scanning electron microscope 144

The samples for examination by SEM are mounted onto a specimen stage, which is within the vacuum system; therefore the samples have to be dry and able to withstand the vacuum.

A fine probe of electrons interacts with the specimen to produce a variety of different signals: high energy, backscattered electrons, low energy secondary electrons, absorbed electrons, X-rays and cathodoluminescence. All interaction products can be collected and amplified to produce a signal that can be used to control brightness to the cathode ray tube. The nature of the interaction of the electron beam will be affected by topography, composition, magnetic and electric character of the specimen.

X-ray microanalysis depends on the generation of characteristic X-rays from the sample due to ionisation of the atoms by the inelastic scattering of incident electrons. When an incident electron strikes a sample it may generate an X-ray whose energy and wavelength are characteristic of the element of origin. If the energy, or wavelength, of the characteristic X-ray can be detected and counted with a suitable spectrometer, chemical information can be obtained about the specimen. In the electron microscope this is achieved by irradiating the sample with a beam of electrons of sufficient energy to remove electrons from the inner orbital shells of the sample atom.

SEM was used to investigate fracture surfaces. Samples were fractured, having being cooled in liquid nitrogen, by the use of a hammer. Four samples were mounted onto each stub via double-sided carbon tape. To make the samples electrically conductive an E500 Gold Sputter Coater was used to coat all the samples, 30 second bursts were used totalling 5 minutes, after which the sample was left to cool for 30 seconds. The following conditions were used:

Instrument:	JEOL 840A
Attachments:	Energy dispersive X-ray analysis
Accelerating Voltage:	20kV
Magnification:	500-8000x
Coating:	Gold-Palladium
Coating Time:	Five minutes (10 x 30 seconds)
Minimum Sample Number:	2

3.9.2

Transmission Electron Microscopy

Transmission Electron Microscopy (TEM) has been in this study to establish the extent of delamination or exfoliation of the clay layers within the nanocomposite. To achieve a successful result using TEM, it is necessary to consider several factors, including: resolution, operating conditions, sample preparation, etc.^{141,145}.

A transmission electron microscope consists of an evacuated column containing an electron gun, electromagnetic lenses, apertures and specimen stage. In modern TEM's all of the control functions with the possible exception of aperture changing are electronically performed.

Transmission electron microscopes produce a coherent beam of virtually monochromatic electrons that are focused by an electromagnetic lens onto the sample ¹⁴⁵. The most common electron source is the thermionic emission gun, consisting of a bent tungsten filament, cathode, with a V shaped tip about 100 μ m radius. Electrons are emitted from the filament tip if it is heated to above 2700K. The electrons are accelerated away from the gun by applying a high negative voltage between the cathode and the anode. By applying a bias voltage of between 0-500V between the cathode and the cathode shield, the electrons can be focused to a point below the cathode.

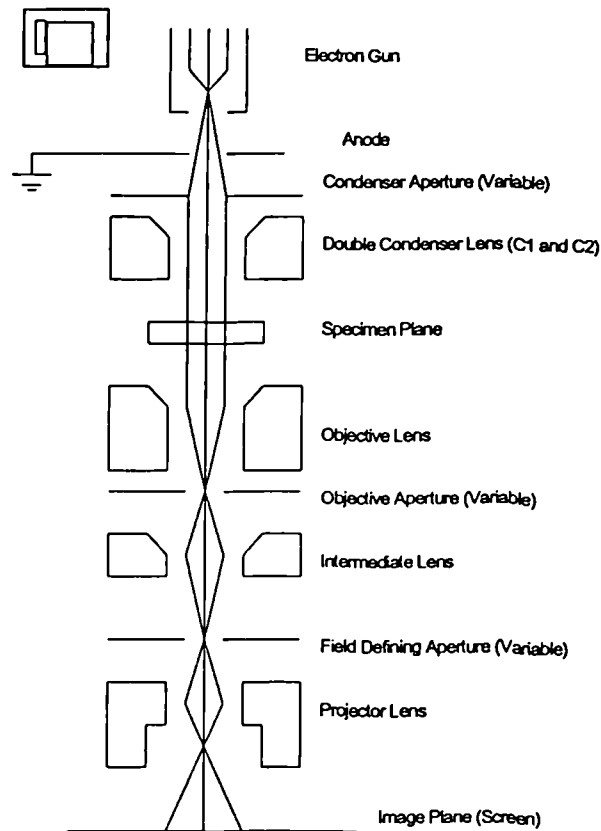


Figure 3.12
Schematic cross-section of a typical electron column 145

Electron microscopes use electromagnetic lenses that are designed to provide a magnetic field almost parallel to the direction of travel of the electrons. The effect of the lens on the electrons is inversely proportional to the accelerating voltage applied to the gun. The function of an electron lens is to bring to focus the beam of electrons produced by the gun, the Focal Point of the lens. The focal length of a lens is the distance between the lens and the focal point, i.e. it is inversely proportional to the strength of the magnetic field. The TEM has three-lens system, a condenser lens system, which provides a coherent beam of electrons, an objective lens system that focuses the image and also gives a small amount of magnification and the projector/intermediate lens system that provides the bulk of the magnification.

The samples for examination by TEM are mounted onto a specimen stage, which is within the vacuum system; therefore the samples have to be dry and able to withstand the vacuum. The stage is electronically grounded to the microscope to provide a conducting pathway for the electrons.

When electrons interact with atoms of the specimen, they are scattered to various directions. The angular distribution of the scattering is dependent on the atomic number and thickness of the specimens; heavy atoms and thicker specimens will scatter electrons to larger angles. Removing the scattered electrons from the beam by the objective lens aperture usually forms the images with amplitude contrast. The image contrast could be very weak for thin specimens and light elements; or very strong for heavy elements or crystalline material, where strong scattering due to Bragg diffraction occurs. An image can also be formed from scattered electrons only, "Dark Field"; the strongly scattered objects appear bright on a dark background. The intensity of the dark field image is usually very low, but contrast is greater than in bright field imaging. Not only is this very useful for the study of weakly scattering objects, but also for the interpretation of diffraction patterns and analysis of image contrast.

In order to visualise the ultrastructure of the clay filled polymers it was necessary to microtome the material to give ultra-thin sections of approximately 150nm in thickness. The materials were first cut with a glass knife but it was not possible to produce usable sections due to the softness of the polymers. A diamond knife was then used which, even though these sections contained compression striations, areas were produced which were usable. The ultra-thin sections were floated onto water after sectioning and were collected onto copper microscope grids. The analysis was conducted using an electron beam with the section at the stage eucentric point. The sections were examined under the following conditions:

Instrument:	JEOL 2000FX
Attachments:	Oxford Instruments ISIS energy dispersive X-ray analyser
Accelerating Voltage:	200kV
Magnification:	5000-50 000x
Minimum Sample Number:	2

3.10

Mechanical Properties

Mechanical properties were monitored in order to ascertain, quantitatively, any differences arising from possible reinforcing effects owing to the clay contained within the nanocomposite structure. For each mechanical test at least three of each material were tested, so as to establish reproducibility. Prior to testing all materials were stored in a desiccator for at least 48 hours, in order to minimise any moisture sensitivity.

3.10.1

Charpy Impact Test

The Charpy test is a widely used method for obtaining the impact strength of a material by physical means. This test involves the breaking of test specimen by the swinging action of a pendulum. Two posts support the test piece so that the specimen forms a horizontal beam, which the hammer (on the end of the pendulum) will swing through. This method is applicable to notched or un-notched samples. For notched samples the Charpy test involves the hammer hitting the sample from behind the notch, (i.e. the notch is facing away from the hammer) as illustrated by the Figure 3.13.

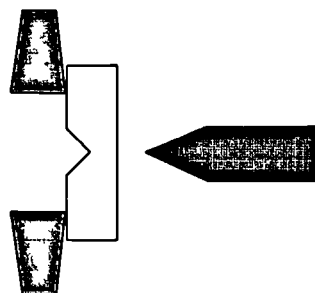


Figure 3.13
Charpy impact test

A notch will facilitate the propagation of a crack, as it is effectively an area of stress concentration. The presence of the notch makes this the most likely site of failure; hence the fracture of the test specimen is controlled. Thus the failure of each specimen

is comparable, as the same initiation site and the same mechanism of failure for each specimen is consistent.

Impact strength is calculated from the energy removed from the pendulum as a result of work done fracturing the test piece divided by the cross-sectional area of the specimen. The calculation used is as follows:

$$\frac{\text{Absorbed Energy (J)}}{\text{Notch Width x Thickness}} = \text{Impact Strength (Jm}^{-2}\text{)}$$

(m) (m)

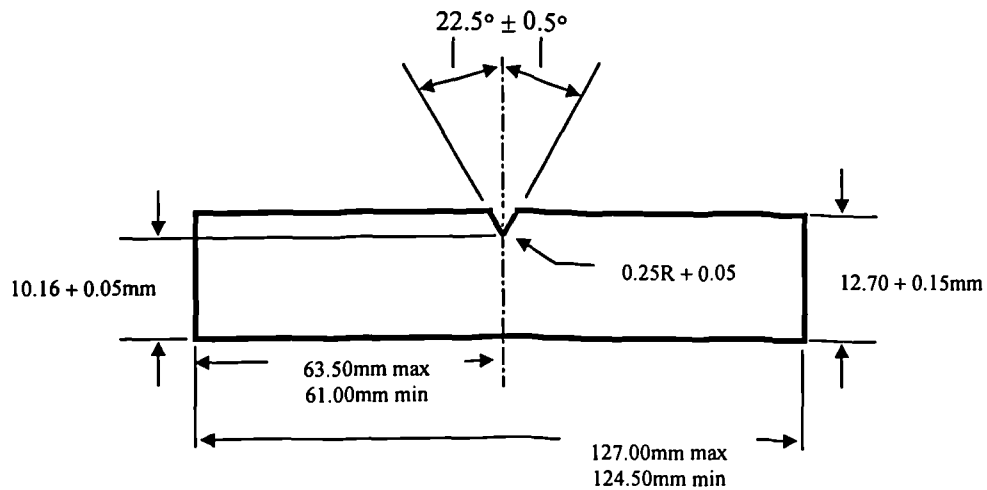


Figure 3.14
Notch types 147

The dimensions of the impact test bars were taken from the gauge length of the injection moulded tensile test bars, as documented by ASTM standard D256, Figure 3.14. Notching of the specimen was carried out using a manual Charpy notch-broaching machine, Blacks Equipment, Ltd. Testing was conducted at room temperature, 23°C, under the following conditions:

Instrument:	Ceast 6456/000
Hammer:	2J
Cross-sectional Area:	80 x 4mm
Minimum Sample Number:	5

3.10.2

Tensile Test

The most common form of mechanical measurement of polymeric materials is the measurement of tensile stress-strain properties ¹⁴⁷. The evaluation of such properties will involve monitoring the application of a force to a test piece until it fails. Measurement of the force and elongation at various stages of the process will help to build a picture of the stress-strain properties of the material, which is generally illustrated by graphical representation in the form of a stress-strain curve. From this curve strength, elongation, and modulus can be calculated.

Tensile test equipment consists of grips to hold the test piece, a means of applying a strain or stress, a force measurement device, and an extension measurement device (extensometer). Testing tensile properties is a convenient and relatively simple process, which acts as a general guide to quality. However, given that test piece geometry will influence the result, tensile properties are considered arbitrary rather than absolute.

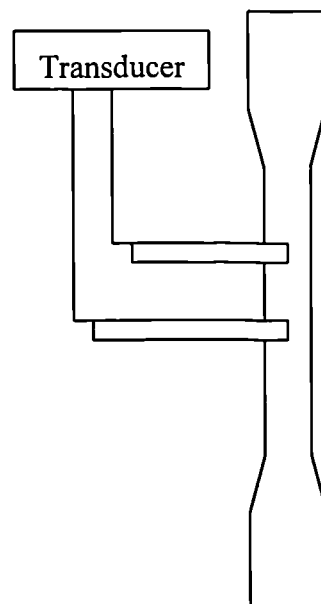


Figure 3.15
Schematic of a contact extensometer

Tensile test pieces are often in the form of two-dimensional dumbbell shapes, the reason being that stresses can be concentrated at the narrow portion (gauge length) of the test

piece, as opposed to the gripped ends. Injection-moulded tensile test bars are most commonly used, as the accuracy of injection moulding results in any differences in geometry being negligible.

Testing was conducted at room temperature, 23°C. The injection moulded tensile testing bars were tested as follows, in order to evaluate the tensile modulus, the displacement and stress, at both peak and at break:

Instrument:	Instron 4206
Load Cell:	5kN
Sample Size:	80 x 10 x 4mm
Specimen Grip Distance:	115mm
Maximum Extension:	600mm
Speed of Testing:	5mm/min
Minimum Sample Number:	5

3.10.3

Flexural Test

Flexural tests are frequently applied to plastic materials ¹⁴⁷. There are various types of testing apparatus, but the 3-point bend method is the most common. In this test the stresses and strains are not uniform throughout the specimen. They change from a tensile form on the outer surface opposite the loading point, through a neutral plane of zero stress or strain, to the compression form on the surface adjacent to the loading point. For isotropic materials the neutral plane is along the centre of the test piece.

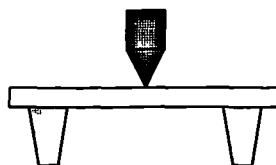


Figure 3.16
Schematic three-point bend test

Ductile materials will generally tend to keep bending until it slips from the outer supports and hence does not reach a point of fracture. The test piece geometry for flexural testing uses the gauge length of dumbbell shaped test bars. The speed of testing is usually 2mm/min. This is used because in the majority of cases it is the closest speed corresponding to a strain of 1% per minute.

The injection moulding the test specimen results in any differences in geometry were very small and deemed negligible. Testing was conducted at room temperature, 23°C, under the following conditions:

Instrument:	Instron 4206
Load Cell:	5kN
Sample Size:	54 x 10 x 4mm
Span:	80mm
Maximum Extension:	40mm
Speed of Testing:	2mm/min
Minimum Sample Number:	5

3.10.4

Dynamic Mechanical Thermal Analysis

Dynamic mechanical thermal analysis (DMTA) is designed to observe the visco-elastic properties of a material with respect to temperature, humidity, vibration frequency, dynamic strain amplitude, or static strain amplitude against time. In practice, the DMTA will excite the material with a periodic stress and monitor the resultant strain while conducting a temperature scan at a constant frequency ¹⁴⁷. The response of the material will depend on its visco-elastic properties. For example, a steel spring will behave completely elastically whilst grease will behave in a viscous manner. Investigation of a material undergoing a temperature scan at a constant stimulated frequency will give a quantitative analysis of how the elastic properties (Young's modulus) of the material will vary with temperature. From this the heat distortion temperatures (i.e. the behaviour of the material at a given temperature) can be

measured ¹⁴⁸. Although there are a number of test fixtures that can be used to collate heat distortion data, the three-point bend method is the most commonly used method.

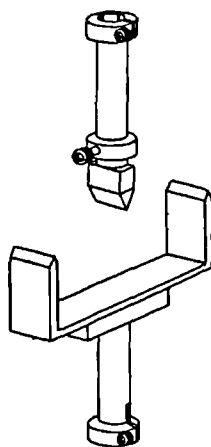


Figure 3.17
Three-point bend test fixture ¹⁴⁹

This dynamic mechanical test was undertaken in order to evaluate the heat distortion characteristics. A plot of elastic and loss moduli of the material versus temperature provides a graphical representation of elasticity and damping as a function of temperature or frequency. The modulus indicates stiffness of a material, and the mechanical damping (internal friction) gives the amount of heat dissipated as heat during the deformation ¹⁵⁰. The injection moulded tensile testing bars were tested as follows, in order to calculate the dynamic storage modulus (E'), the dynamic Young's modulus (E'') and the loss factor ($\tan \delta$):

Instrument:	Rheometrics Solids Analyser RSA II
Temperature Range:	-100-260°C
Sample Size:	54 x 10 x 4mm
Span:	48mm
Testing Frequency:	6.28 rads/s (1Hz)
% Strain:	0.05%
Force:	-200N
Minimum Sample Number:	5

The magnitude of the dynamic storage modulus (E'), the dynamic Young's modulus (E'') and the loss factor ($\tan \delta$) were measured at 4°C increments.

CHAPTER FOUR

RESULTS AND DISCUSSION

4.1

Introduction

This chapter deliberates the experimental results obtained and subsequent trends observed in reaction cast and reaction extruded nanocomposites. Samples C001 – C010 were primarily used to ascertain catalyst to activator combinations, and practical aspects of processing. The samples subsequently produced using this data were used to study the influence of the polymerisation conditions, residual monomer content and the nature of the composite structure produced are discussed, as well as the effects that these have on the mechanical properties observed.

4.2

Polymerisation of ϵ -Caprolactam

And Residual Monomer Content

Gas Chromatography and Gel Permeation Chromatography were used to assess and quantify the amount of residual caprolactam monomer within the samples. These techniques also allow the degree of the polymerisation to be assessed.

4.2.1

Gas Chromatography: Cast System

Monomer residue remaining in the polymerised castings was measured by Gas Chromatography (GC) based on a monomer concentration in distilled water. Known aqueous caprolactam solutions were vaporised and the corresponding elutant peak areas obtained, this data was used to construct a calibration curve, Figure 4.1. A second order polynomial approximation was fitted to this curve thus allowing the calculation of elutant peak areas as a function of monomer content.

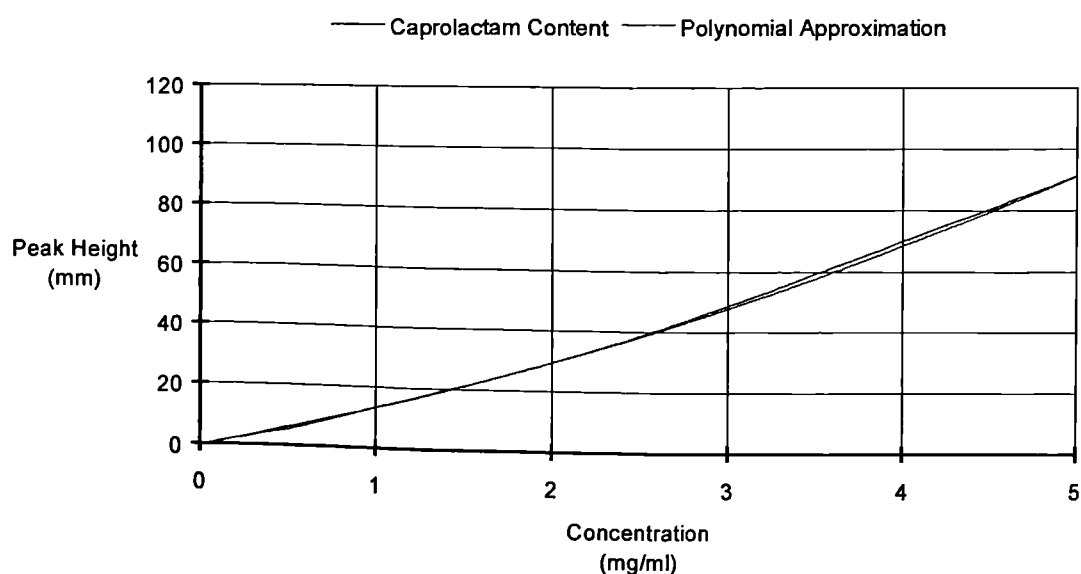


Figure 4.1
Calibration curve for caprolactam monomer content by Gas Chromatography

From this calibration curve the residual monomer content of the different cast samples were determined, the results are as shown in Table 4.1. The C-PA6 sample yielded one of the highest residual monomer contents. Inferring that the clay content rather than inhibiting the reaction conversely seems to encourage more complete conversion to the polymer. The exception to this is the NCH, which has the highest residual monomer content, thus comparison of these results suggests that a higher degree of polymerisation is obtained in the samples containing the organically modified clay.

Sample	Average (%)	SD	Rank
C-PA6	8.7	0.0	8
B-PA6	0.0	0.0	1
C020	5.6	0.9	4
C021	6.7	1.7	6
C022	5.0	0.9	3
C024	6.3	1.6	5
C028	6.8	1.8	7
C029	4.1	0.0	2
NCH	9.0	0.0	9

Table 4.1
Residual caprolactam monomer content assessed by Gas Chromatography

4.2.2

Gas Chromatography: Reaction Extruded System

Monomer residue remaining in the polymerised samples was measured by Gas Chromatography (GC) based on a monomer concentration in distilled water. Known aqueous caprolactam solutions were vaporised and the corresponding elutant peak areas obtained. This data was used to construct the calibration curve, shown in Figure 4.2. A second order polynomial approximation was fitted to this curve thus allowing the calculation of elutant peak areas as a function of monomer content.

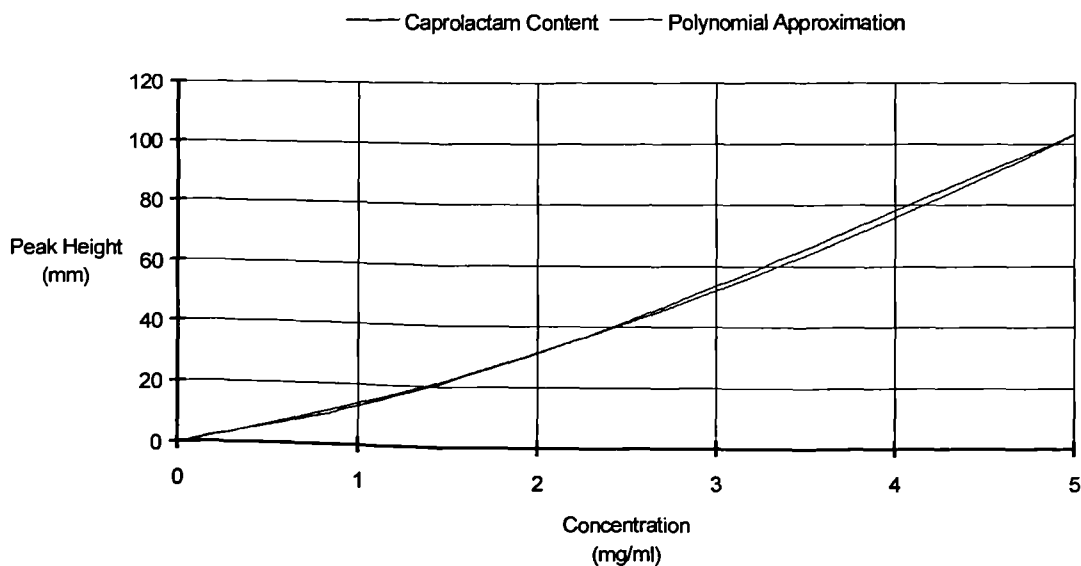


Figure 4.2
Calibration Curve for caprolactam monomer content by Gas Chromatography

From this calibration curve the residual monomer content of the different extruded samples was determined, and the results shown in Table 4.2. The B-PA6 sample had no discernible caprolactam remaining, inferring complete polymerisation. The reactive extruded J-PA6 sample produced the highest residual monomer content, suggesting that the reactive extrusion procedure itself was not optimal. The addition of clay to either material resulted in the same effect; in both cases the addition of untreated clay yielded a lower residual monomer content than that of the treated clay. Whilst the addition of treated or untreated clay improved the reactive extruded polymerisation, it was detrimental to the B-PA6 in effect depolymerising the sample.

Sample	Average (%)	SD	Rank
C-PA6	8.7	0	7
B-PA6	0.0	0	1
B-PA6(U)	1.2	0	3
B-PA6(T)	2.9	0	4
J-PA6	14.6	0.8	8
J-PA6(U)	6.7	0.8	5
J-PA6(T)	7.0	0.5	6
UBE	0.0	0	1

Table 4.2
Residual caprolactam monomer content assessed by Gas Chromatography

4.2.3

Molecular Weight And Molecular Weight Distribution: Cast System

The results for Gel Permeation Chromatography (GPC) carried out on the cast samples are summarised in Table 4.3. There are several ways of defining average molecular weight¹⁵⁹. Dividing the number chains into a series of size ranges and then determining the number fraction of chains with each size range obtain the number size average, \bar{M}_n . This number average molecular weight is expressed as:

$$\bar{M}_n = \sum x_i M_i$$

Where M_i represents the mean molecular weight of size range i , and x_i is the fraction of the total number of chains within the corresponding size range.

A weight average molecular weight \bar{M}_w is based on the weight fraction of molecules within the various size ranges. It is calculated according to:

$$\bar{M}_w = \sum w_i M_i$$

Where, again, M_i represents the mean molecular weight within a size range, where as w_i denotes the weight fraction of molecules within the same size interval.

All the samples have been analysed using RAPRA's standard procedure for 1,3 cresol at 120°C. The GPC of polyamides is at best difficult and there are frequent problems due to the very weak refractive index detector response and distinguishing signal from baseline. For reasons that are not clear, work on these samples seems to have been particularly complex. In the majority of instances it has been difficult to get two runs, for each sample, in reasonable agreement. All the samples, with exception of NCH, C-PA6 and B-PA6, contained small amounts of gel-like material and were very difficult to filter.

Sample	Mw	Mn	Polydispersity
C-PA6	33,489	12,523	2.674
	32,922	13,118	2.510
B-PA6	56,024	25,305	2.214
	55,853	27,560	2.027
C020	77,232	16,324	4.731
	82,287	17,886	4.516
C021	40,702	16,896	2.409
	37,445	17,886	2.093
C022	39,503	14,648	2.697
	46,549	11,982	3.885
C024 A	37,651	22,382	1.682
	31,897	19,304	1.652
C024 B	37,788	24,287	1.556
	37,207	22,931	1.623
C028	33,446	13,617	2.456
	30,943	12,739	2.429
C029	62,638	15,636	4.006
	49,063	13,213	3.713
NCH	2,470	1,053	2.346
	2,776	1,243	2.234

Table 4.3
Calculated molecular weight averages and polydispersity

The C-PA6 was also submitted for the extruded samples and differing results were obtained. The B-PA6 was also submitted for both cast and extruded GPC results analysis, and the results for these samples were also different. The very different results observed these occasions cannot easily be explained, but it is emphasised that the results are best considered in a simple comparative manner. The procedure was modified to dissolve at a higher temperature or the difference could simply be due to differences in the calibration: which is defined by a third order polynomial on a log (molecular weight) versus linear (retention volume) relationship, small shifts in retention volume for a very high molecular weight calibrant can have a dramatic effect on calculated molecular weight.

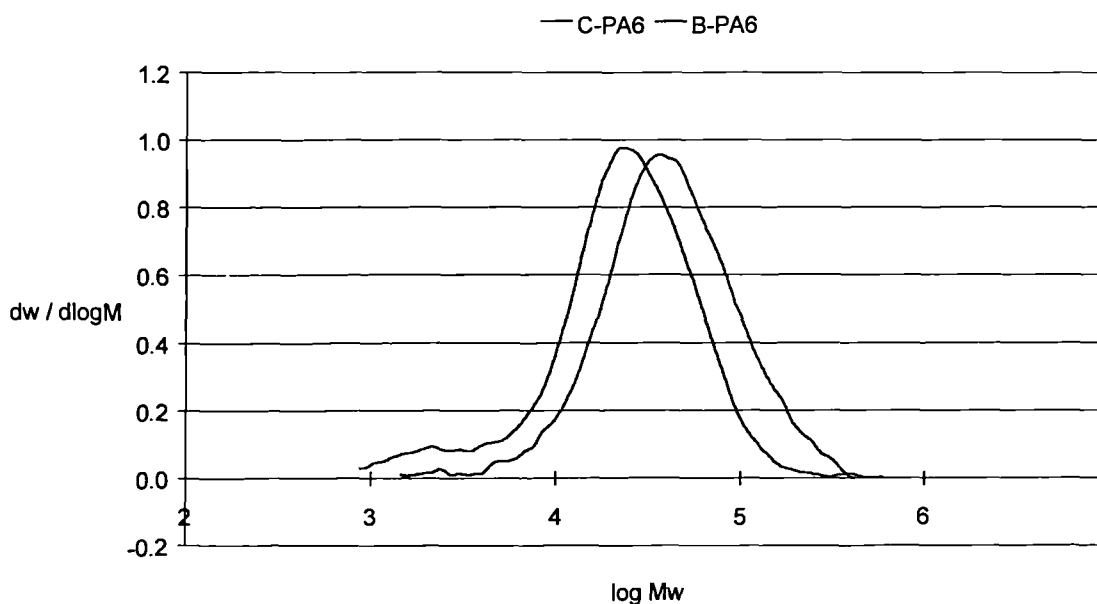


Figure 4.3
Overlay of the computed molecular weight distributions for the C-PA6 and the B-PA6 samples

The C-PA6 and B-PA6 were essentially used as controls for comparison between the cast series of materials. Typical commercial grades of polyamides have reported average molecular masses of 18,000-52,000⁶. These results infer that C-PA6 has an average molecular mass of 33,200 and of 55,940 for B-PA6. These results are relatively high and infer a comparatively high degree of polymerisation. However the molecular mass distribution is not highly variable and the ratio of mass number average/ number average is typically 1.9-2.0. The polydispersity index and gives an indication of the distribution of molecular mass. The distribution is relatively high; therefore the extent of reaction is also relatively high.

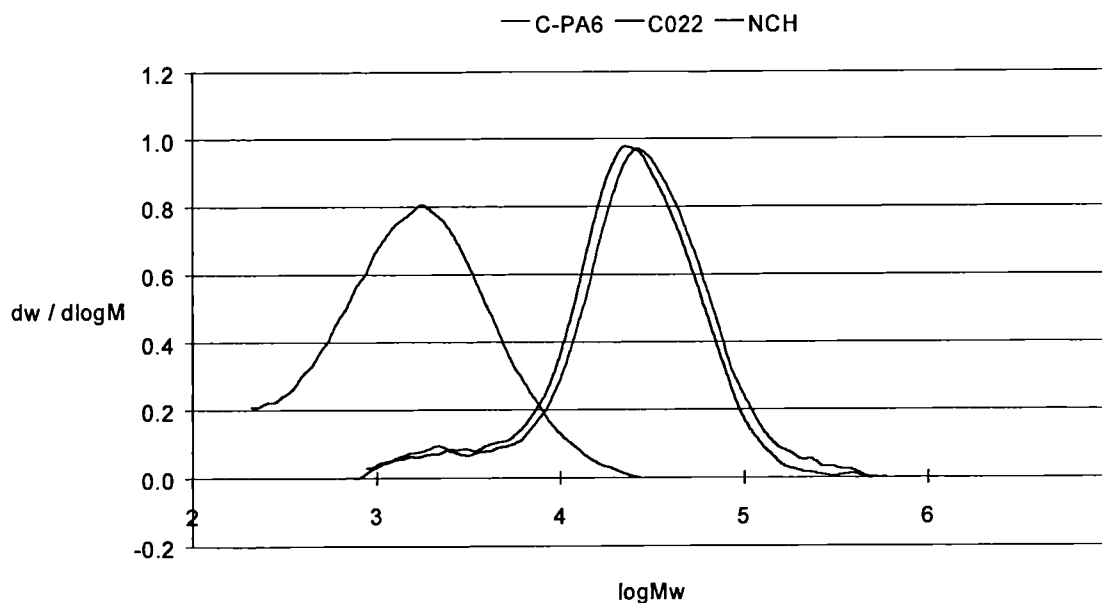


Figure 4.4
Overlay of the computed molecular weight distributions for the C-PA6, C022 and NCH samples

The NCH displays a relatively low molecular weight and infers a comparatively low degree of polymerisation. But surprisingly the polydispersity index is relatively high; which could suggest that the extent of reaction is also relatively high. However, in this instance given the high degree of residual caprolactam it may be better to take the polydispersity index in its mathematical context of defining the breadth of the distribution curve. Inferring that there is a broad distribution of polymer chain lengths within the NCH sample.

The results for C022 are higher than those for the C-PA6, so compare favourably. The increased molecular weight results can be directly attributed to an increase in the extent of the reaction, as reflected by the polydispersity index.

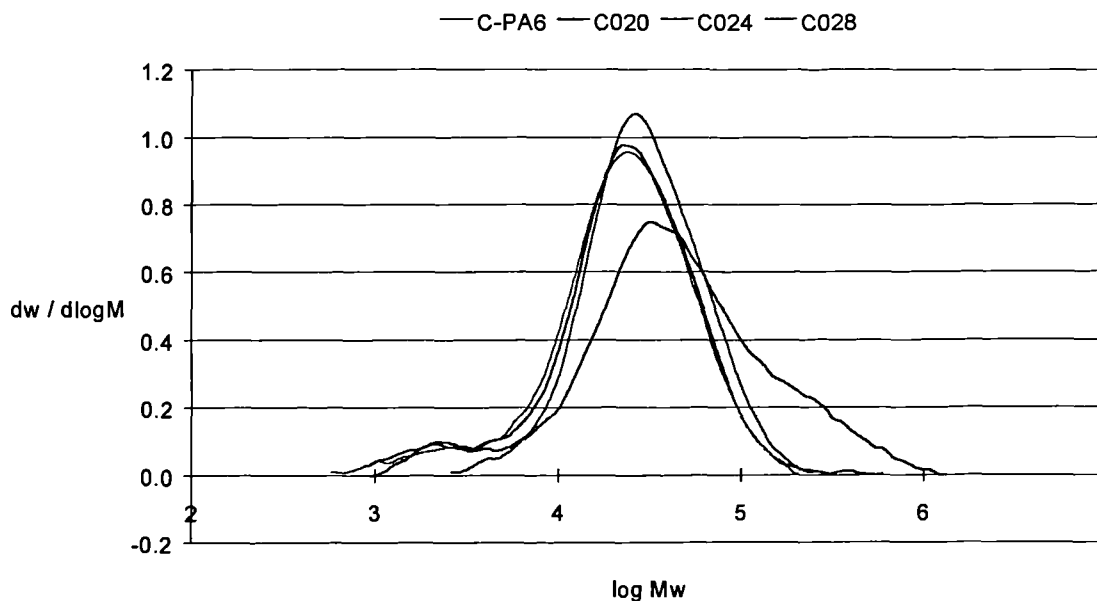


Figure 4.5

Overlay of the computed molecular weight distributions for a selection of the Cast series of samples

All of the cast series display relatively high molecular weights, inferring comparatively high degrees of polymerisation. All of these samples show good correlation with reported results.

Sample C020 displays the highest molecular weight and the highest polydispersity index. Although the peak itself is very much broader and somewhat more erratic than those for other samples tested. The clay used in C020 contains organically modified clay, and it is quite possible that the reactive end on the chain grafted onto the clay had unexpected reactions and terminations accounting for the unusual curve shape. This sample also had the highest recorded polydispersity.

Both C024 & C028 contain 4% of clay, and in both cases the chain length is once more comparable with the cast standard. C024 contains additional activator and demonstrates an increased molecular weight, despite the polydispersity suggesting that the completion of the reaction was lowest recorded.

All of the plots are normalised to equal area and are shown with the same axes. Overall the repeatability for the duplicate runs reported is poor, but the overlay plots do suggest some differences between samples. The low molecular weight for the NCH sample is very clear. It appears that C020 is of higher molecular weight than the other cast series of samples, and compares favourably with the industrial polyamide-6 samples. On the whole the addition of clay seems to increase the molecular mass of the sample compared with the C-PA6. Which is in agreement with the GC results, again inferring that the clay content seems to encourage conversion to a high molecular weight polymer.

Sample	Average Polydispersity	Rank	Average Mn	Rank
C-PA6	2.592	4	33,206	7
B-PA6	2.121	8	55,939	2
C020	4.624	1	79,760	1
C021	2.251	7	39,074	5
C022	3.291	3	43,026	4
C024	1.628	9	36,136	6
C028	2.443	5	32,195	8
C029	3.860	2	55,851	3
NCH	2.290	6	2,623	9

Table 4.4
Rankings of molecular weight and polydispersity

Owing to the chain nature of polymers it is necessary to deal with an average molecular size. The ratio of the mass average to the number-average of the molecular mass is known as the polydispersity index δ , and gives an indication of the distribution of molecular mass. If the extent of reaction is low, the distribution will be corresponding low; although it is possible to achieve a low polydispersity index with a high molecular mass polymer.

4.2.4

Molecular Weight And Molecular Weight Distribution: Extrusion System

The results for Gel Permeation Chromatography (GPC) carried out on the extruded samples are shown in Table 4.5, results are summarised as the calculated molecular weight averages and polydispersity. All the samples have been analysed using RAPRA's standard procedure for 1,3 cresol at 100°C. The GPC of polyamides is at best difficult and there are frequent problems due to the very weak refractive index detector response and distinguishing signal from baseline. The B-PA6 sample solution was easy to filter but all of the other solutions gave some problems on filtration. It was suspected that the thixotropic nature of the clay complicated the filtration process.

Sample	Mw	Mn	Polydispersity
C-PA6	141,409	61,582	2.296
	151,533	69,301	2.187
	133,866	67,309	1.989
B-PA6	24,233	11,529	2.102
	24,343	11,427	2.130
	24,434	11,356	2.152
J-PA6	27,348	11,438	2.391
	28,869	11,260	2.564
	30,605	12,108	2.528
J-PA6(U)	24,244	10,437	2.323
	22,565	9,931	2.272
	24,917	10,529	2.367
J-PA6(T)	35,256	14,421	2.445
	31,469	14,447	2.178
	39,812	17,496	2.275
UBE	27,352	12,405	2.205
	27,624	11,805	2.340
	27,009	12,343	2.188

Table 4.5
Calculated molecular weight averages and polydispersity

The C-PA6 and B-PA6 were also analysed with the cast samples, and as can be seen from Table 4.6 differing results were obtained for each submission, confirming that the long-term reproducibility of this particular GPC system is not very stable. So it is highlighted that the results are best considered in a simple comparative manner with the emphasis being placed on any observed differences between samples and not simply on the numerical values of the results themselves and not too much should be deduced from the actual numerical values for the average molecular weights.

Sample	Mw	Mn	Polydispersity
C-PA6 (Run One)	33,489	12,523	2.674
	32,922	13,118	2.510
C-PA6 (Run Two)	141,409	61,582	2.296
	151,533	69,301	2.187
	133,866	67,309	1.989
B-PA6 (Run One)	56,024	25,305	2.214
	55,853	27,560	2.027
B-PA6 (Run Two)	24,233	11,529	2.102
	24,343	11,427	2.130
	24,434	11,356	2.152

Table 4.6
Calculated molecular weight averages and polydispersity

The detector response for polyamides is typically weak and the quality of GPC results obtained is much poorer than for other polymer types. Triplicate runs were carried out instead of the usual duplicate runs to try and compensate for the poorer repeatability. However with this set of samples, the results appear to be possibly poorer than usual. Reasonable results have only been obtained by excluding any possible low molecular weight tail – the signal noise and possible low molecular weight impurities making this part of the chromatograms particularly variable. All of the plots are normalised to equal area and are shown with the same axes, and show an overlay of the computed molecular weight distributions for each sample.

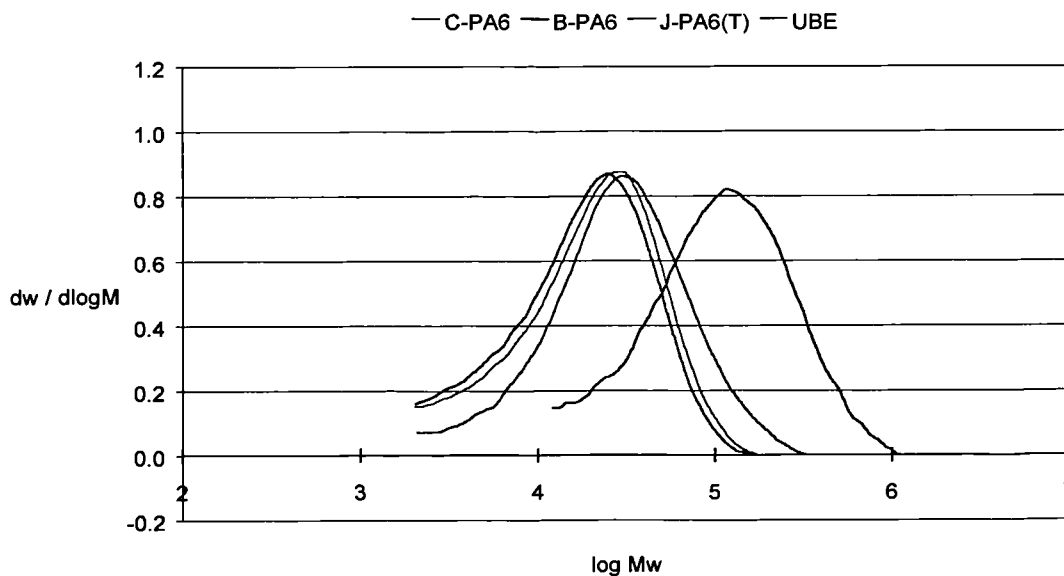


Figure 4.6
Overlay of the computed molecular weight distributions for C-PA6, B-PA6, J-PA6 and UBE

Clearly the C-PA6 sample is of significantly higher molecular weight than the other samples. This C-PA6 appears to be of significantly higher molecular weight than normally observed for polyamides. The chromatogram peak area for this sample is low and taken with the difficulty of filtering; it appears that some polymer has been removed at the filtration stage. The reactively extruded J-PA6 sample compares favourably with the industrial samples, and the presence of the treated clay yields a higher molecular weight material.

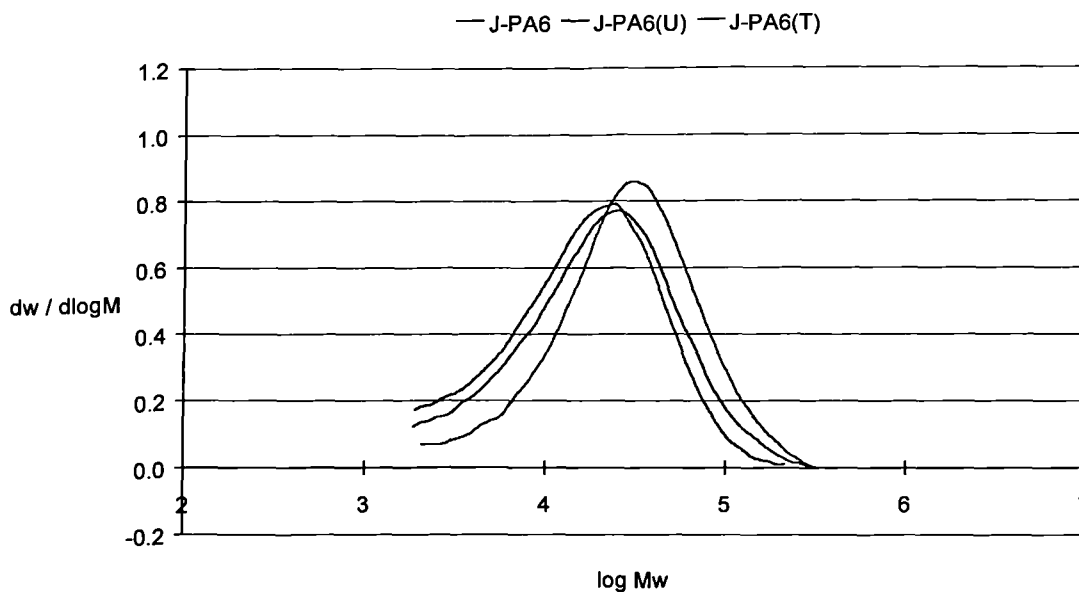


Figure 4.7
Overlay of the computed molecular weight distributions for the JAL series of samples

The J-PA6(T) which contains 4% of treated montmorillonite clay demonstrates a higher molecular weight than J-PA6, which does not contain any clay. This confirms that the treatment of the clay is no longer poisoning the polymerisation reaction, which was an issue with early reactive extrusion trials - owing to excess remaining protonated acid. There is not much variance between J-PA6 and J-PA6(U), although there is no reason why there should be any significant difference. The untreated clay contains no excess acid and clay is a well-documented filler of polyamides.

The average molecular size, as determined by the polydispersity index, gives an indication of the distribution of molecular mass. If the extent of reaction is low, the distribution will be corresponding low. So despite there being residual monomer content, as determined by Gas Chromatography, the extent of reaction appears to be higher in the reactively extruded samples.

Sample	Average Polydispersity	Rank	Average Mn	Rank
C-PA6	2.157	5	142,269	1
B-PA6	2.128	6	24,337	5
J-PA6	2.494	1	28,941	3
J-PA6(U)	2.321	2	23,909	6
J-PA6(T)	2.299	3	35,512	2
UBE	2.244	4	27,328	4

Table 4.7
Rankings of molecular weight and polydispersibility

4.3

Structural Analysis

Thermo-Gravimetric Analysis was used to assess the amount of inorganic material per sample, and also as a primary indication of clay distribution. Owing to the differing melting points of the various crystal forms of polyamide-6 Differential Scanning Calorimetry can be used to establish the nature of the crystallisation. The crystalline types present in polyamide-6 have distinct X-ray Diffraction peaks, which can be correlated with Differential Scanning Calorimetry data. Microscopic techniques were used to view the composite microstructure.

4.3.1

Thermo-Gravimetric Analysis: Cast System

Thermal Gravimetric Analysis (TGA) was used to ascertain the weight of clay present, once the polymer had been totally degraded. As relatively small amount of samples (5-10mg) were tested repeated from varied areas of casting, these result providing a crude indication of dispersion through the sample as a whole.

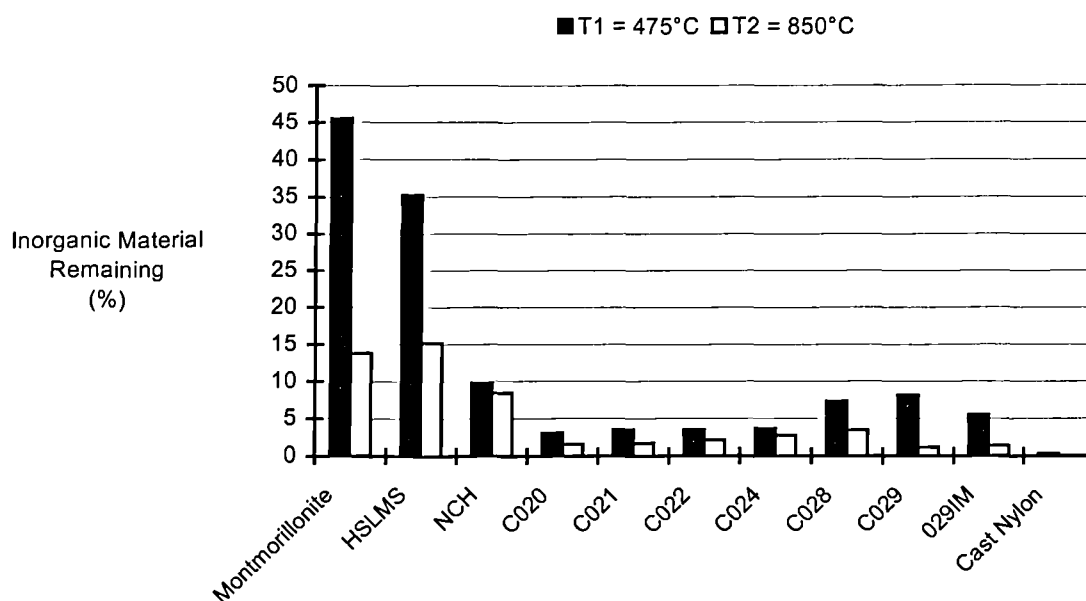


Figure 4.8
Summary of thermal gravimetric analysis results

Adsorbed water is lost at approximately 105°C from the external surfaces of the clay, but a much higher temperature, from 120-300°C, is required for the evolution of inter-layer water and water associated with the exchangeable cations. Hence at a temperature of 475°C it can be assumed that loss of water owing to these processes is complete. However this is prior to the main decomposition endotherm, which occurs at about 700°C, when the hydroxyl groups are removed as water. It is for these reasons that results were collated at 475°C and 850°C. The initial dehydration products formed are probably amorphous alumina and silica.

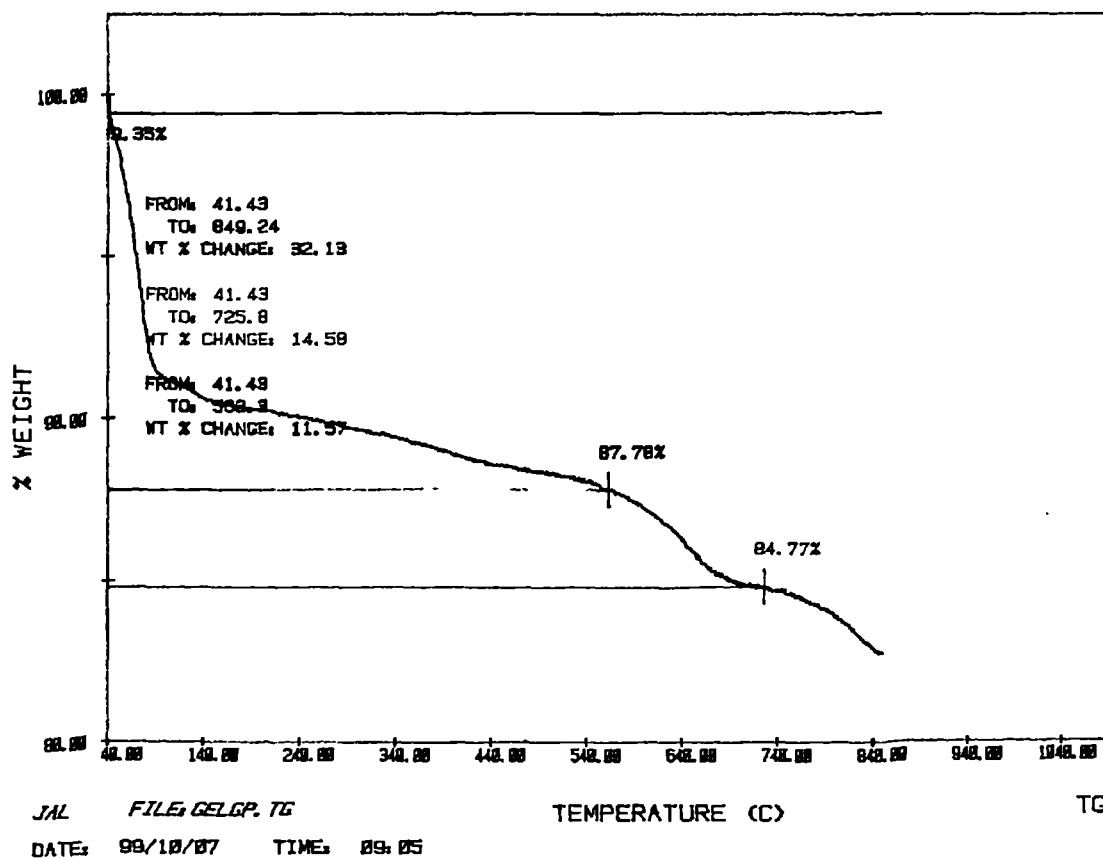


Figure 4.9
Thermogram of montmorillonite

C-PA6 appears to have some inorganic matter present up to 475°C; this is most likely to be the aluminium compounds, which are present in the catalyst. Therefore if this inorganic matter is present in the C-PA6, it can be assumed that it will be present in all of the cast series of materials, and thus comparable. After 850°C, the remaining inorganic content of the polyamide-6 is negligible. Hence it can safely be assumed that any organic matter remaining in the cast series of polymer is solely due to the clay.

Injection moulding of the previously cast C029 yields no real change in the residual clay content. As the sample material has just been subjected an additional process, thus is to be expected.

Sample	T1 (475°C)	T2 (850°C)	Clay (%)
C020	3.07	1.57	2
C021	3.55	1.72	2
C022	3.47	1.65	2
C024	3.68	2.82	4
C028	4.65	3.43	4
C029	4.47	1.18	2
029IM	3.50	1.37	2
NCH	9.70	8.41	5

Table 4.8
Theoretical and experimental clay content

By 850°C there will have been some decomposition of the clay structure itself, considering this factor there appears to be agreement between the amount of clay used in the formulation and the residual clay. A small variance was found between samples of the same batch type; hence initial indications infer that high shear mixing has distributed the clay relatively evenly through out the casting.

4.3.2

Thermo-Gravimetric Analysis: Reaction Extruded System

Thermal Gravimetric Analysis (TGA) was used to ascertain the weight of clay present, once the polymer had been totally degraded. As relatively small amount of samples (5-10mg) were tested repeated from varied areas of casting, these result providing a crude indication of dispersion through the sample as a whole.

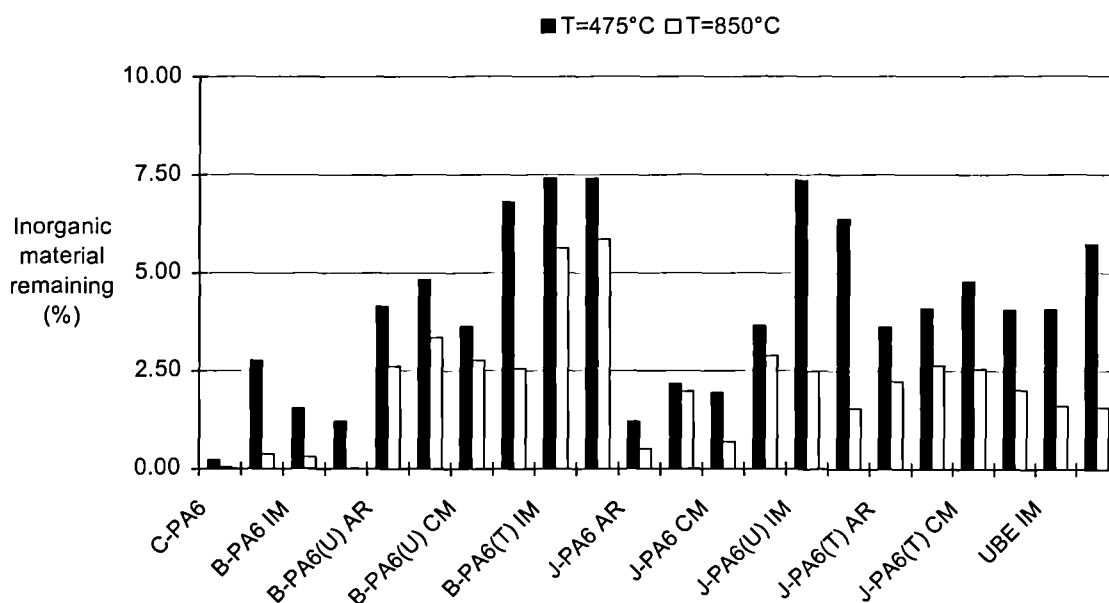


Figure 4.10
Summary of thermal gravimetric analysis results

Adsorbed water is lost at approximately 105°C from the external surfaces of the clay, but a much higher temperature, from 120-300°C, is required for the evolution of inter-layer water and water associated with the exchangeable cations. Hence at a temperature of 475°C it can be assumed that loss of water owing to these processes is complete. However, it is prior to the main decomposition endotherm, which occurs at about 700°C, when the hydroxyl groups are removed as water. It is for these reasons that results were collated at 475°C and 850°C. The initial dehydration products formed are probably amorphous alumina and silica.

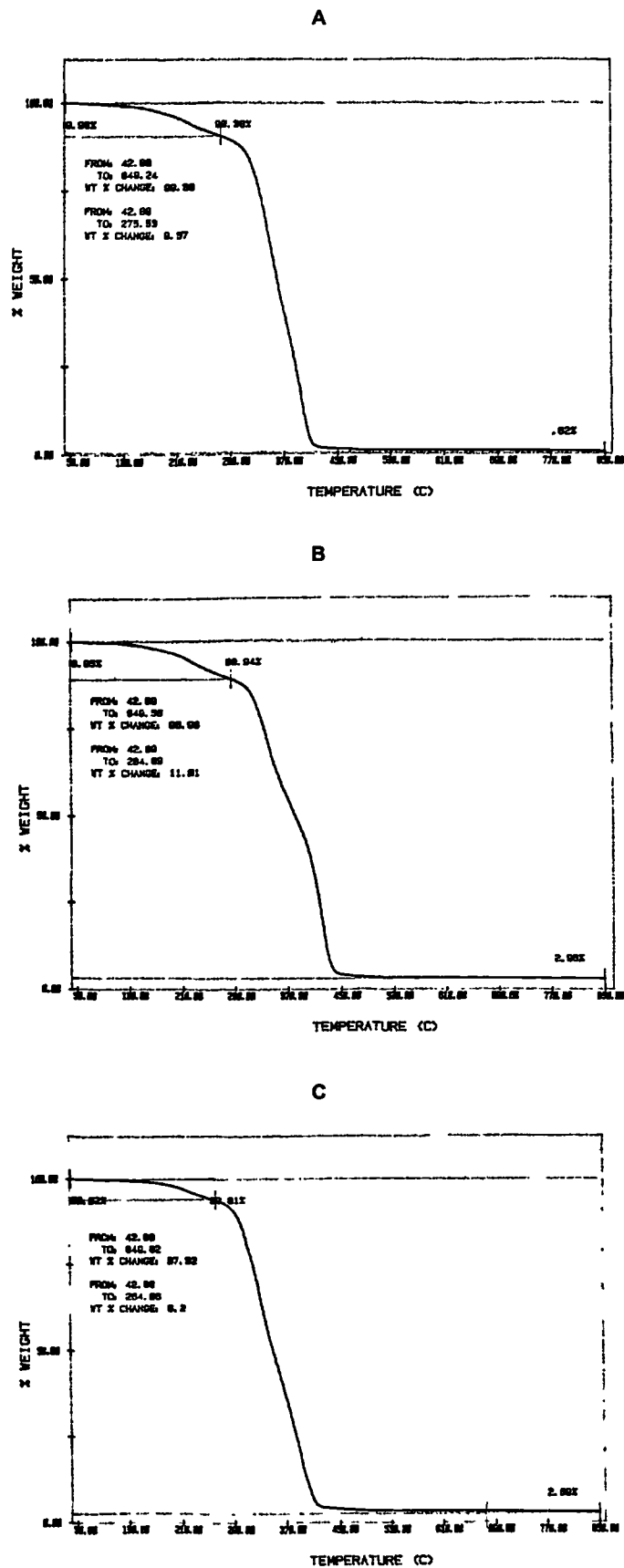


Figure 4.11
TGA Thermograms of J-PA6 (A), J-PA6(U) (B) and J-PA6(T) (C)

C-PA6 appears to have some inorganic matter present up to 475°C; this is most likely to be the aluminium compounds, which are present in the catalyst, and therefore will be present in all of the JPA series of materials. After 850°C, the remaining inorganic content of the polyamide-6 is negligible.

Injection moulding of the previously cast C029 yields no real change in the residual clay content, which as the sample material has just been subjected an additional process, is to be expected.

Sample		T1 (475°C)	T2 (850°C)	Clay (%)
C-PA6		0.23	0.04	-
B-PA6	AR	2.76	0.38	-
	IJM	1.55	0.30	-
	CM	1.21	0.01	-
B-PA6(U)	AR	4.14	2.61	4
	IJM	4.83	3.34	4
	CM	3.63	2.76	4
B-PA6(T)	AR	6.82	2.56	4
	IJM	7.42	5.64	4
	CM	7.42	5.85	4
J-PA6	AR	1.21	0.51	-
	IJM	2.18	1.99	-
	CM	1.94	0.69	-
J-PA6(U)	AR	3.65	2.88	4
	IJM	7.37	2.49	4
	CM	6.37	1.59	4
J-PA6(T)	AR	3.62	2.24	4
	IJM	4.09	2.64	4
	CM	4.79	2.55	4
UBE	AR	4.05	2.01	2
	IJM	4.08	1.61	2
	CM	5.73	1.57	2

Table 4.9
Theoretical and experimental clay content

By 850°C there will have been some decomposition of the clay structure itself, considering this factor there appears to be a good tally between the amount of clay used in the formulation and the residual clay – which is to be expected. There was also not found to be significant variance between samples of the same batch type; hence initial indications infer that high shear mixing has distributed the clay relatively evenly through out the casting.

4.3.3

Differential Scanning Calorimetry: Cast System

Differential Scanning Calorimetry (DSC) was used to monitor melting behaviour and the crystallisation temperature of the polyamide-6. The polymer melting points and the crystallisation temperatures obtained, as well as the heats of fusion ($\Delta H =$ Heat of Fusion) are listed in Table 4.12. For the purpose of comparison a cast polyamide-6 standard was produced, in which melting started at 217°C peaked at 221°C and had a peak crystallisation temperature of 169°C. This is comparable with reported values of melting at 220°C, a peak at 224°C and a peak crystallisation temperature of 170°C⁶.

The way in which a sample crystallises is dependent on multiple factors, for example the cooling rate and the presence nucleation centres. Nucleation centres, sites such as additives, remaining crystallinity and even roughness of the sample pan, are responsible for uncontrolled nucleation. The very nature of these sites means that they are not exactly reproducible.

Crystallisation is, in most systems, initiated by heterogeneous nucleation. Foreign surfaces are used to reduce the free energy opposing nucleation. The presence of these nucleating agents does not alter the crystallisation kinetics of the polymer, the whole volume of the polymer melt will start to crystallise at a temperature which is close to its melting point irrespective of these additives. During the crystallisation process heat is released, which is observed as an exothermic peak. As the rate of nucleation increases the system reaches maximum crystallinity at a higher temperature, hence exotherms for nucleated systems are detected at higher temperatures than for un-nucleated systems.

Material	Melting Point (Heating Cycle, I)						
	Onset	Peak	ΔH	Onset	Peak	ΔH	Deviation from standard
	(°C)	(°C)	(J/g)	(°C)	(°C)	(J/g)	(°C)
C-PA6				217.04	221.83	82.60	0
C020	210.86	217.76	54.96	218.45	221.77	15.79	-0.06
C021				208.74	218.23	74.66	-3.60
C022				210.65	220.18	78.01	-1.65
C024				209.29	218.97	60.98	-2.86
C028				211.53	220.50	63.22	-1.33
C029				216.12	224.15	84.03	2.32
C029 (IJM)	192.05	199.57	1.96	212.89	217.72	16.20	-4.11
NCH	169.55	188.01	37.54	199.20	203.73	112.58	-18.10

Material	Recrystallisation Temperature (Cooling Cycle, II)					
	Onset	Peak	ΔH	Onset	Peak	ΔH
	(°C)	(°C)	(J/g)	(°C)	(°C)	(J/g)
C-PA6	176.84	168.63	40.37			
C020				180.65	174.95	37.37
C021	172.98	169.73	2.63	182.86	178.53	15.92
C022				181.33	176.26	36.23
C024				182.42	178.10	38.41
C028				181.27	178.02	37.08
C029	173.20	166.38	1.20	180.80	178.64	0.35
C029 (IJM)				189.10	185.80	50.12
NCH				173.05	168.82	55.46

Table 4.10
Differential Scanning Calorimetry data of Cast series of samples

It was observed that all the reactively cast samples containing clay yielded consistent melting temperatures of between 217°C-224°C and peak crystallisation temperatures of 174°C-185°C. Compared to the cast polyamide-6 standard, which had a melting temperature of 221°C and had a peak crystallisation temperature of 169°C it is evident that crystallisation tends to occur more quickly in the presence of clay. These samples also showed a more gradual melting onset of between 7°C-10°C compared to just under 5°C for the reactively C-PA6. In the presence of a layered silicate an increase in the

crystallisation temperature is observed, which may be attributed to an increase in the nucleation rate.

In fact other layered silicates, notably talc, have been documented as being effective nucleating agents ¹⁶⁰, this has been attributed to molecule segments orientated in a zigzag conformation and attached to the substrate in the direction of the substrate. Characteristic of good nucleating agents is their small particle size and narrow size distribution, which is a benefit of the nano-scale clay.

The NCH demonstrates a significantly lower melting point, as well as a relatively broad melting peak. This could be attributed to the melting of smaller less perfectly formed crystals, which occurs at a lower temperature, and corresponds to the lower crystallisation temperature measured.

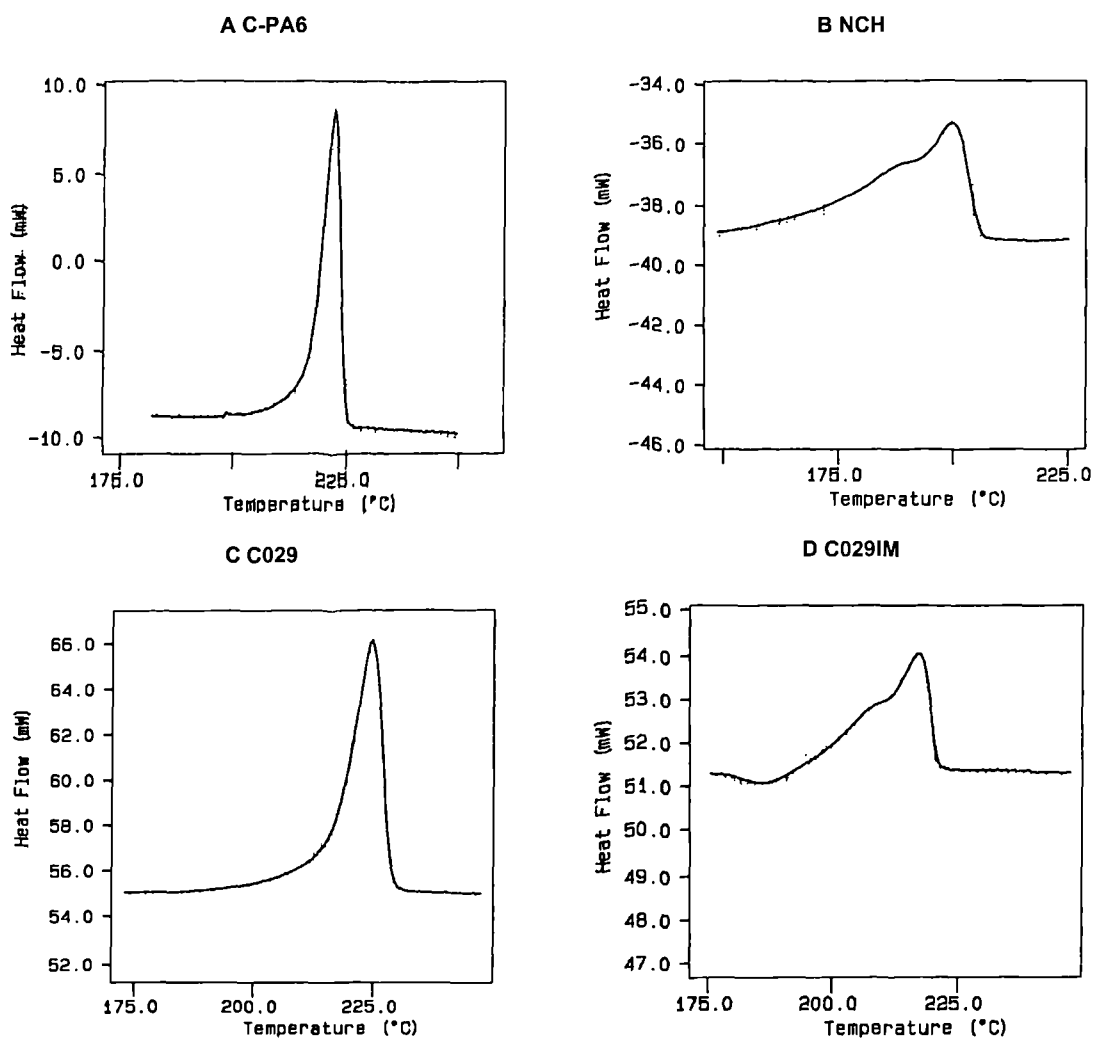
The α -phase is the most thermodynamically stable crystalline form and can be obtained by slow cooling the melt, as occurs in the casting process. The γ form can be converted into the α form by melting followed by recrystallisation. The α -phase has a reported melting range of 222-229°C, and 195-219°C for the γ -phase ¹⁶¹. However, the crystallisation of these phases is affected by the thermal treatment of the system. So a comparative method may be a more appropriate, with the α -phase having a higher melting point than the γ -phase.

Sample C029 was injection moulded after casting, to enable comparison between forms. The cast sample appears to consist mainly of α crystallites, characterised by the higher melting point; but on cooling the less thermodynamically stable γ -phase forms, hence the lower crystallisation temperature. Where as the converse is true for injection moulded samples, where on cooling the stress induced γ crystallites are recrystallised to form the more thermodynamically stable α -phase, hence the increased crystallisation temperature.

The heat of fusion (ΔH) is associated with crystallinity; a low ΔH value on heating suggests either low levels of crystallinity or that crystals formed are relatively small, and thus in both cases less energy is required to melt the crystals. Enthalpy values

observed on the heating cycle are relatively low, whilst upon the cooling cycle an increase is observed in the recrystallisation temperature and the ΔH values. Inferring that large numbers of small crystals have been formed as a result of the numerous clay particles acting as nucleating agents.

Where samples contained double peaks it is harder to compare the ΔH values, as these values are of the individual peaks, rather than the composite peak. The distinct double melting peaks, as shown in Figure 4.12, are well-documented artefacts of DSC traces. They are symptomatic of different types of crystallisation, indicating that two spherulite types are present. The first peak is attributed ¹⁶¹ to the melting of original polymer crystallites and the second peak to the melting of crystallites that have grown as a result of the DSC heating cycle. During the heating cycle the original crystals are perfected, these crystals then melt concurrently with the recrystallisation and melting of the recrystallised crystals.



Sample	DSC				XRD	
	Heating cycle I (°C)		Cooling cycle II (°C)		(°)	
	α	γ	α	γ	Figure in brackets denotes relative intensity	
C-PA6	-	221.83	-	168.63	20.12 (79)	23.79 (100)
NCH	188.01	203.73	-	168.82	19.95 (95)	23.94 (100)
C029	-	224.15	178.64	166.38	20.07 (99)	23.92 (100)
C029IM	199.57	217.72	185.80	-	21.17 (100)	-

Figure 4.12

Differential Scanning Calorimetry thermograms of Cast samples contrasted against DSC results

The NCH displays both phases from both techniques, as does C029. With the C029IM the second peak the is observed during the heating cycle could be due to melting of

crystallinities that have grown as a result of the DSC heating cycle. Hence why only one peak is observed under the cooling cycle, which correlates with the XRD result. However, the C-PA6 does not seem to display the α -phase that the XRD trace indicates is present.

4.3.4

Differential Scanning Calorimetry: Reaction Extruded System

Differential Scanning Calorimetry (DSC) was used to monitor melting behaviour and the crystallisation temperature. The polymer melting points and the crystallisation temperatures obtained, as well as the heats of fusion ($\Delta H = \text{Heat of Fusion}$) are listed in Table 4.11.

For the purpose of comparison a commercially available polyamide-6, BPA-6, was used as a control. In its as received form this materials started melting at 204°C and indicated a melting point of 219°C, which is 5°C lower than the reported values. The peak crystallisation temperature was 167°C, which is 3°C lower than the reported values. When compared to the C-PA6 the B-PA6 series, irrespective of any clay content and its nature, a decrease of approximately 2.3°C is observed.

The UBE showed the least variance in melting point, at a decrease of approximately 1.2%. The crystallisation temperature also showed very little least variance at 180°C.

With the JAL series showing the greatest decrease in melting point at on average approximately 12.1%. The crystallisation temperature also showed a small degree of variation, with the average temperature 176°C.

It was difficult to observe any trend as a result of either the absence or presence clay; or as a result of processing technique. Although these crystallinity factors influencing these results can be better understood from interpretation of the XRD results.

Material		Melting Point (Heating Cycle, I)						
		Onset	Peak	ΔH	Onset	Peak	ΔH	Deviation
		(°C)	(°C)	(J/g)	(°C)	(°C)	(J/g)	°C
C-PA6					217.04	221.83	82.60	0
B-PA6	AR				204.94	219.75	91.43	-2.08
	CM	204.53	212.11	0.38	213.84	219.97	26.84	-1.86
	IJM				209.12	220.26	52.82	-1.57
B-PA6(U)	AR	209.63	224.17	4.81	215.49	220.93	17.43	-0.90
	CM	202.97	207.05	10.71	213.50	219.75	5.19	-2.13
	IJM	207.61	212.80	-0.53	216.04	220.04	23.69	-1.79
B-PA6(T)	AR	196.08	202.10	-1.21	213.26	219.70	21.62	-2.13
	CM	193.04	198.49	3.81	210.66	217.48	10.36	-4.35
	IJM	203.29	207.07	-0.45	213.71	218.33	22.27	-3.50
J-PA6	AR				195.12	207.99	53.47	-13.84
	CM	121.90	125.37	0.78	197.12	208.78	43.27	-13.05
	IJM	121.57	125.92	0.48	199.94	212.42	53.47	-9.41
J-PA6(U)	AR				186.12	207.07	43.51	-14.76
	CM				188.29	208.43	45.14	-13.40
	IJM	112.41	121.59	2.05	199.15	209.82	57.71	-12.01
J-PA6(T)	AR				193.36	208.89	60.34	-12.94
	CM	123.67	126.61	0.43	203.79	210.95	4.57	-10.88
	IJM	119.74	126.73	1.63	205.57	212.94	65.44	-8.89
UBE	AR	208.75	210.90	2.29	216.10	221.02	15.68	-0.81
	CM	205.69	212.42	21.20	216.80	220.47	6.99	-1.36
	IJM				214.83	220.48	16.81	-1.35

Material		Recrystallation Temperature (Cooling Cycle, II)					
		Onset	Peak	ΔH	Onset	Peak	ΔH
		(°C)	(°C)	(J/g)	(°C)	(°C)	(J/g)
C-PA6		176.84	168.63	40.37			
B-PA6	AR	177.52	167.01	-52.68			
	CM	176.38	169.65	-18.42	188.18	182.20	-2.32
	IJM				186.16	182.77	-53.50
B-PA6(U)	AR				187.71	184.37	-48.41
	CM				187.88	184.86	-44.88
	IJM				190.63	186.91	-48.92
B-PA6(T)	AR				184.35	183.28	-43.60
	CM				184.44	183.46	-43.03
	IJM				186.41	186.41	-46.24
J-PA6	AR				177.60	173.54	-50.17
	CM	113.69	111.15	-0.92	179.34	174.67	-49.14
	IJM	113.38	111.11	-0.49	183.48	179.25	-52.76
J-PA6(U)	AR				177.73	172.83	-42.84
	CM				179.45	175.11	-44.68
	IJM	106.97	104.42	-1.38	183.45	178.66	-52.29
J-PA6(T)	AR				174.82	173.00	-50.26
	CM	114.19	111.90	-0.55	178.97	174.13	-48.28
	IJM		115.43	-0.86	182.48	179.18	-51.68
UBE	AR				183.56	180.87	-32.26
	CM				184.47	180.75	-48.70
	IJM				183.51	179.67	-51.94

Table 4.11
Differential Scanning Calorimetry data of extruded polyamide-6 samples

The α -phase is the most thermodynamically stable crystalline form and can be obtained by slow cooling the melt, as occurs in the casting process. The γ form can be converted into the α form by melting followed by recrystallisation. Therefore processing techniques (i.e. injection moulded and compression moulding) post-extrusion should result in changes in the crystalline structure. The α crystallites are more thermodynamically stable and are typically characterised by their higher melting point. With the less thermodynamically stable γ -phase having a lower crystallisation temperature.

The way in which a sample crystallises is dependant on multiple factors, for example the cooling rate and the presence nucleation centres. The very nature of these sites means that they are not exactly reproducible. Crystallisation is, in most systems, initiated by heterogeneous nucleation. During the crystallisation process heat is released, which is observed as an exothermic peak. As the rate of nucleation increases the system reaches maximum crystallinity at a higher temperature, hence exotherms for nucleated systems are detected at higher temperatures than for un-nucleated systems.

Again the distinct double peaks are present as artefacts of the DSC technique. They are symptomatic of different types of crystallisation, indicating that two spherulite types are present. There was also an emergence of a very small melting and re-crystallization peaks at 120-125°C and 110-115°C respectively, for the J-PA6 series of materials. One possibility is that it reflects reorganisation of the polyamide structure.

4.3.5

X-Ray Diffraction: Cast System

Intercalation changes the dimensions between the silicate layers, so an increased layer distance indicates the formation of a nanocomposite. This is seen as a reduction in the diffraction angle, which corresponds to an increase in distance between the silicate layers. However, care must be taken, as what may well appear intercalated using X-ray Diffraction (XRD), may under Transmission Electron Microscopy be exfoliated.

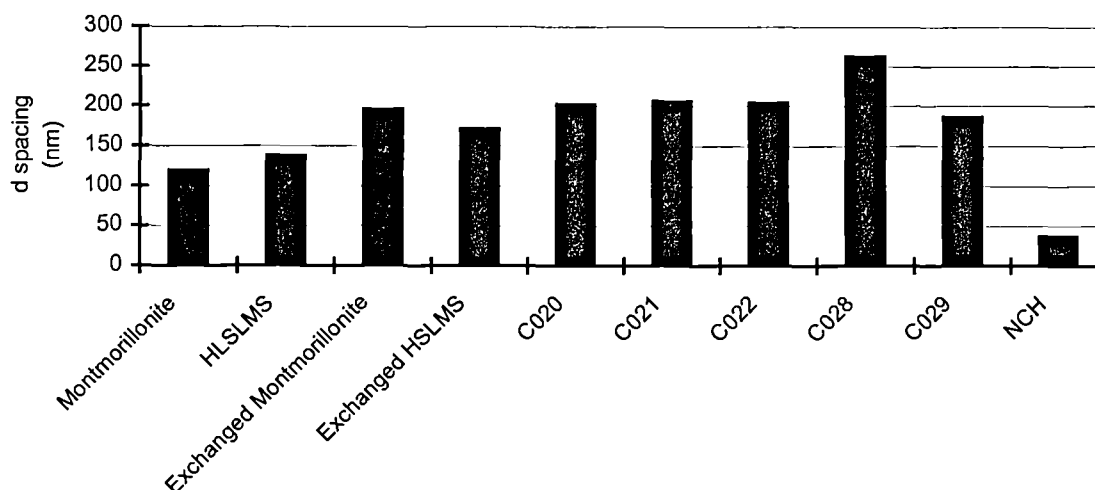


Figure 4.13
Summary of *d*-spacings from X-ray Diffraction Traces

A computer connected to the X-ray diffractometer running Traces V3 software calculated the *d*-spacing from the angle obtained using the Bragg equation, as discussed in section 3.8.3. A full listing of XRD results is located in Appendix IV.

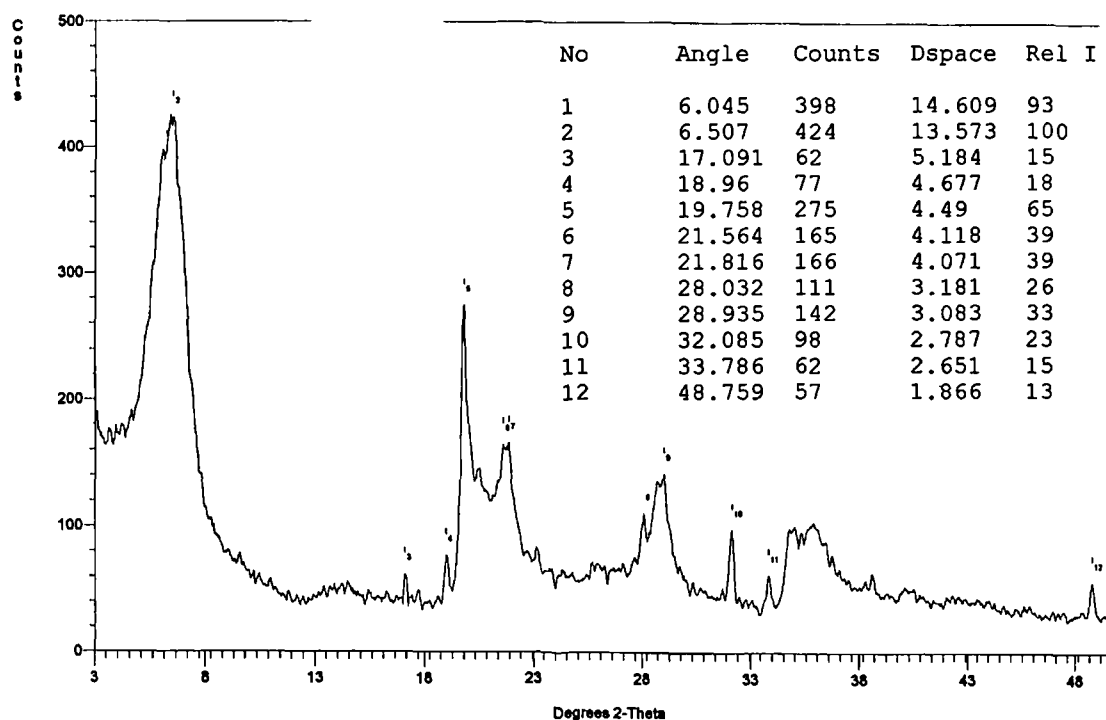


Figure 4.14
XRD Trace for Montmorillonite

The *d*-spacing for natural montmorillonite has reported as being of 1.31nm⁵⁷, 1.14nm⁹³, 1.32nm¹⁶⁸ and for the basal (001) plane. There is a degree of variation, which has to be expected with natural minerals. The experimental result obtained was approximately 1.20nm, which is comparable to the reported values. Once exchanged both the montmorillonite and the hydrous sodium lithium magnesium silicate demonstrate an increase in *d* spacing compared with their untreated states. Intercalated basal spacings have been reported at 1.66nm⁵⁷ and 1.77nm⁹³. However this figure was exceeded with experimental results of over 1.95nm recorded, Figure 4.13. These results are summarised in Table 4.12.

Clay Sample	Untreated Clay <i>d</i> -spacing (nm)	Treated Clay <i>d</i> -spacing (nm)	Increase in <i>d</i> -spacing (nm)
Montmorillonite	1.20	1.96	0.76
Hydrous sodium lithium magnesium silicate	1.38	1.72	0.34

Table 4.12
Summary of silicate layer spacings

Hydrous sodium lithium magnesium silicate is a synthetic form of montmorillonite, synthetic clays tend to be cleaner and more consistent than their natural counterparts. Yet the increase in interlayer spacing observed is approximately half that of montmorillonite. So perhaps this very inconsistency and impurity of natural clay lends itself to the natural clay being more susceptible to alterations within the layer structure. So on the basis of this result it was decided to use the montmorillonite clay for the exchange process.

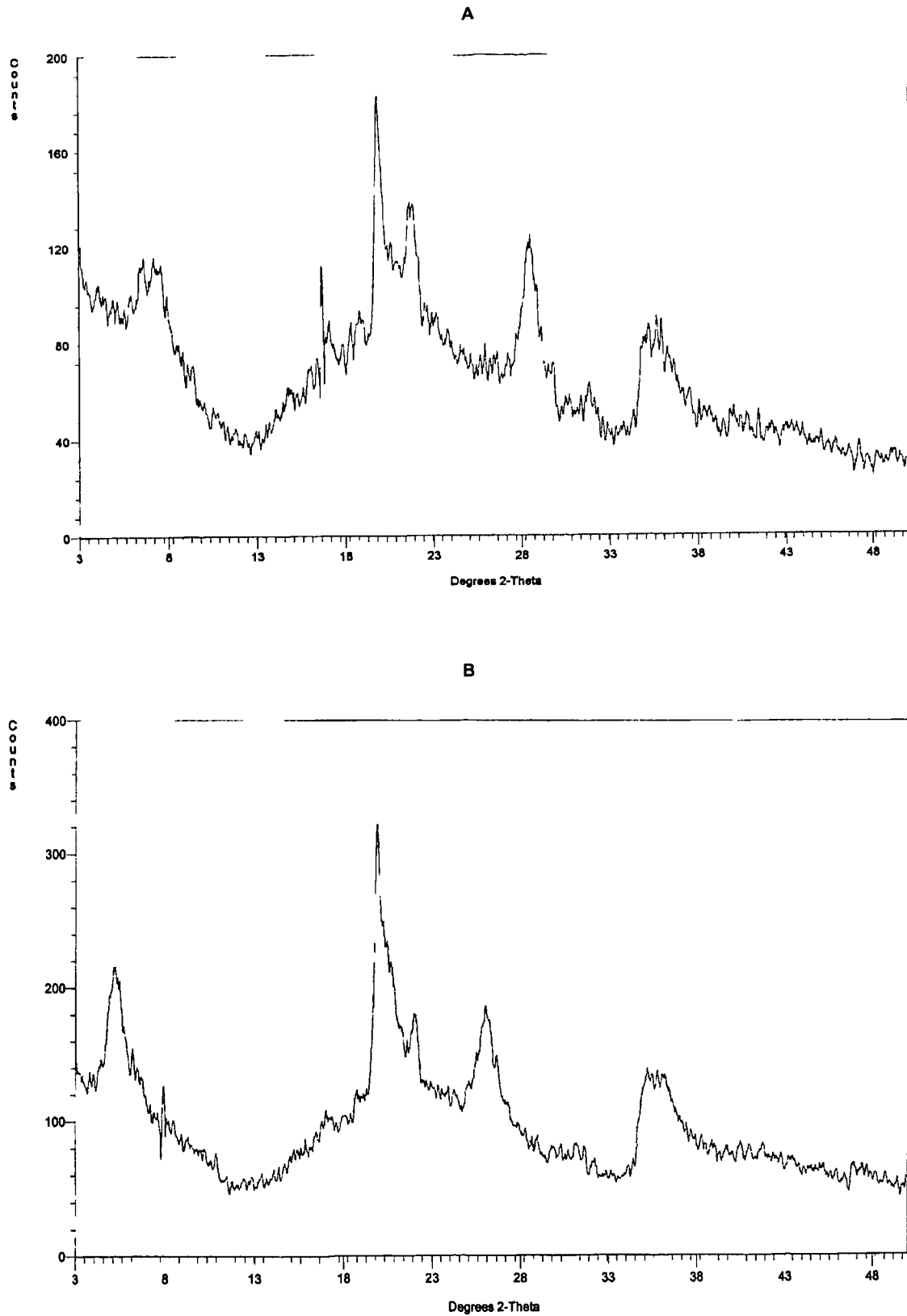


Figure 4.15
Comparison of XRD traces for untreated (A) and treated (B) montmorillonite

The diffraction pattern of completely amorphous polyamide-6 would be a broad diffuse halo with maximum intensity at ca. 22°. Reported values of 2θ for the crystalline phases are 158:

Phase	Plane	2θ (°)
α_1	200	21
α_2	002 + 202	24
γ_1	100	22
γ_2	$\bar{2}01 + 200$	23

Table 4.13
Reported 2° values for metastable crystalline phases in CPA-6

As can be seen from the XRD trace of the C-PA6, Figure 4.16, the alpha peaks occur at 20.24° corresponding to α_1 , and at 23.94° corresponding to α_2 . The gamma peaks are harder to discern. One peak is visible at 21.44° corresponding to the γ_1 peak; there is a shoulder on the base of the α_2 peak that could be the γ_1 peak. But the relative intensity of the gamma phase peaks infers that there is not much γ present, which is not surprising as this phase tends to be induced under stress, a factor that was absent in the casting process. Note the absence of any 2θ peaks in the 3-5° range, as these peaks are associated with the presence of a layered silicate.

Sample	Untreated Clay d -spacing (nm)	Difference in d -spacing Post Exchange Process (nm)
C020	2.03	+ 0.07
C021	2.06	+ 0.11
C022	2.04	+ 0.09
C028	2.63	+ 0.67
C029	1.86	- 0.09

Table 4.14
Difference in d -spacings after exchanging compared with untreated clay

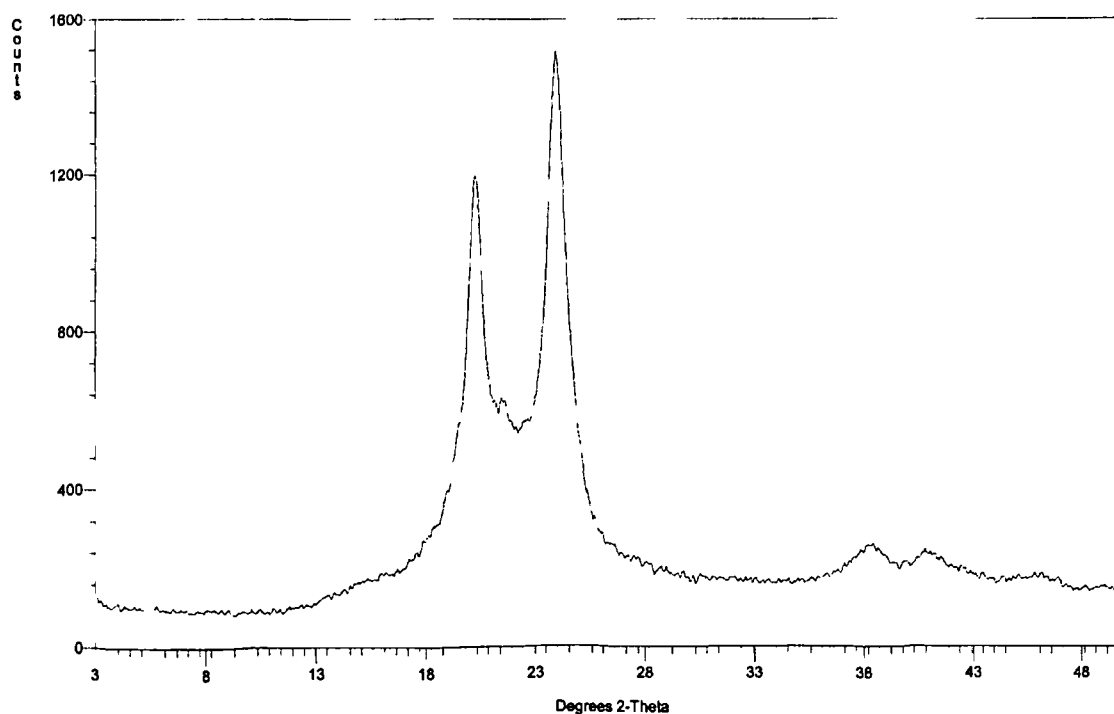


Figure 4.16
XRD trace of C-PA6

The cast (C020*) series of composites, in general, display a further increase in the interlayer spacing compared with exchanged montmorillonite. So this increase in d -spacing could well be caused by polymerisation occurring between the silicate layers. The biggest increase was observed in C028, which contained double the amount of clay compared to the other samples tested.

An exception is that within the cast series, C029 exhibits a decrease in d -spacing. A possible explanation for this includes that polymerisation did not only occur between the layers, rather polymerisation outside these silicate layers, lead to them being compressed rather than expanded.

These two observations are exemplified in Figure 4.17. The difference in the inter-layer spacing is visible by the difference in relative intensity of the first peak, which corresponds to the basal spacing of the clay. Inferring that the cast series of materials are have formed an intercalated nanocomposite, where as the NCH has not. So in this case of the NCH sample if polymerisation has occurred between the layers it has not lead to any further expansion of these layers. However, this result is not conclusive, microscopy has to be used to qualify this.

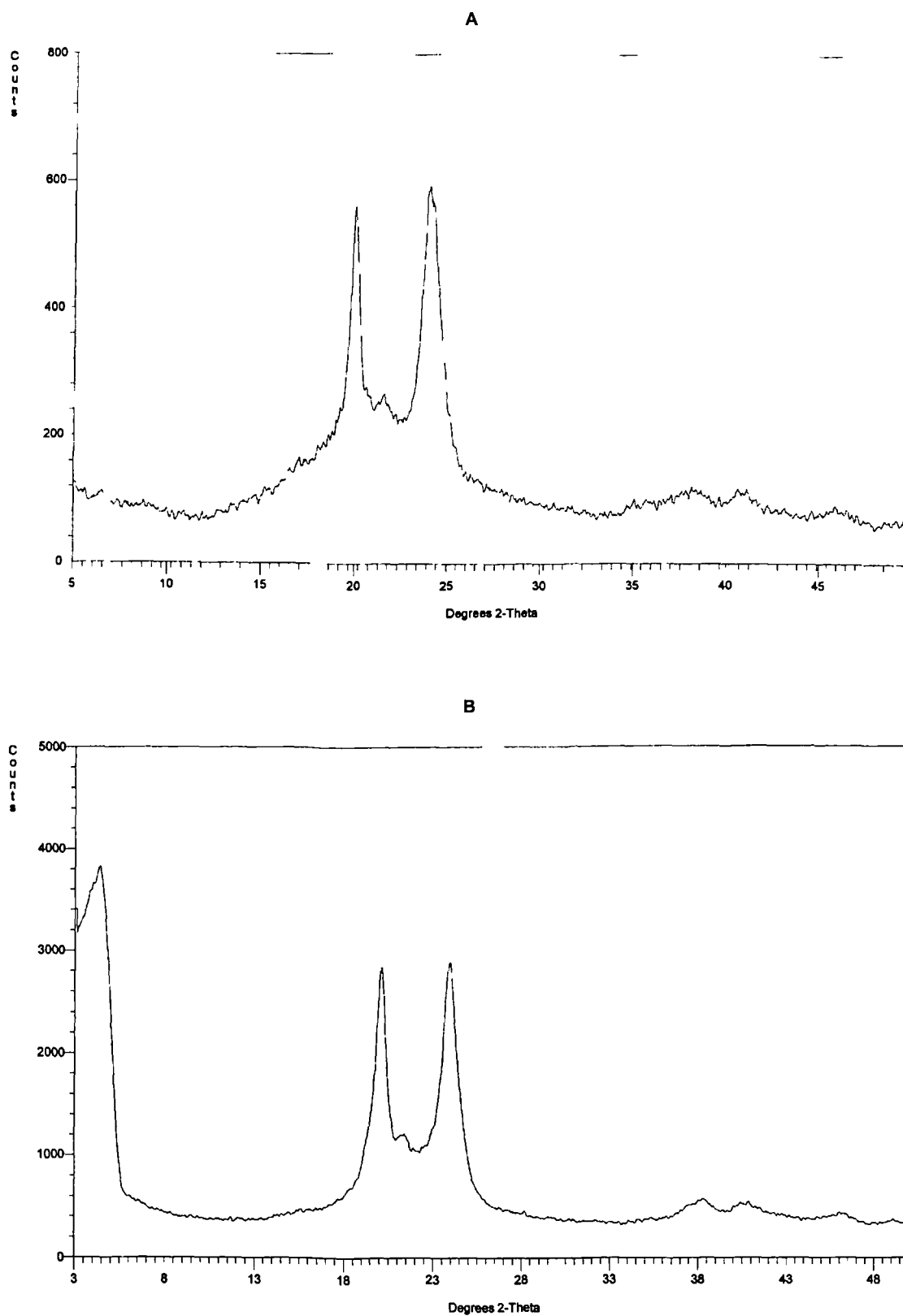


Figure 4.17
Comparison of NCH (A) and C028 (B) X-ray Diffraction traces

4.3.6

X-Ray Diffraction: Reaction Extrusion System

Intercalation changes the dimensions between the silicate layers, so an increased layer distance indicates the formation of a nanocomposite. This is seen as a reduction in the diffraction angle, corresponding to an increase in distance between the silicate layers. A full listing of XRD results is located in Appendix IV.

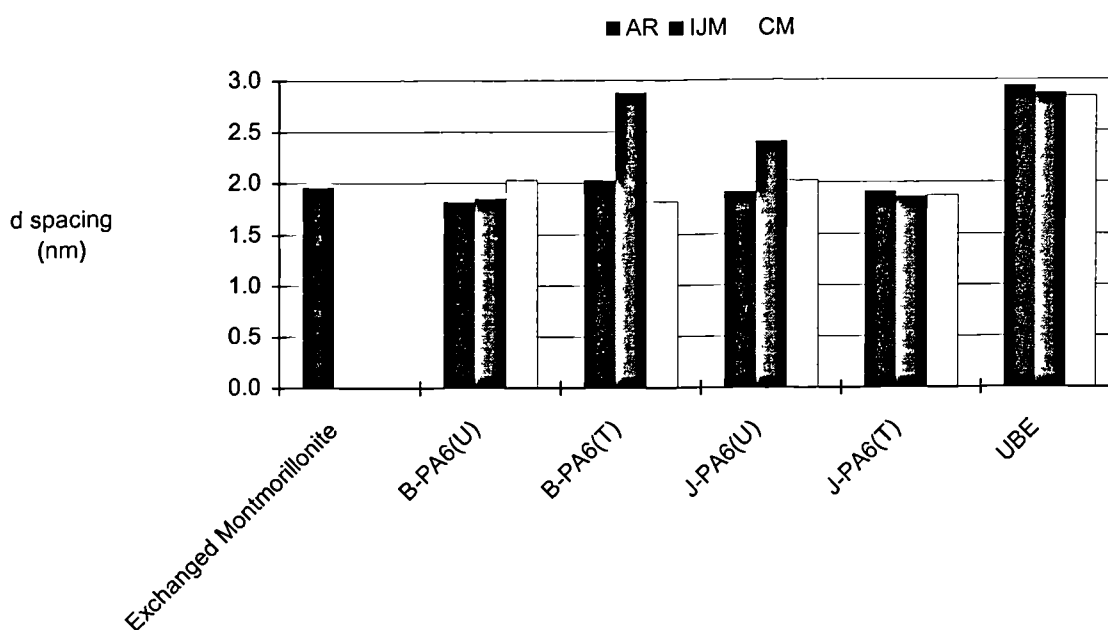


Figure 4.18
Summary of *d*-spacings from X-ray Diffraction Traces

The *d*-spacing for natural montmorillonite is reported as being of 1.31nm for the basal (001) plane, the experimental result obtained was approximately 1.20nm. This is slightly lower in comparison, however a degree of variation has to be expected with natural minerals. Intercalated basal spacings have been reported at 1.66nm. However this figure was exceeded with experimental results of over 1.95nm recorded, Table 4.15.

Clay Sample	Untreated Clay <i>d</i> -spacing (nm)	Treated Clay <i>d</i> -spacing (nm)	Increase in <i>d</i> -spacing (nm)
Montmorillonite	1.20	1.96	0.76

Table 4.15
Summary of silicate layer spacings

The UBE material demonstrated the greatest inter-layer expansion, on average approximately 0.93nm. Such a large increase in *d*-spacing could well be caused by polymerisation occurring between the silicate layers, especially as this material contained 2wt% clay compared to 4wt% in the other samples.

Most of the samples exhibit a decrease in *d*-spacing, although this is still in excess of the untreated clay *d*-spacing. Possible explanations for this result could be that polymerisation did not only occur between the layers, but outside the silicate layers as well, leading to the layers being compressed rather than expanded.

Sample		<i>d</i> -spacing of composite (nm)	Difference in <i>d</i> -spacing compared with exchanged montmorillonite (nm)
B-PA6(U)	AR	1.82	- 0.14
	CM	2.03	0.08
	IJM	1.85	- 0.11
B-PA6(T)	AR	2.03	0.08
	CM	1.82	- 0.13
	IJM	2.8	0.92
J-PA6(U)	AR	1.91	- 0.05
	CM	2.02	0.06
	IJM	2.40	0.44
J-PA6(U)	AR	1.91	- 0.04
	CM	1.87	- 0.09
	IJM	1.86	- 0.09
UBE	AR	2.94	0.99
	CM	2.84	0.88
	IJM	2.87	0.91

Table 4.16
Difference in d-spacings after exchanging compared with untreated clay

The XRD results do not display much information by the way of trends. Neither the type of clay (treated or untreated) nor the processing technique (compression or injection moulded) appears to yield consistent results.

The diffraction pattern of completely amorphous polyamide-6 would be a broad diffuse halo with maximum intensity at ca. 22°. Reported values of 2θ for the crystalline phases are ¹⁵⁸ shown in Table 4.17 and experimentally can be seen from the XRD trace of CPA-6 in Figure 4.17.

Phase	Plane	2θ (°)
α_1	200	21
α_2	002 + 202	24
γ_1	100	22
γ_2	201 + 200	23

Table 4.17
Reported 2° values for metastable crystalline phases in CPA-6

In Figure 4.19 the transformations within the J-PA6 series are visible. Note the absence of any 2θ peaks in the 3-5° ranges, these peaks are associated with the presence of a layered silicate. The sample starts off being predominately α , with some γ present. Upon injection moulding the crystal phase is mainly in the γ -phase. Which as this phase tends to be induced under stress is to be expected. With the compression-moulded samples, which are produced under conditions of constraint, are once more predominately α , with some γ present.

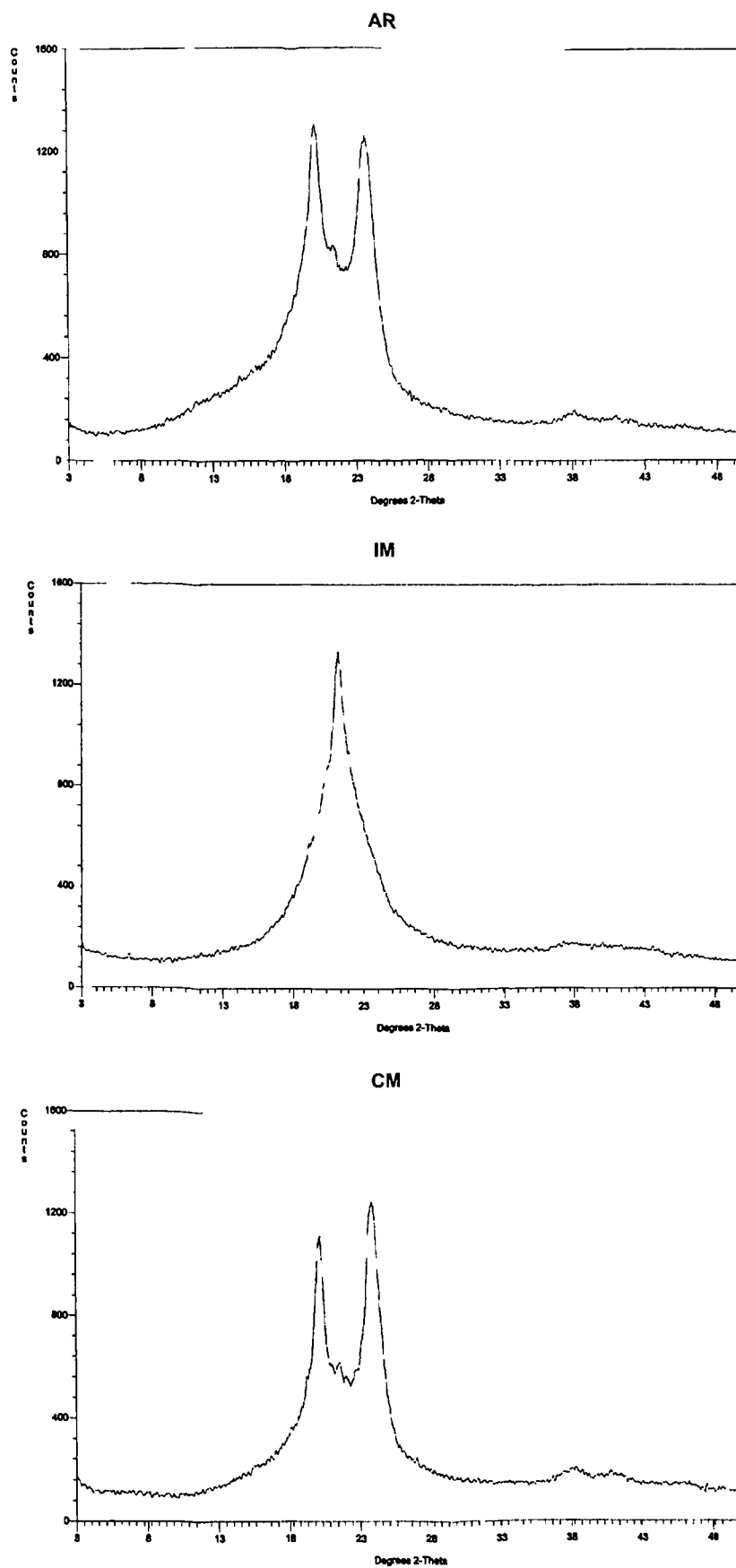


Figure 4.19
J-PA6 X-ray Diffraction Traces

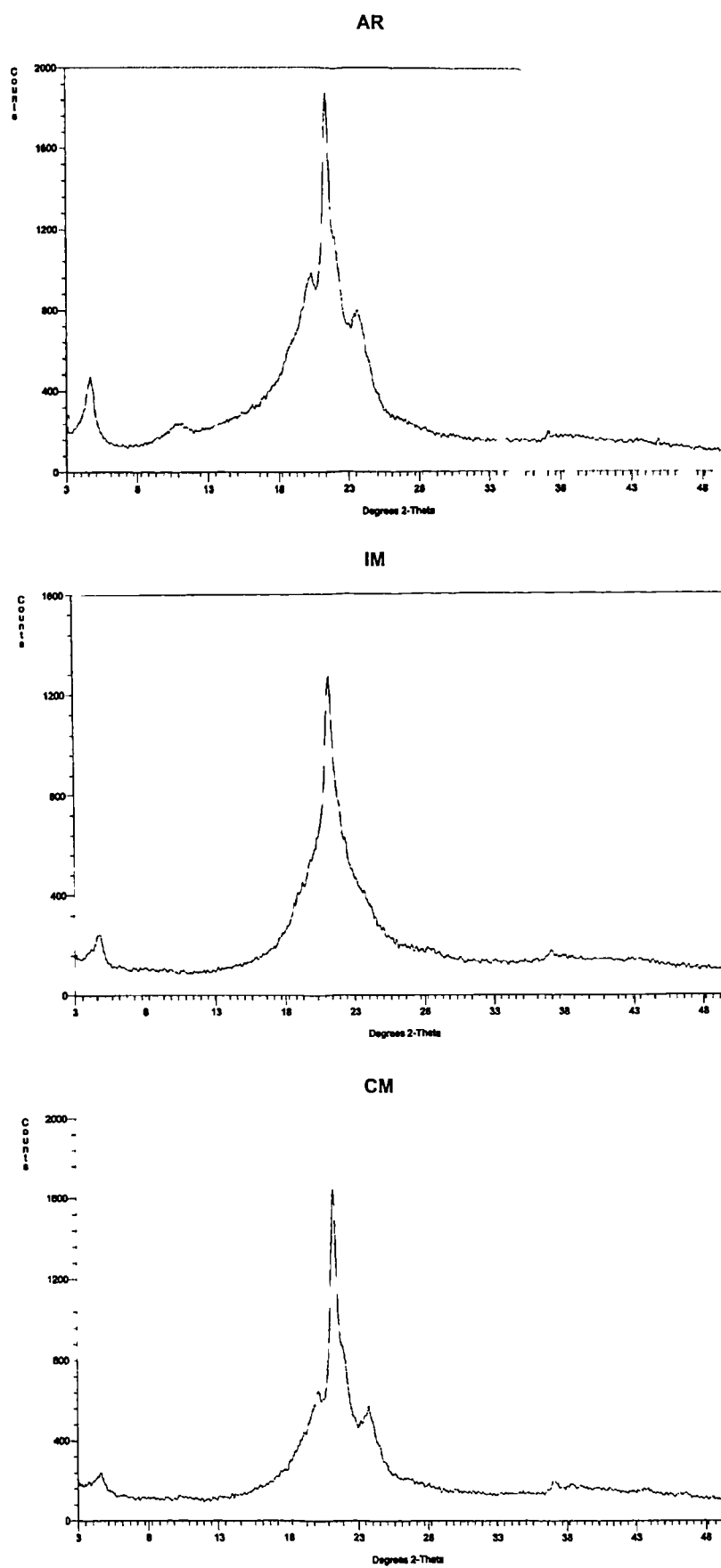


Figure 4.20
J-PA(U) X-ray Diffraction Traces

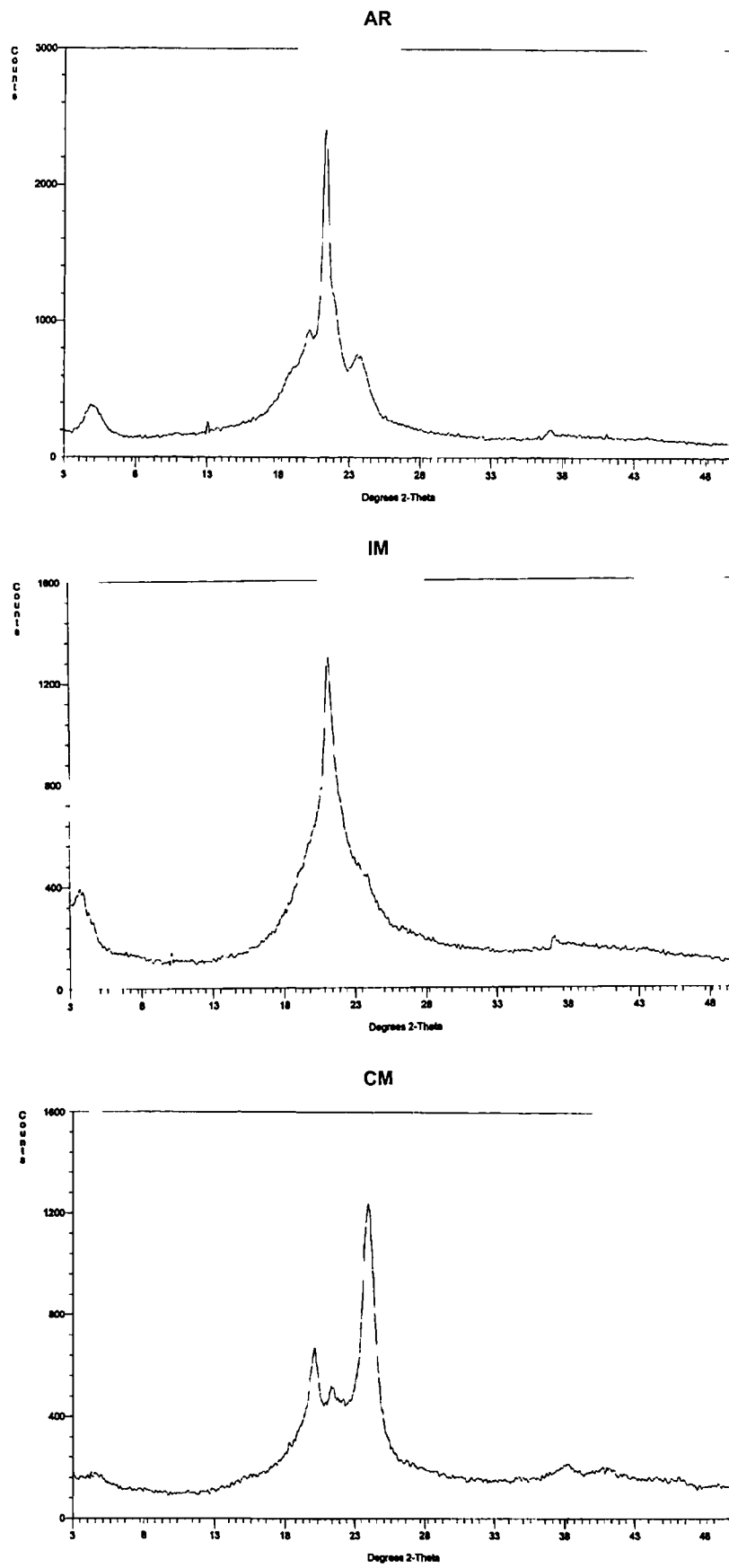


Figure 4.21
J-PA(T) X-ray Diffraction Traces

In Figure 4.20 the transformations within the J-PA6(U) series are visible. Note the presence of the 2θ peaks in the $3-5^\circ$ ranges; these peaks are associated with the presence of a layered silicate. The sample starts off being predominately γ , with some α present. Upon injection moulding the crystal phase is mainly in the γ -phase. Which as this phase tends to be induced under stress is to be expected. With the compression moulded samples, which are produced under conditions of constraint, the sample returns to being predominately α , with some γ present.

In Figure 4.21 the transformations within the J-PA6(T) series are visible. Once again the 2θ peaks are associated with the presence of a layered silicate peaks are present the $3-5^\circ$ ranges. The sample starts off being predominately γ , with some α present. Upon injection moulding the crystal phase is mainly in the γ -phase. Which as this phase tends to be induced under stress is to be expected. With the compression-moulded samples, which are produced under conditions of constraint, the sample returns to being predominately α , with some γ present.

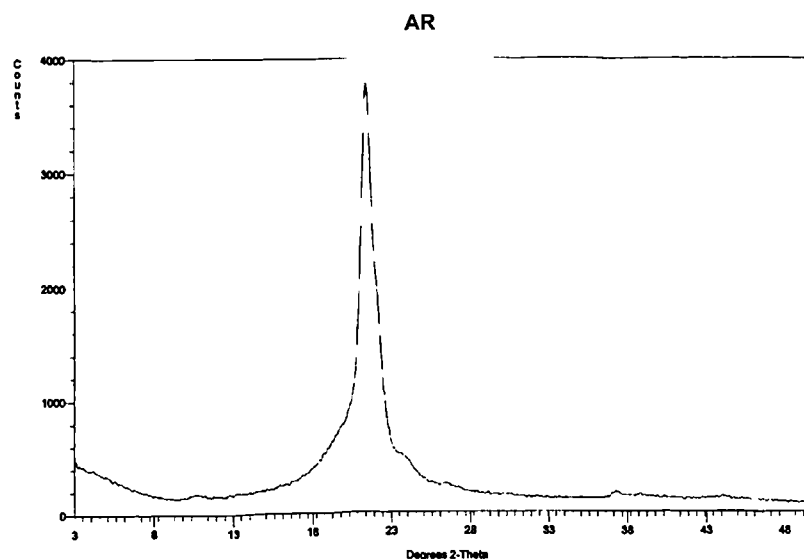


Figure 4.22
UBE X-ray Diffraction Traces

Figure 4.22 is representative of the crystal structure of the UBE material. The 2θ peak associated with the presence of a layered silicate peaks are present the $3-5^\circ$ ranges, but is a more gradual incline. The sample displays γ crystal structure in all three states: as received, injection moulded and compression moulded the crystal phase is mainly in the γ -phase.

4.4

Microscopic Analysis

Initially a series of test pours were conducted to ascertain the best method for treating clays. Having identified the method that produced the best result, the corresponding process was then used to treat all the clays in the subsequent experiments.

4.4.1

Scanning Electron Microscopy: Cast System

Test pours C003 and C007 both contain the same amounts of catalyst and activator, with neither containing clay. There does not appear to be significant difference between the samples. The former however, contains 1wt% of an anti-foaming agent. This additive is primarily added to reduced the foaming that occurs when the samples are transferred between containers. Although when the samples were transferred from the glass bottles to the specimen tubes, there was no appreciable visible difference to the naked eye in sample consistency.

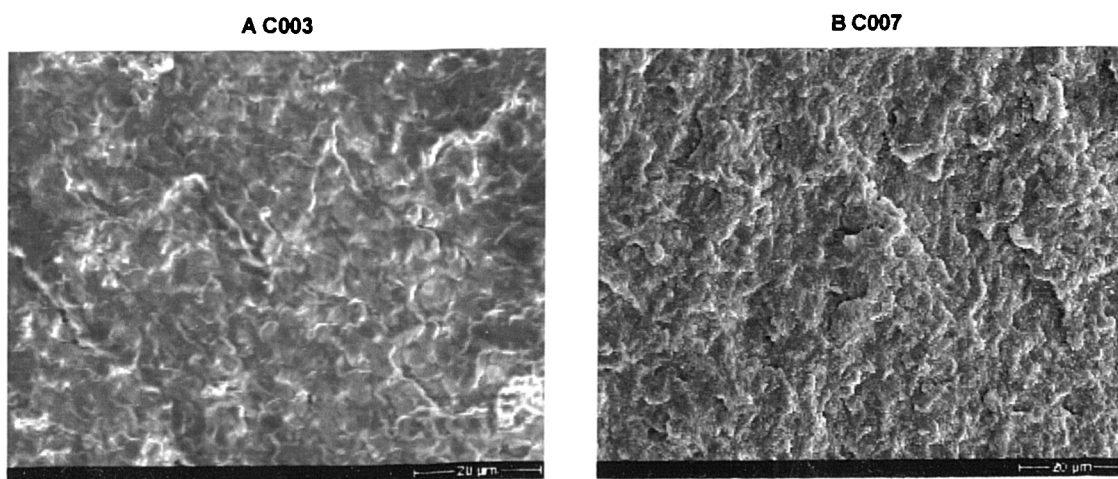


Figure 4.23
SEM images of initial test pours

On the basis of this inspection it was decided to continue the test pours without the addition of the anti-foaming agent, largely because it appears to have little effect where

these small volumes are concerned, but also because Figure 4.23 **B** exhibits an increased surface texture. This texture may provide an increased number of possible nucleation sites enabling increased crystallisation.

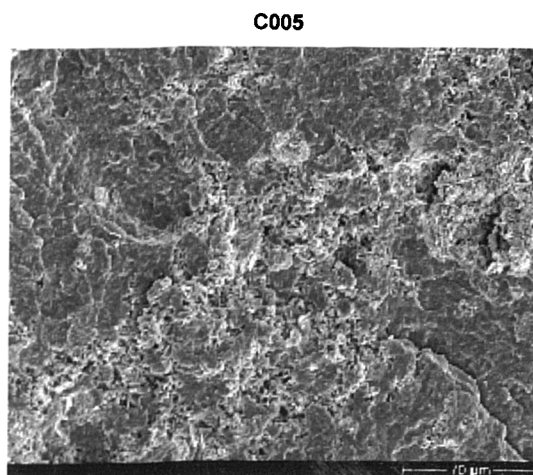


Figure 4.24
SEM image of initial test pours

Sample C005, Figure 4.24, contained 4wt% clay, during production much of this clay sank to the bottom of the specimen tube during the polymerisation process. So there was unequal dispersion of the clay and clay agglomerates can be observed on the surface. There was little expectation of polymerisation being able to occur between the layers, and there is no evidence to suggest that it has, as the clay had not undergone any modification.

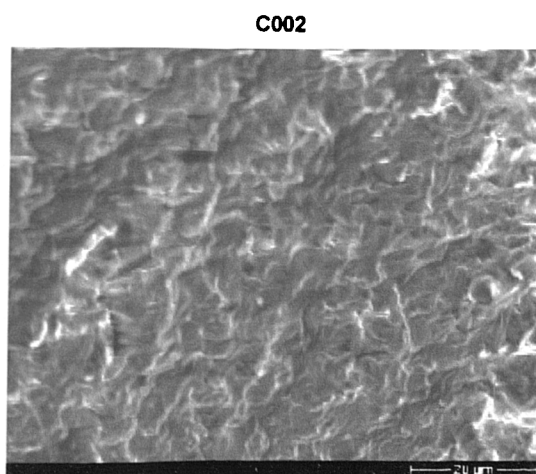


Figure 4.25
SEM image of initial test pours

The sample shown in Figure 4.25 was prepared using the (MG) exchanged clay. During production nearly all of the clay content sank to the bottom of the specimen tube before polymerisation had occurred. A few clusters aggregates are present, but the structure is mainly comparable with that of C007, a cast polyamide-6.

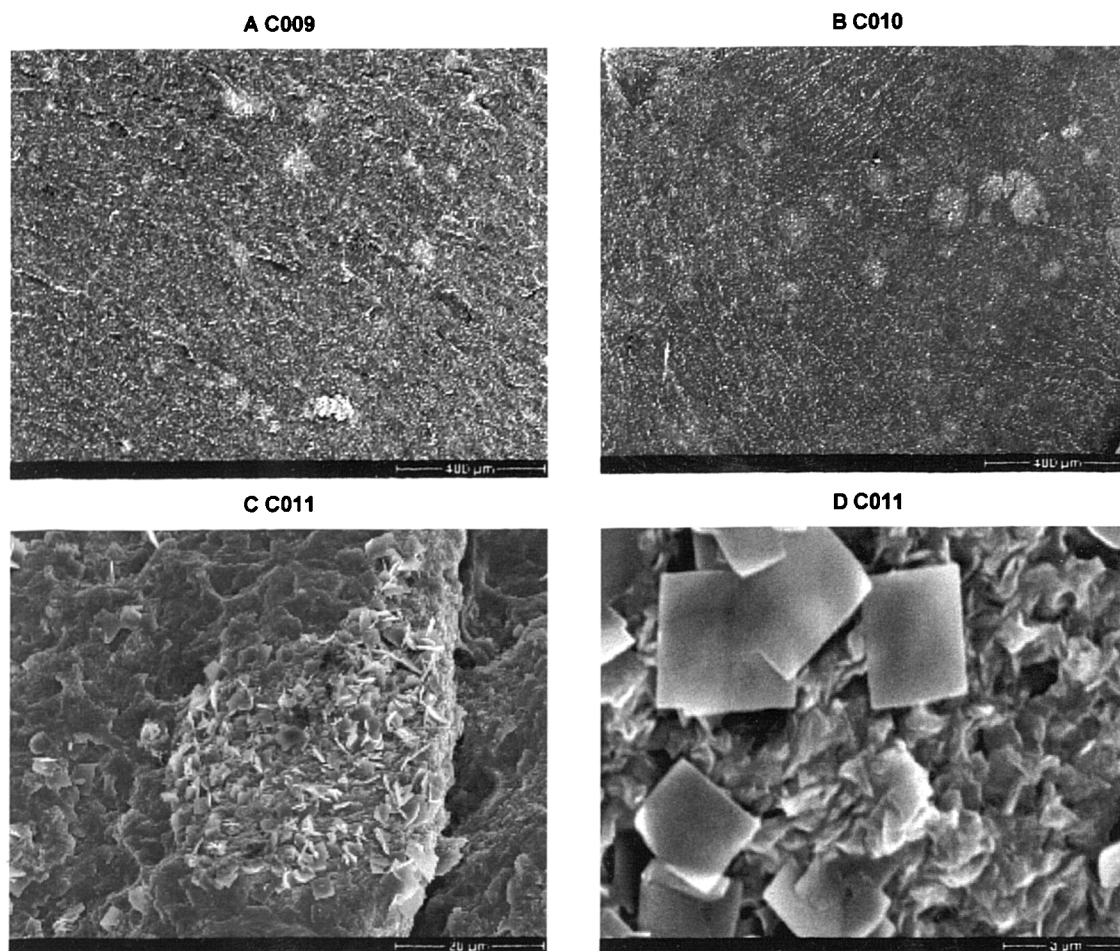


Figure 4.26
SEM images of initial test pours

Sample C011, Figure 4.26 c, contains large areas of poorly dispersed catalyst, exemplified by the increased magnification image, Figure 4.26 d. Hence there was concern that in this instance the individual components were not able to mix properly and that this was inhibiting the polymerisation process. With samples C009 and C010 the activator was added, there was a ten-minute interval; the catalyst was then added, there was another ten-minute interval; and finally the clay was added. The concept being that the activator and catalyst were completely dispersed within the ϵ -caprolactam, and that polymerisation had conceivably started when the clay was added. Reducing the possibility of the clay addition poisoning polymerisation.

Sample C010, contains twice as much treated clay as C090, in both cases areas of poor dispersion are visible, Figure 4.26 A and B. Clay agglomerates are still present in this (AU) Series, but the clay appears to be dispersed through out the sample. Inferring that the clay treatment itself still needed to be optimised, as the presence of an aggregate precludes interlayer polymerisation.

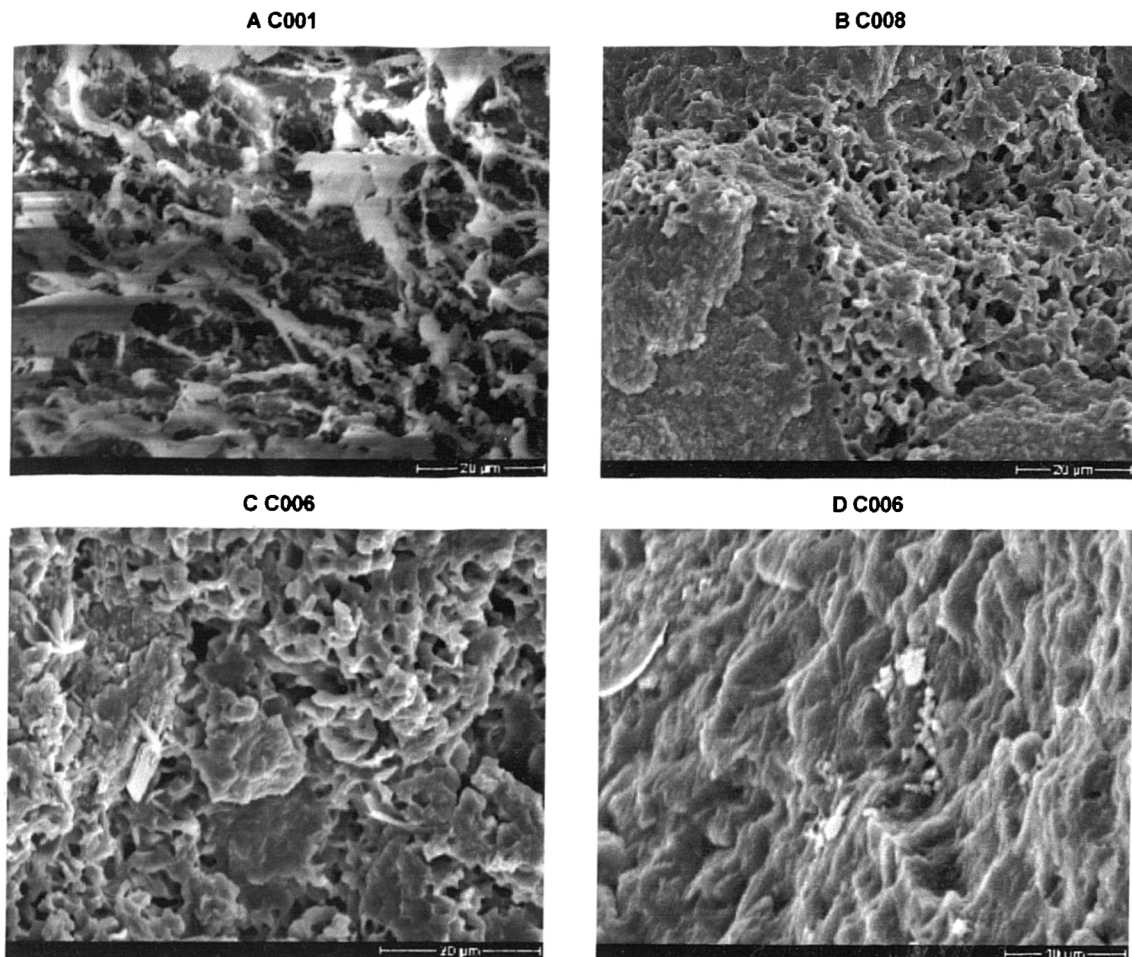


Figure 4.27
SEM images of initial test pours

As shown in Figure 4.27 sample C001 has formed a very porous sample, with what appears to be large clay agglomerates. Although it is difficult to be precise as the sample was of very poor quality and consequently difficult to prepare, resulting in the charging lines visible across the sample surface.

Sample C006 contained the minimum amount of catalysts and activator used. The sample is again of a very porous nature, increasing the amount of catalyst and activator, as for C008, appears to reduce this porosity – compare Figure 4.27 **b** and **c**. Clay agglomerates are still present, as shown in Figure 4.27 **d**, although the average size of these is relatively small when compared with previous samples.

On the basis of these images it was decided to proceed using the (AU) method of exchanging clay and to stagger addition of the reagents. The ratio of activator to catalyst that was subsequently used was in the order of 2%: 5%.

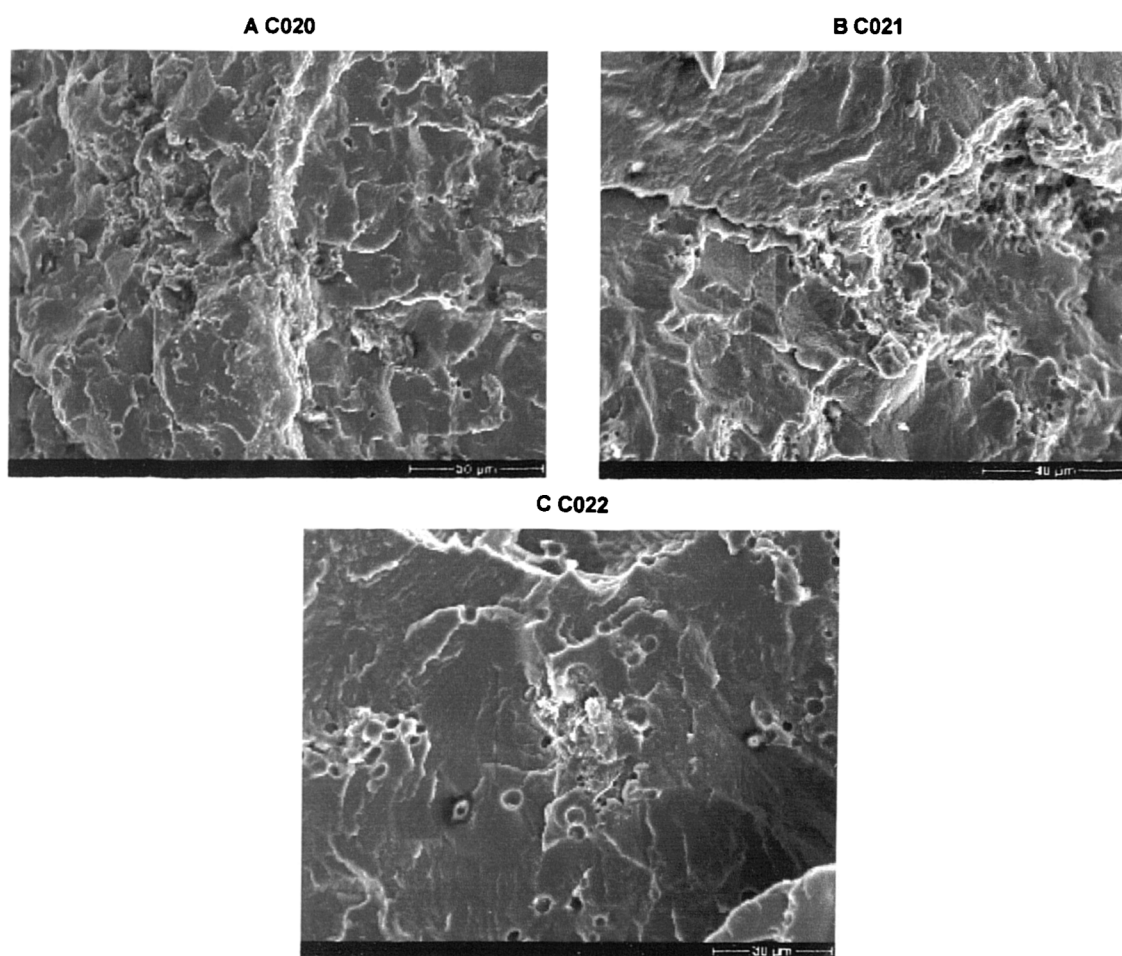


Figure 4.28
SEM images of initial test pours

Porosity is present in several of the samples; there are various possibilities as to why it is present. The first being the adsorption of water, which is known to affect the polymerisation of polyamide, and given the length of time that the polymer took to cast some adsorption of atmospheric moisture is inevitable. A greater factor is air being

contained within the sample. The samples were produced using high shear mixing, during this process air would undoubtedly enter the mixture owing to the stirring mechanism. The casting was not pressurised so there was no way to force the air out, hence pores were formed as the trapped air slowly rose to the surface of the casting.

The primary reason for conducting trials using these materials was to compare a montmorillonite clay, which has been previously surface treated. These three clays already contained an organic chain, which had been grafted onto the montmorillonite. This organic chain increased in length, as follows: 30B > 25A > 15A, Figure 4.29. So correspondingly decreased in hydrophobicity over that range.

All the samples C020, C021 and C022 demonstrate the presence of air bubbles, which will obviously compromise their physical performance, although the addition of an anti-foaming agent may reduce this occurrence. Clay agglomerates are also visible on the surface, inferring that despite the changes in hydrophobicity this is not sufficient to induce interlayer exfoliation. Although porosity does not appear to be such a major factor with these range of clays.

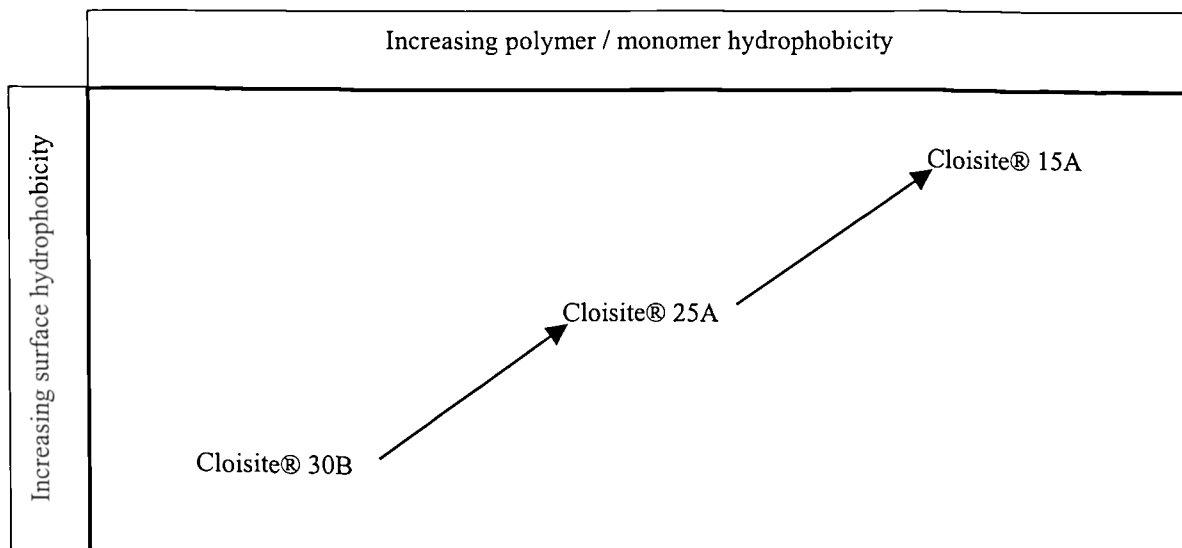


Figure 4.29
Structure of the Cloisite® clays

The polymerisation reaction appears to have occurred more uniformly through these samples. However, the results achieved do not demonstrate that the addition of the organic surface treatment has any beneficial effect on the inter-layer expansion.

The image of the B-PA6 material, Figure 4.30, shows no areas of porosity. Also the surface texture appears to be very uniform. Thus highlighting that the polymerisation reaction does not appear to be optimal with the cast range of materials.

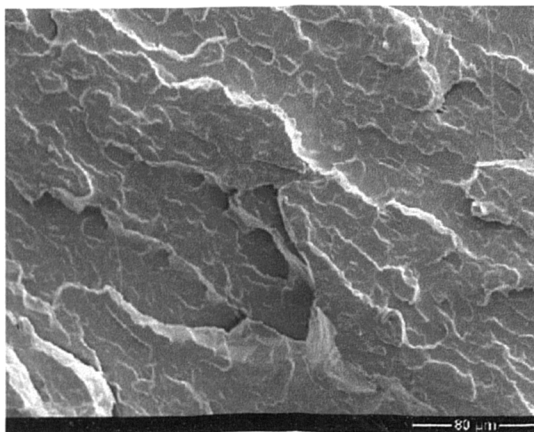


Figure 4.30
SEM image of B-PA6

With the NCH material a very different structure is observed. The clay has aggregated into large clusters visible on the surface of the sample; inferring that little or no interlayer intercalation has occurred. This observation is verified by the XRD trace, which shows no 2θ peaks in the $3-5^\circ$ range, typically associated with the presence of a layered silicate. The surface texture is also quite different to that observed for the other cast samples. There appears to be extensive porosity within the NCH material. These NCH samples are a replication of an experiment and they contain 5wt% of treated clay. These images suggest relatively poor samples quality, however with out optimising this process that observation could be too stringent.

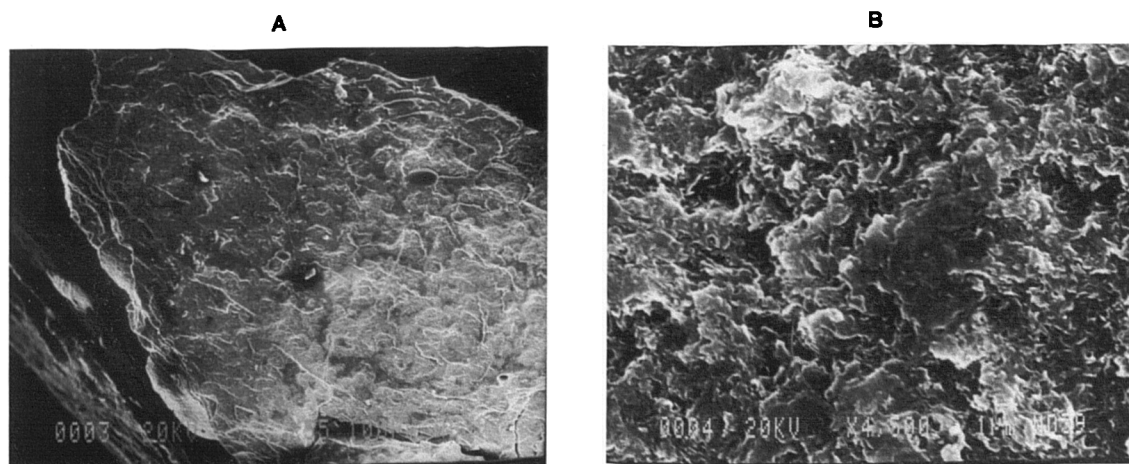


Figure 4.31
SEM images of NCH

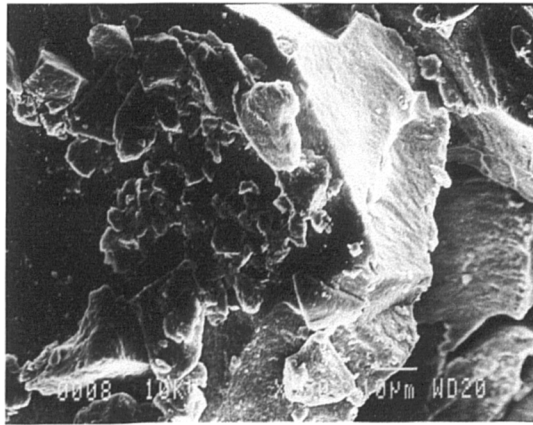


Figure 4.32
SEM image of Montmorillonite clay

SEM was also used to examine the clay itself, in order to verify that the angular shapes suspected as being clay, were indeed so. Where suspected particles of clay were observed X-ray Fluorescence (XRF) was used to identify traces of silicon, a high silicon content was taken to be evidence for the presence of a layered silicate; as shown in Figure 4.33.

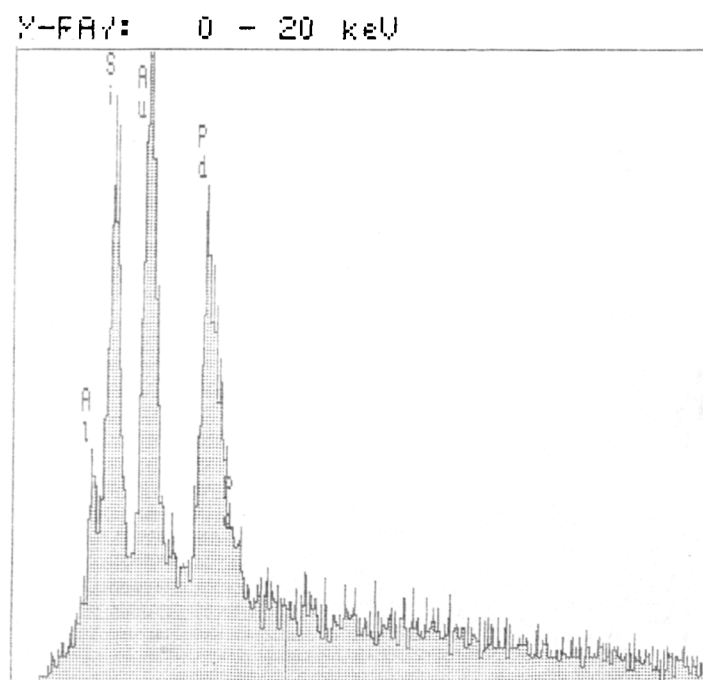


Figure 4.33
XRF trace of a layered silicate

4.4.2

Scanning Electron Microscopy: Reaction Extruded System

The image of the B-PA6 material, Figure 4.34, shows no areas of porosity. Also the surface texture appears to be very uniform. The J-PA6 material appears to have an increased surface texture and has small patches of white material, this material appears in all of the samples, with the exception of the BASF. This material could possibly be either residual activator or catalyst.

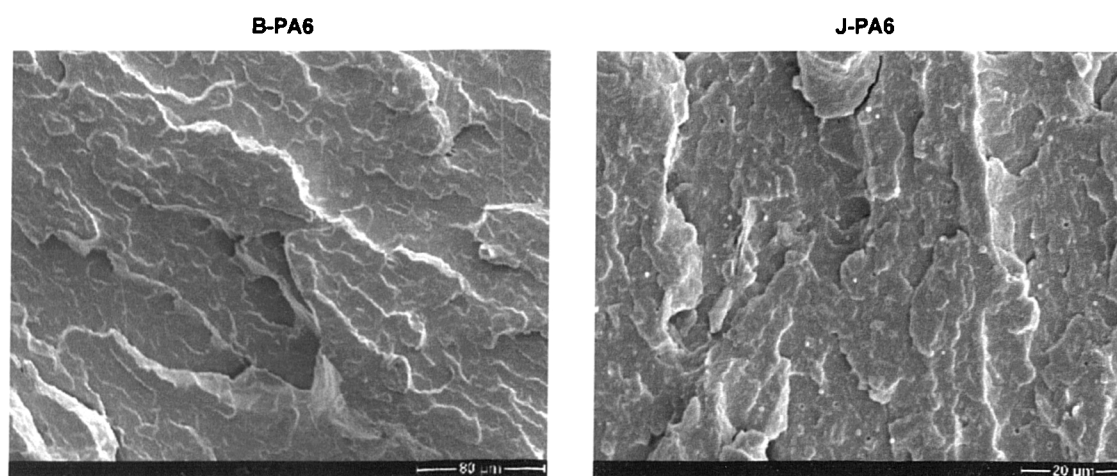


Figure 4.34
SEM images of B-PA6 and J-PA6

In Figure 4.34, there does not appear to be any large agglomerates visible in either sample, although there are some white patches in both cases that could be clay. However as they appear in the J-PA6 also, which has no clay additive, they are likely to be either residual activator or catalyst.

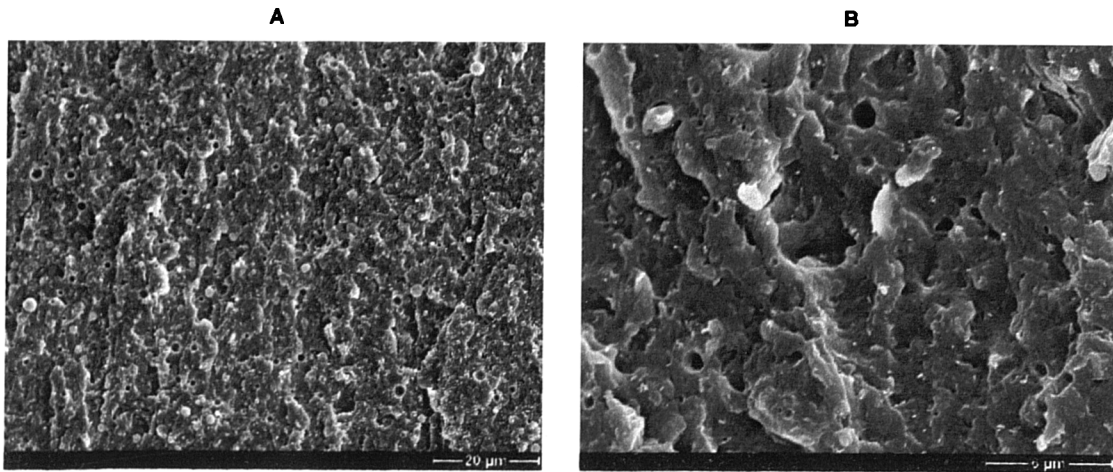


Figure 4.35
SEM images of J-PA6(U)

The JAL(T) clay appears to have very much more porous sample surface than the J-PA(U) material. But in neither case does the polymerisation process appear to have been optimal. But there is still significant improvement on the cast samples.

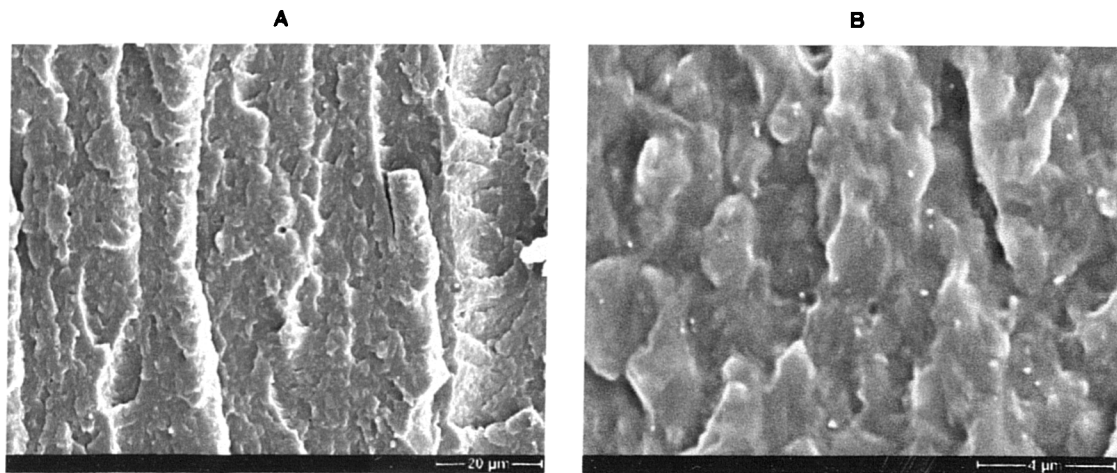


Figure 4.36
SEM images of J-PA6(T)

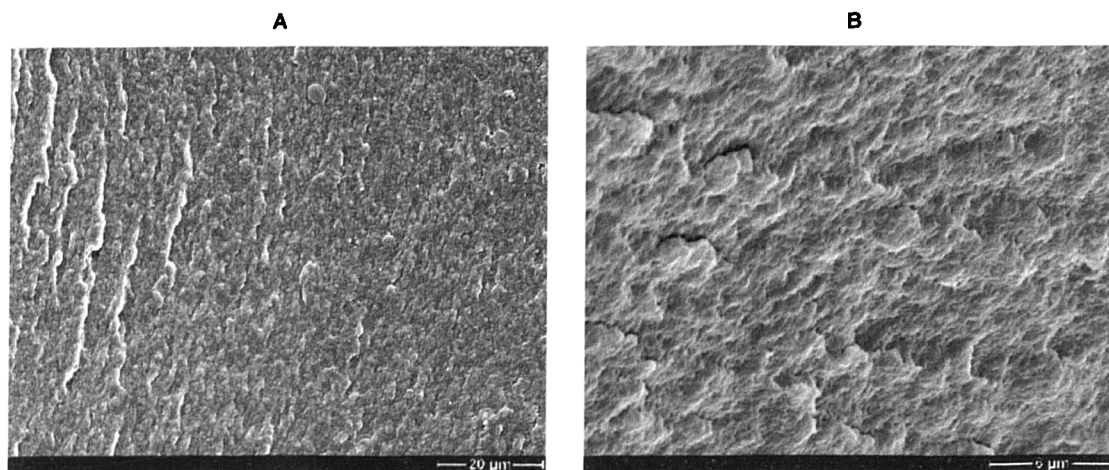


Figure 4.37
SEM images of UBE

There are not any large agglomerates visible on the surface of the sample. The surface texture is also very uniform inferring a good degree of polymerisation and dispersion. It is possible that the UBE material is a predominately exfoliated hybrid, whereas the JAL series is a predominately an intercalated hybrid. The UBE has d -spacings of approximately 3nm, whilst for the Cast series the d -spacings between the clay layers is approximately 2nm. Larger d -spacings infer exfoliation, whilst smaller d -spacings infer intercalation. Therefore the UBE material may contain more areas of exfoliated material compared with the reactively cast samples; although further analysis is required to confirm this.

4.4.3

Transmission Electron Microscopy: Reaction Extruded System

This was used to ascertain whether interlayer separation had occurred and if the layers had been expanded in the direction of extrusion, hence samples were sectioned in direction parallel to the flow direction (transverse) and perpendicular to the flow direction (longitudinal). With the treated material, Figure 4.38, alignment majority of the clay is aligned with the direction of the flow, and interlayer expansion has occurred but not to the maximum extent of the separation of all individual layers. There also appear to still be a few agglomerates, but their size is relatively small.

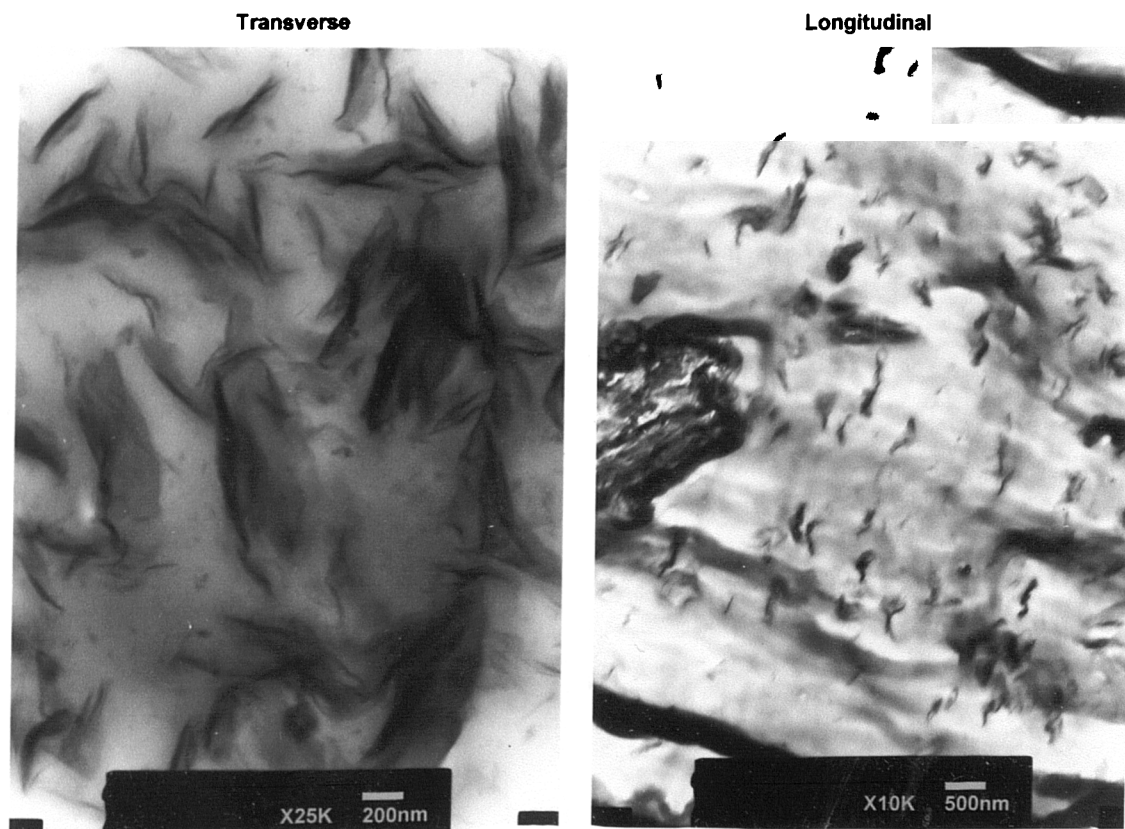


Figure 4.38
TEM photographs of J-PA6(T)

This was used to ascertain whether interlayer separation had occurred and if the layers had been expanded in the direction of extrusion, hence samples were sectioned in direction parallel to the flow direction (transverse) and perpendicular to the flow direction (longitudinal). With the UBE material, Figure 4.39, majority of the clay appears to be aligned with the direction of the flow. The interlayer expansion has occurred to a great extent, and the separation of individual layers can be seen. Again there also appears to be a few agglomerations, but their size is relatively small.

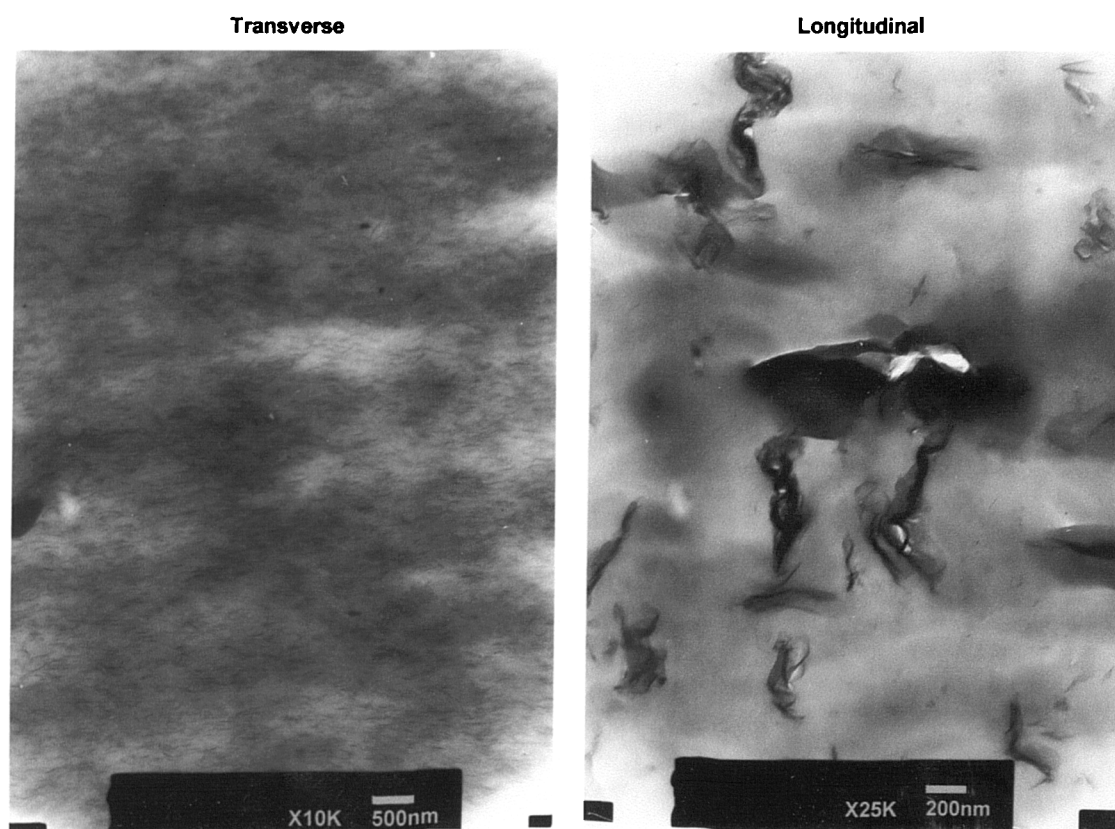


Figure 4.39
TEM photographs of UBE

4.5

Physical Properties

The mechanical properties of the samples were studied in order to ascertain the effects of nanocomposite fillers on the mechanical behaviour of the composites. The mechanical behaviour of materials is described by data produced as the result of simple, idealised tests. Hence caution should be exercised in interpreting results from such relatively limited sample sizes.

It was only possible to machine a limited number of cast samples. Therefore it was decided to use these samples for Dynamic Mechanical Thermal Analysis, as these would give an indication of how the samples perform over a range of temperatures. The NCH sample was very porous in nature and despite repeated attempts it just was not possible to machine a suitable sample. Given that porosity was greater for the J-series, it must be taken into consideration when comparing the properties of the J-series against the UBE and BASF commercially available material.

4.5.1

Impact Properties: Reaction Extruded System

Impact properties are based on the failure of the largest flaw, presupposing that the notch is the largest flaw. The addition of clay to a polymer usually yields detrimental impact properties. Although the filler loading is relatively low, so the effect on the impact properties may also be relatively low.

The crystalline morphology is important in these results, the γ -phase is more tightly packed and benefits from a higher degree of hydrogen bonding compared to the α -phase. Therefore the greater the amount of γ -phase the greater the impact energy required to fracture the sample.

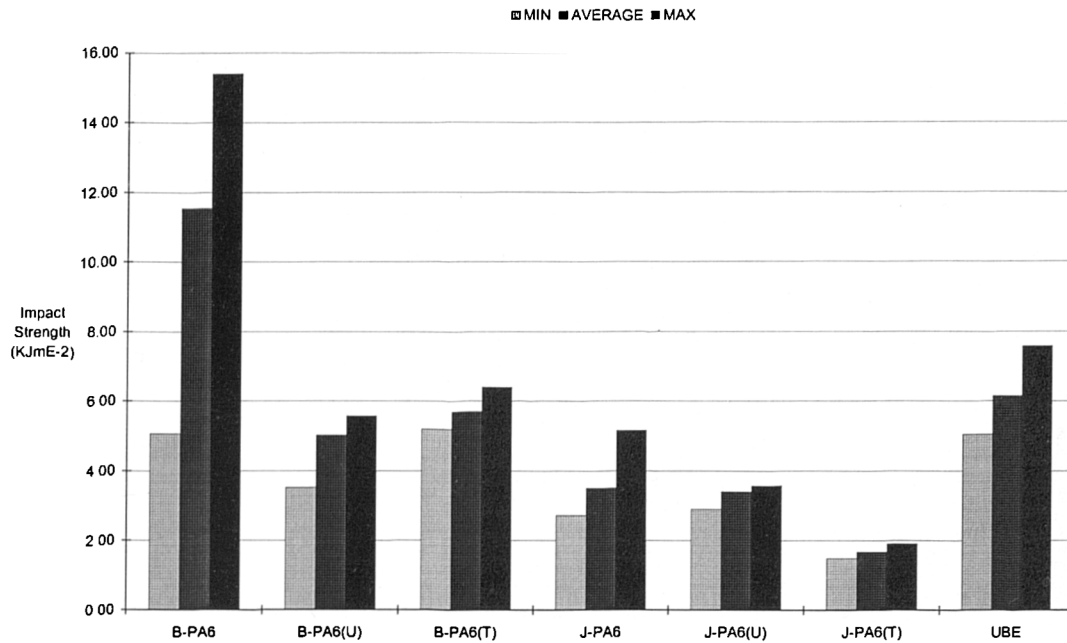


Figure 4.40
Impact properties

The J-PA6 series of samples show greatly reduced impact strength when compared with the other materials. It appears that the addition of treated clay is producing weaker interfacial bonds therefore a reduced amount of absorbed energy is required to overcome these bonds. The similarities between the impact strengths and absorbed energies for the J-PA6 series, suggests that the level of interfacial bonding in the untreated is almost as strong as the forces that bind the matrix J-PA6. It is also possible that owing to the small clay loading, these results may just be reflecting the strength of the matrix and thus account for the similar values between the J-PA6 and modified materials.

Material	Average Impact Strength	
	(GPa)	SD
B-PA6	9.75	1.13
J-PA6	3.51	0.96
J-PA6(U)	3.41	0.29
J-PA6(T)	1.68	0.18
UBE	8.31	1.59

Table 4.18
Summary of impact results

As observed from DMTA according to the damping loss factor ($\tan \delta$), the J-PA6 was mechanically tested just above its glass-transition while the J-PA6(U) and J-PA6(T) operated just below theirs. This will have major repercussions on the impact properties of the samples. Firstly, the J-PA6 having been seen to operate above its Glass Transition Temperature (T_g) will yield impact strength that is superior to that which it would be if it were operating below its T_g . With the converse being true for the J-PA6(U) and J-PA6(T). So given this, the increased impact strength of the UBE material is solely to do with the reinforcement of the UBE being better than the J-PA6 series, as the UBE is operating well below its T_g . Another factor to consider is the moisture content of J-PA6 series, which will result in increased impact properties of the samples, owing to the plasticising effect of water on the polyamide-6.

4.5.2

Tensile Properties: Reaction Extruded System

The effect of the polymer-clay orientation may have also had an influence on this result, with respect to the alignment of the clay within the sample. The degree of interfacial bonding strengths between the polymer and clay would have also been critical.

Clay reinforcement is suspected to be due to the strong, almost ionic interaction, between the silicate layers and nylon molecules. This ionic interaction has been attributed to a positive polarisation of the ammonium atoms within the polyamide-6 structure enabling it to interact with the overall negative charge of the silicate layers. Assuming there is substantial bonding strength at the polymer-clay interface, then the clay layers are acting as a 'pinning' phase restricting the movement and rotation of polymer chains.

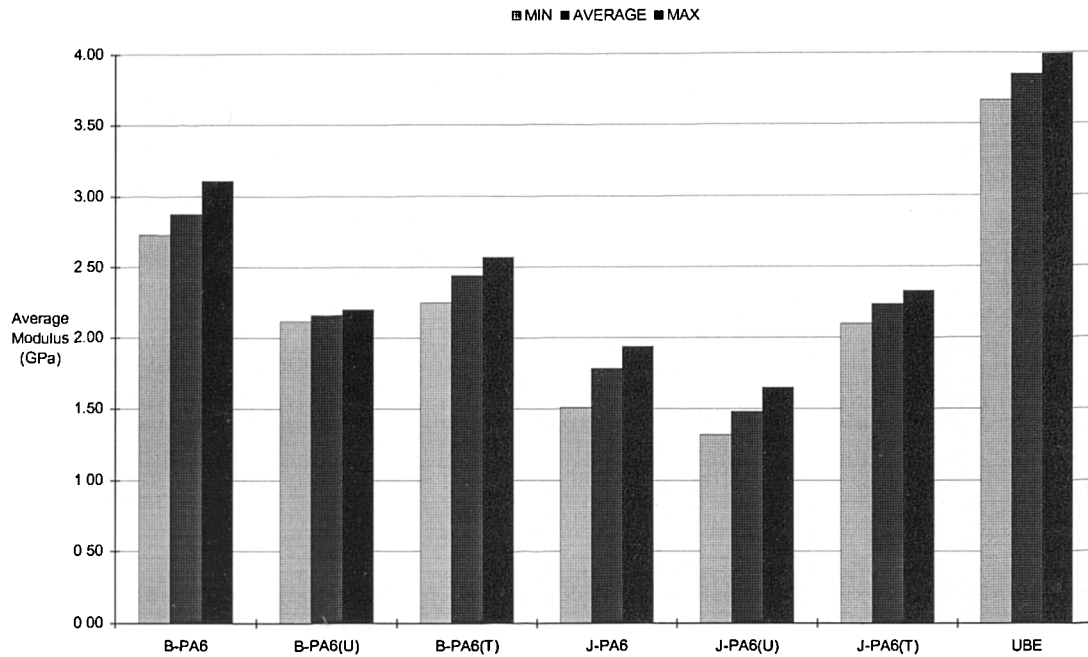


Figure 4.41
Tensile Properties

The tensile properties associated with the UBE material indicate that it has tensile properties that exceed those of the commercially available B-PA6. This result reflects the typical effect of reinforcement on polymeric materials. The comparison of tensile properties for the J-PA6 series of materials showed the J-PA6 to have a higher tensile modulus than the untreated but a lower tensile modulus than the treated samples. Which concurs with the basic concept of the initial clay treatment being to increase the interfacial bonding. However, the damping loss ($\tan \delta$) curve shows the J-PA6 to be operating just below its T_g while the J-PA6(U) and J-PA6(T) are operating just above theirs.

Material	Strain at Peak (%)	Stress at Peak (Mpa)	Strain at Break (%)	Stress at Break (Mpa)	Average Modulus (GPa)	SD of Average Modulus
B-PA6	0.45	12.19	0.44	12.10	2.88	0.22
B-PA6(U)	4.88	91.55	9.96	62.85	2.16	0.04
B-PA6(T)	4.50	70.70	24.04	44.60	2.44	0.12
J-PA6	0.27	3.42	0.27	3.39	1.78	0.18
J-PA6(U)	0.26	3.97	0.26	3.95	1.48	0.14
J-PA6(T)	0.40	7.49	0.40	7.44	2.24	0.11
UBE	0.54	20.05	0.54	19.19	3.85	0.12

Samples were tested at a sample rate of 10pts/sec and a crosshead speed of 1mm/min, with the exception of B-PA6(U) and B-PA6(T) which were tested at the same sample rate and a crosshead speed of 50mm/min.

Table 4.19
Summary of tensile properties

The factors that could affect the properties include porosity, degradation, molecular weight, polymer-clay orientation, morphology, residual monomer content and interfacial bonding strengths at the polymer-clay interfaces. Porosity was a recurrent problem with the J-PA6 series. Morphology i.e. the amounts of γ -phase present also has a contributory effect on the physical properties. There is also the possibility that the plasticising effect due to the presence of water reduced the tensile modulus of the treated and untreated materials. The influence of plasticisers is to increase polymer-chain distances, culminating in easier movement of the polymer-chains, thus reducing the tensile modulus but increasing the toughness. Therefore perhaps the major contribution to improvement in physical properties coming from the polymer-clay interfacial bond strengths.

4.5.3

Flexural Properties: Reaction Extruded System

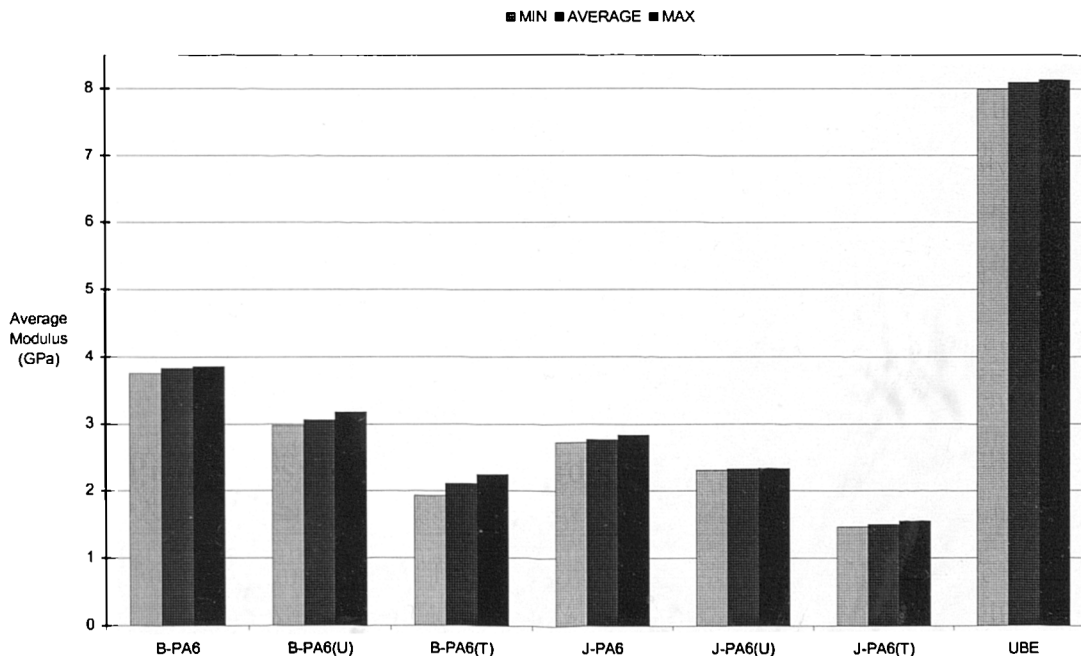


Figure 4.42
Flexural Properties

UBE demonstrates significant flexural property enhancements over the B-PA6. This can be attributed to the difference in phase morphology and interactions at polymer-clay interfaces. The morphology for both systems was predominantly γ -phase. However, the ratio of γ -phase to α -phase was significantly higher for the UBE material than for the other materials. The interactions occurring at the polymer-clay interface must be contributing to the rest of the property difference. Clay layers can inhibit polymer-chain motion, which has been well documented as producing stiffening effects in polymer-clay macrocomposites.

Material	Displacement at Yield (mm)	Stress at Yield (MPa)	Strain at Yield (mm/mm)	Average Modulus (GPa)	SD of Average Modulus
B-PA6	11.69	118.90	0.045	3.83	0.04
B-PA6(U)	14.33	108.80	0.054	3.07	0.09
B-PA6(T)	16.34	77.44	0.061	2.11	0.12
J-PA6	12.83	75.83	0.048	2.77	0.05
J-PA6(U)	13.63	66.12	0.051	2.33	0.02
J-PA6(T)	17.52	58.15	0.066	1.50	0.04
UBE	9.12	190.40	0.037	8.09	0.06

Table 4.20
Flexural Summary

J-PA6 demonstrated superior modulus and strength properties over the J-PA6(U) and J-PA6(T) samples. Again this would appear to link back to the glass-transition temperature with J-PA6 operating above its T_g and the J-PA6(U) and J-PA6(T) samples operating below theirs. This could well account for difference in flexural properties. The crystalline morphology for all of the J-PA6 series of materials, are very similar in that they all exhibit a predominantly γ -phase with the clear presence of α -phase and furthermore, that the amounts of α - and γ -phases differ by a very little amount. Therefore, it could be assumed that the influence of crystalline morphology is minimal compared to the effect of interfacial bonding at the polymer-clay interfaces.

The crystalline morphology of the UBE contains considerably more γ -phase than the JAL series. Which could account for the mechanical property differences observed. Porosity levels could also introduce areas of mechanical weakness. Finally the effect of plasticisers present in the J-PA6 series would facilitate chain motion and slippage.

4.5.4

Dynamic Mechanical Thermal Analysis: Cast System

The flexural modulus of polyamides progressively decreases as the test temperature is raised. For the purposes of comparison the flexural modulus of all the samples were compared with reported values, as shown in Table 4.21.

Sample	Flexural Modulus (GPa)
Polyamide-6 Homopolymer	2.2-3.2
Polyamide-6 Impact Modified	0.8-2.2
Polyamide-6 Glass-fibre Reinforced	4.0-11.9
Polyamide-6 Glass-fibre / Mineral Reinforced	7.6-9.2
C-PA6	2.7
B-PA6	2.2
C020	2.0
C021	1.4
C022	2.2
C024	1.4
C028	1.1
C029	2.0

Table 4.21
Theoretical δ and experimental flexural results at 23 °C

Whilst the experimental samples corresponded generally to the shape of the theoretical graphs, the measured flexural modulus of the cast materials at 23°C is disappointingly low. The increase predicted by the mineral addition to the polyamide does not appear to occur, in fact the converse takes place, i.e. a decrease in the flexural modulus is observed. C-PA6 and B-PA6 concur with expected values, ruling out apparatus error.

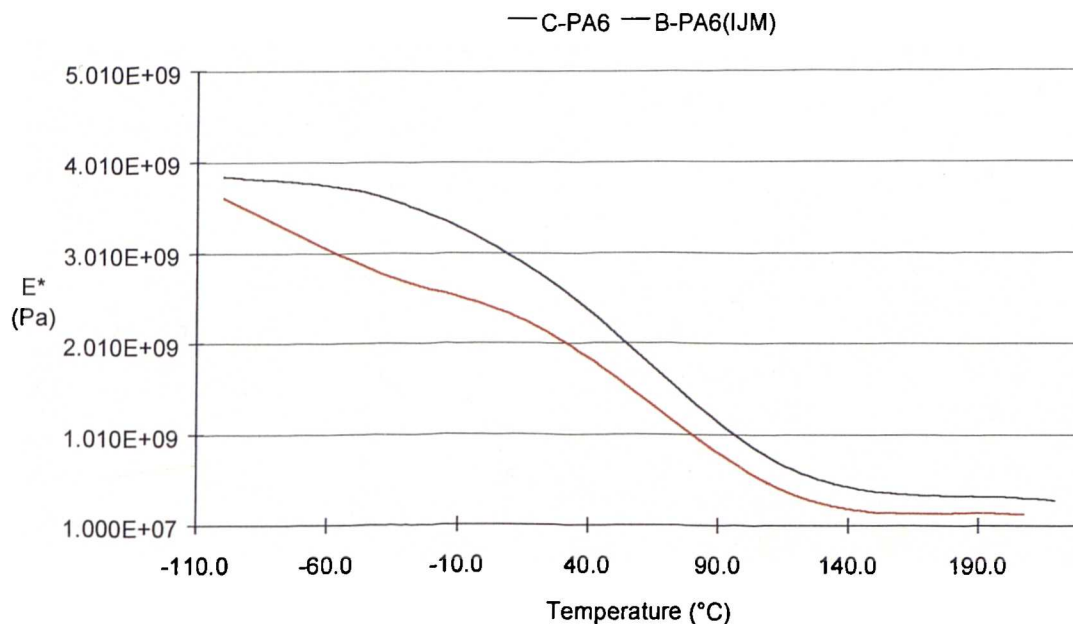


Figure 4.43
DMTA results for C-PA6 and B-PA6

Figures 4.43 and 4.44 both display the performance of organically modified clay with the pure polymer. The initial performance of these materials exceeds that of the C-PA6. As the test temperature is increased the flexural modulus rapidly decreases, over the mid temperature range, though this rate of decrease is slightly less for the materials shown in Figure 4.44. The mechanical performances of all the modified samples are roughly comparable to the C-PA6 at a higher temperature range.

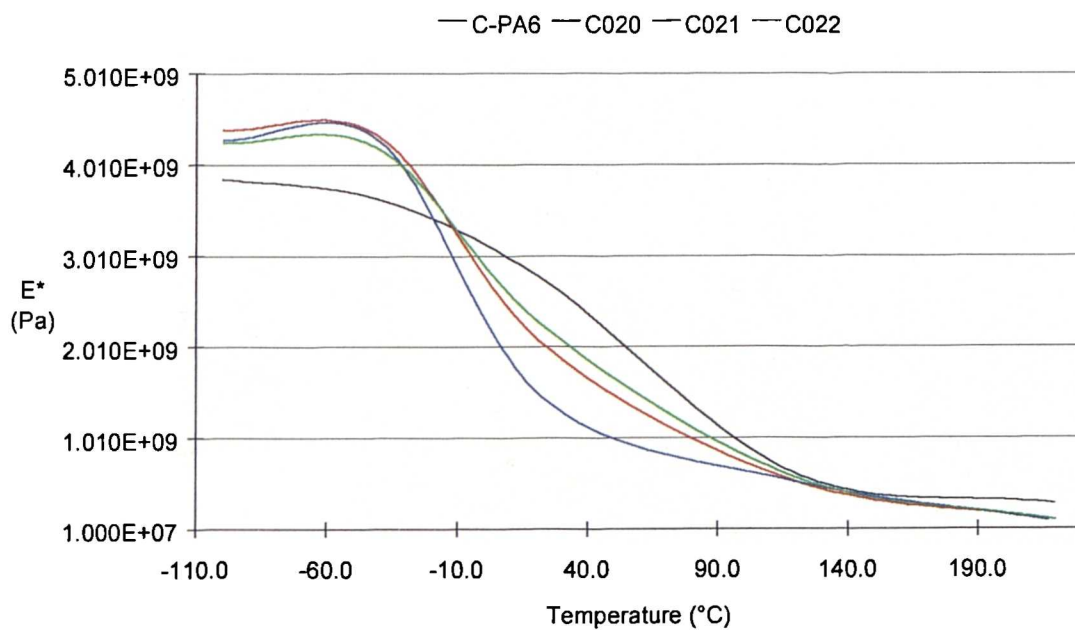


Figure 4.44
DMTA results for C-PA6 , C020, C021 and C022

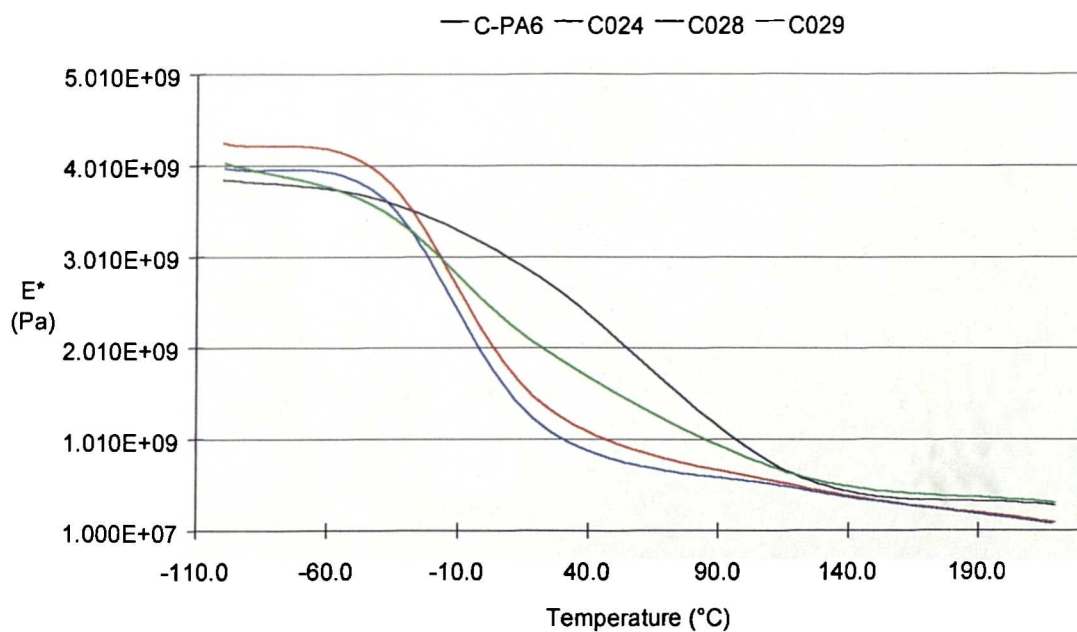


Figure 4.45
DMTA results for C-PA6 , C024, C028 and C029

4.6.5

Dynamic Mechanical Thermal Analysis: Reaction Extruded System

The DMTA results indicate that the heat distortion properties for UBE are superior at elevated temperatures than that of B-PA6 and J-PA6. There is also a drop in modulus at a temperature approximating to the glass-transition temperatures. When the material changes from behaving elastically and to viscously.

Factors that may have introduced deleterious effects on the heat distortion properties of the materials include moisture content, porosity levels, residual monomer content, molecular weight, polymer-clay orientation, crystalline morphology, and polymer degradation. Although the largest factor has to be the morphology of the samples, specifically the crystalline forms. The γ -phase produces better mechanical properties and therefore, will introduce some property enhancement. Another factor that will have a large influence is the interfacial bonding strength.

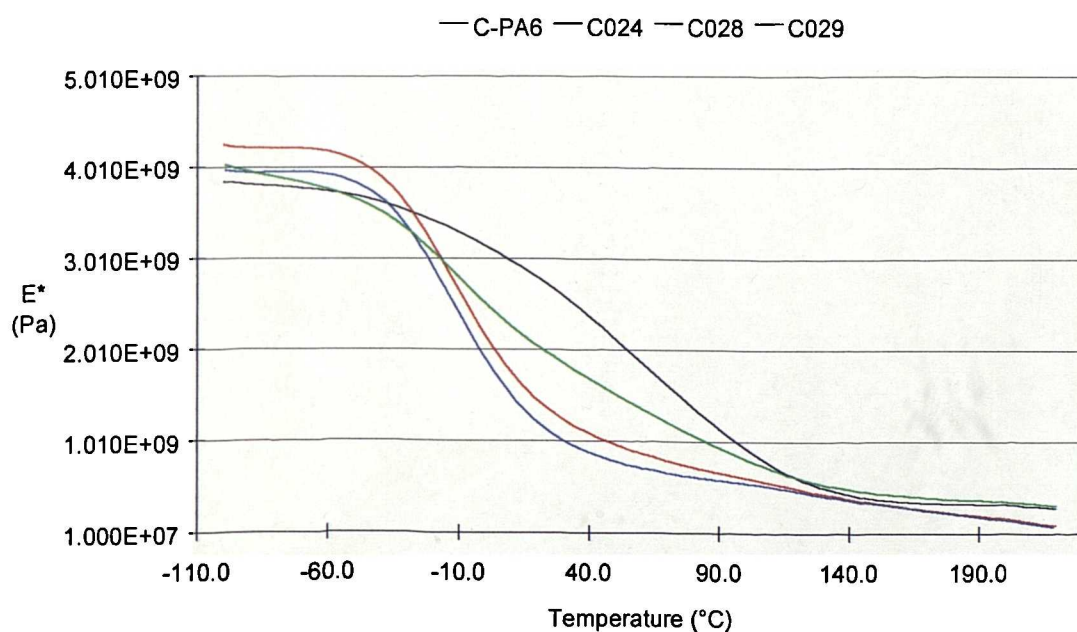


Figure 4.46
DMTA results for C-PA6, B-PA6, B-PA6(U) and B-PA6(T)

The comparison of the C-PA6 to the B-PA6 material, showed the cast material to have increased modulus properties over the entire temperature range. Although the addition of the untreated clay did appear to raise the property profile of the B-PA6 material.

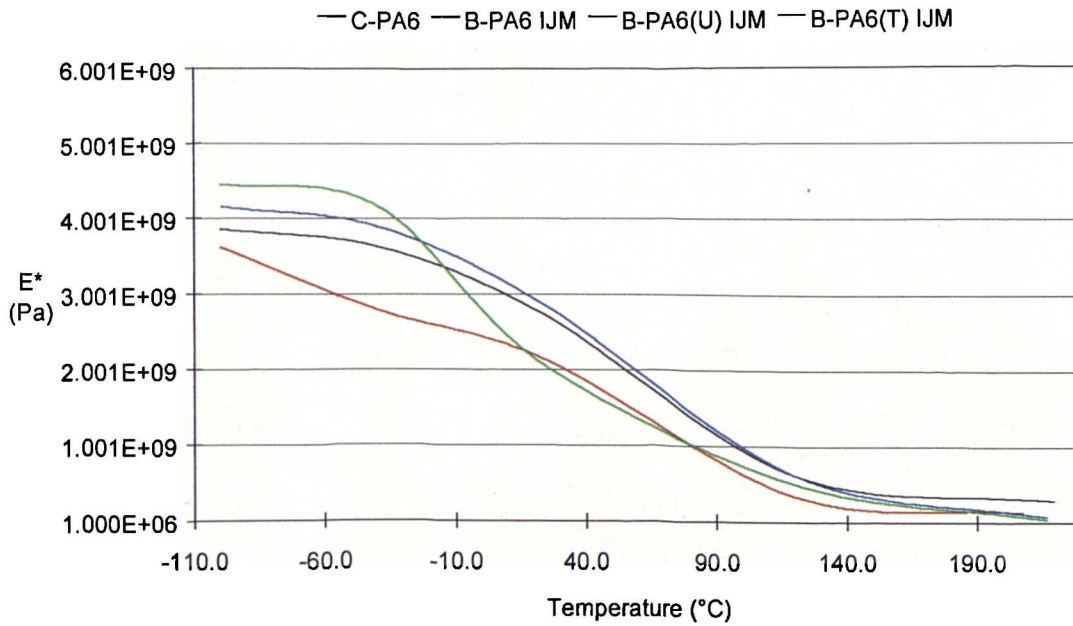


Figure 4.47
DMTA results for C-PA6, J-PA6, J-PA6(U) and J-PA6(T)

With the J- PA6(U) series of materials the untreated samples show superior modulus to both the J-PA6 and the J- PA6(T). Inferring that the clay in its natural form provides reinforcement. The level of porosity was found to be a recurrent problem with the J-PA6 series, which showed excessive porosity when compared to the other materials. However, the porosity levels for the JAL series were similar thus allowing for comparison between them. All of the J-PA6 series of materials all showed a predominately α -phase morphology for the JALN6 with progressively more γ -phase for the untreated and treated materials, which could explain its lower dynamic modulus.

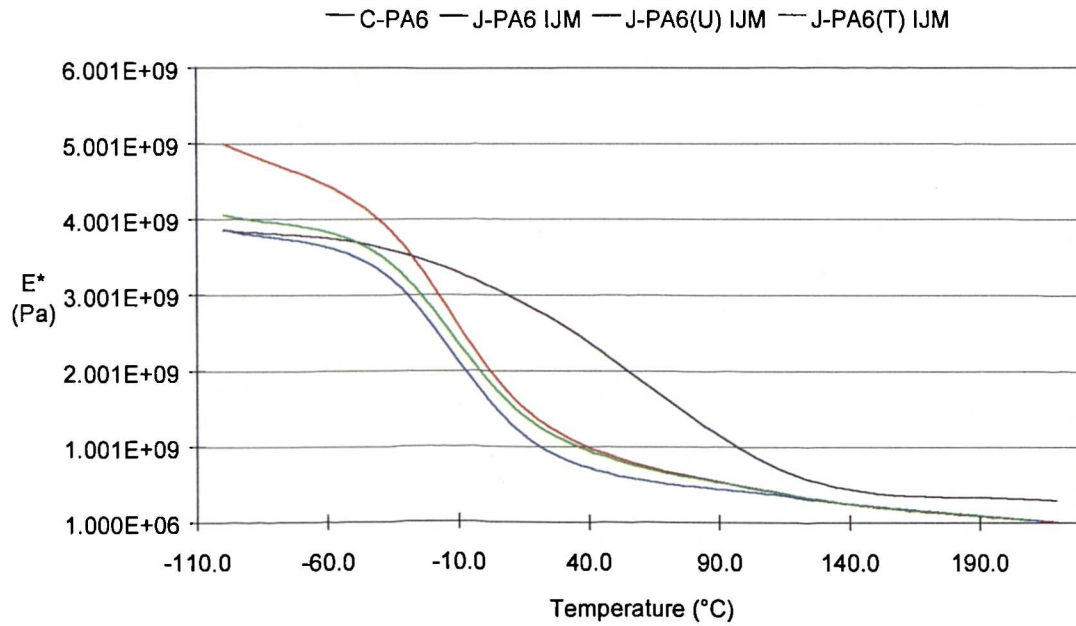


Figure 4.48
DMTA results for C-PA6, J-PA6(T) and UBE

The UBE material displayed superior properties when compared with the J-PA6 series above ambient temperatures. Raising the possibility that there is a plasticising effect. Plasticisers tend to behave as anti-plasticisers at below ambient temperatures and thus could account for the increased modulus values.

A key issue to note at this juncture is differing Tg's between the UBE and J-PA6 series of materials. At room temperature the J-PA6 series of material will be operating above their Tg; whilst the UBE and B-PA6 would be operating well below theirs. Thus causing the difference in modulus values in favour of the commercially available material. The influence of operating above or below glass-transition temperatures is so influential on modulus and hence mechanical properties, it is difficult to discuss other factors such as porosity, degradation, and orientation effects because their effects, if any, would be masked considerably by the Tg difference.

4.6

Cast System

The Cast system was essentially comprised of three phases. The initial range of test pours (C001-C011) provided very basic information about whether the catalyst and activator system, as well as the respective ratios, would be effective on the small experimental scale. Having established the viability of system the process was refined using the experience gathered and a series of samples were generated and their properties analysed. The final stage was to scale up the process to factory trial size with the addition of high shear in order to aid dispersion.

The Cast series of materials all displayed structural improvements, owing to the addition of the modified layered silicate. Yet these improvements did not translate into an increase in physical properties.

4.6.1

Brabender Series

No results were drawn from the Brabender series of materials. None of the Brabender samples polymerised properly, despite the introduction of a nitrogen blanket. This was added to the apparatus in order to prevent moisture from reacting with the caprolactam. However, the Brabender continuously mixes the contents of its reaction chamber, so if polymerisation had occurred the end result would have been the seizure of the apparatus. So the general conclusion is that this particular set-up was not conducive to reactive casting or suitable.

4.6.2

Test Pours

In this section there are two main comparisons, the first between C020, C021 and C022 which all contain an organically modified silicate. C024, C028 and C029 all contained cation exchanged montmorillonite. The interlayer distance of the C020, C021 and C022 were very consistent 203, 206 and 204nm respectively. However, C028 demonstrated significantly greater an interlayer distance of over 262nm realistically an increase in gallery spacing of that magnitude must have been accomplished by polymerisation within the inter-layer area.

The GC results were consistent throughout these series of results, with there being under 7% residual monomer in all these samples. This is in part validated by the GPC findings, although there appears to be a large variation within groups. C020 demonstrates a very high molecular weight and polydispersity. This increase in reactivity could be owing to the organic modification grafted onto the silicate. However, if this was true then there should also be significant improvement for C021, although the polydispersity index for this sample is lower. Sample C024 demonstrates a lower molecular weight. Inferring that the addition of excess activator results in the formation of low chain-length polymer, which given the very nature of an activator is possible. However, these results are so varied and given the difficulties in obtaining meaningful results using GPC caution should be used in drawing conclusions.

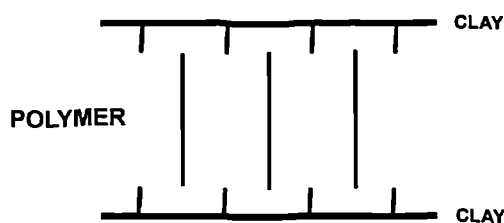
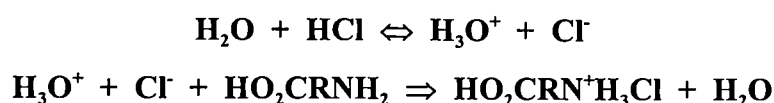


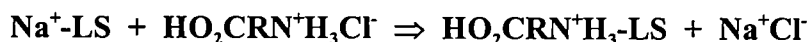
Figure 4.49
Possible Structure

All of the cast series demonstrated increased melting points and crystallisation temperatures. But despite this the alteration in structure of the Cast series of materials, these changes did not translate into an increase in physical properties. All of the physical results obtained were lower than that reported for the homopolymer. A possible explanation for this may be that the polymer is not anchored to the clay, rather aligned with in the layers, as shown in Figure 4.49.

The montmorillonite clay is modified using a cation exchange reaction. Hydrochloric acid is dissociated in water and protonates the 12-aminolauric acid:



The ion exchange reaction between montmorillonite and a protonated amino acid is shown below, where **LS** refers to a Layered Silicate:



The sodium and chloride ions remain in solution and are removed by washing the clay thoroughly with deionised water. The ions present in the clay are not exclusively sodium, for example other ions present include potassium and aluminium, but principles are the same. The preferred theory for the intercalation reaction is as shown in Figure 4.50.

The activator species is a hexamethylene diisocyanate, and propagates the reaction. Thus the growing polymer chain is anchored into the modified clay via a cyanate linkage.

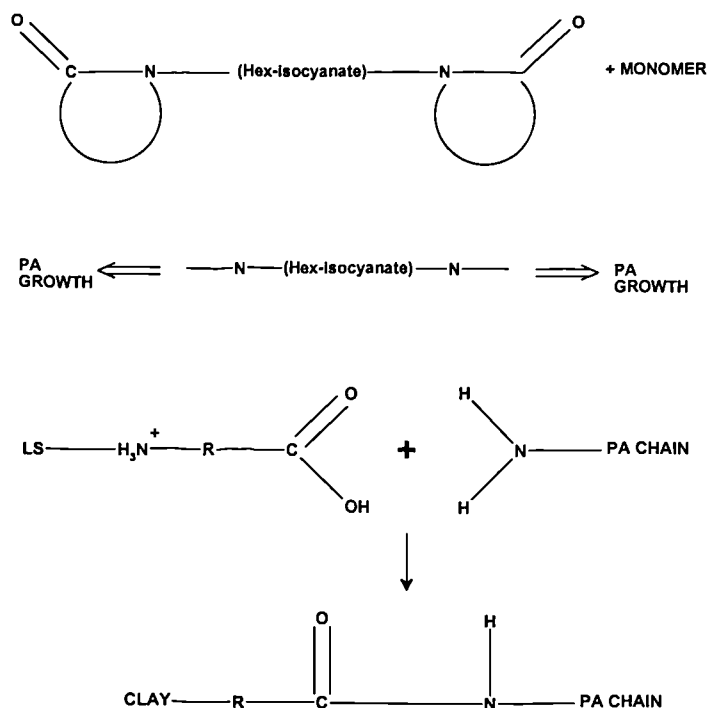
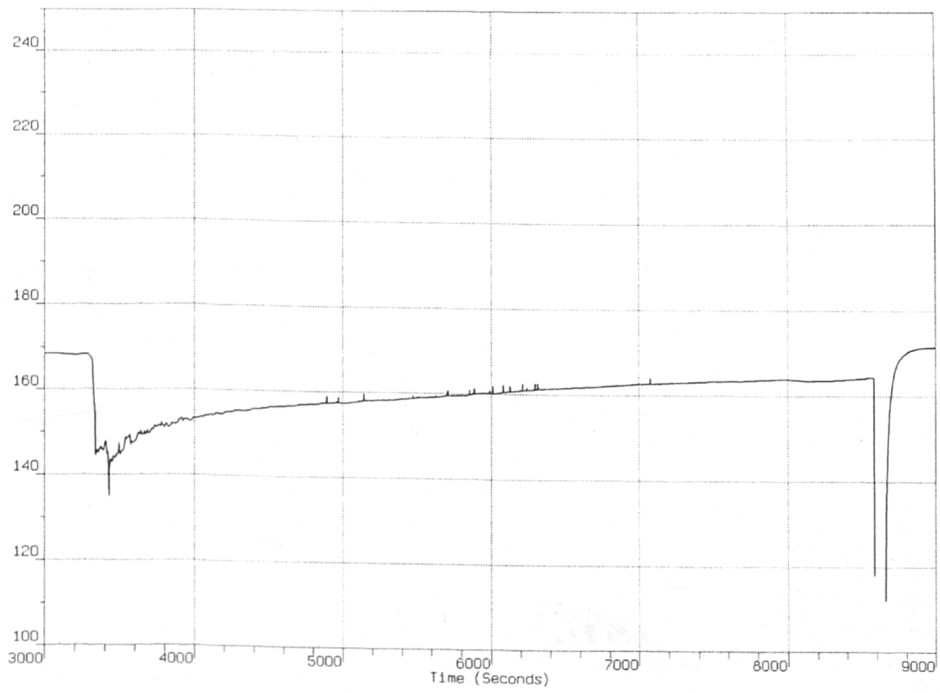


Figure 4.50
Possible intercalation reaction

Upon completion of a successful test pour and its analysis the process would be scaled up to 8kg for a factory trial. With the Factory Pours a thermocouple was placed into the casting. There are two main reasons for this, the first being in order to see if the oven temperature remained constant. The second reason is that polymerisation is an exothermic process, so when it occurs an increase in the temperature of the casting will be observed. This is clearly shown in Figure 4.51. Sample C027, which was an unsuccessful trial, did not polymerise and the temperature of the casting remains at between 150-165°C. In fact the casting does not quite reach the original oven temperature of just under 170°C. Where as C029, which did polymerise successfully, shows a steady increase in the temperature of the casting. It exceeds the initial oven temperature and continues to rise until it reaches a plateau at approximately 205°C. This simple technique provides quantitative and qualitative information on the progression of the reaction. Modifying equipment and apparatus to accommodate this technique would also provide information about reproducibility issues.

A C027



B C029

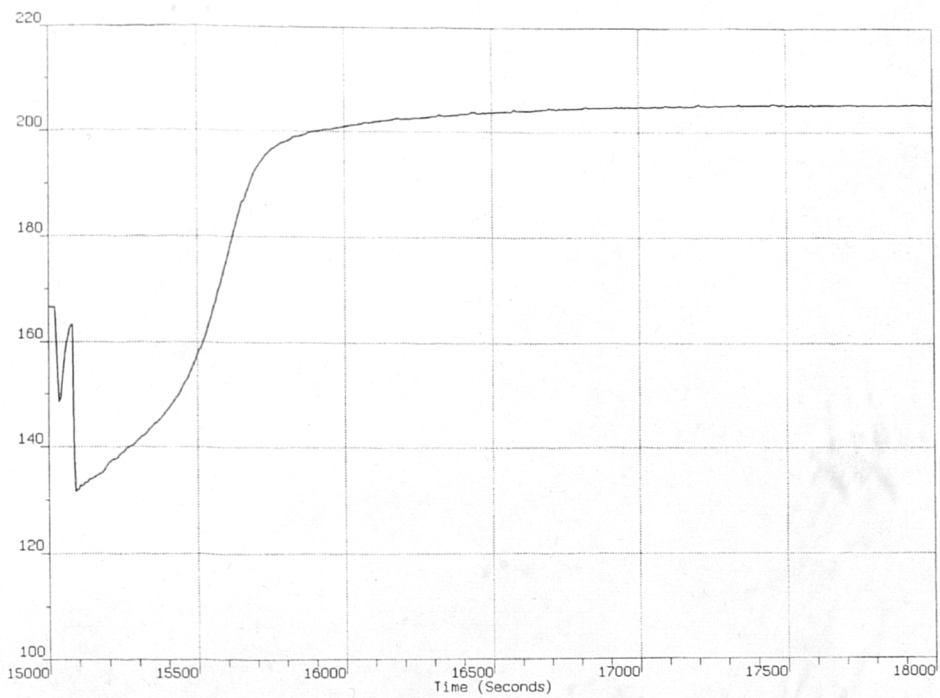


Figure 4.51
Thermographs of two factory trials

4.6.3

Nylon Clay Hybrid

Microscopic analysis showed the NCH sample to be highly porous and in general of very poor quality. In fact it did not prove possible to machine a sample for analysis of mechanical properties.

This sample had residual caprolactam content of 9%. Which correlates with the lower molecular weights recorded. However, the polydispersity result is 2.3, a typical result for commercial polyamides are approximately 2.0. So it would appear that the distribution is relatively high, and therefore the extent of reaction must also be relatively high. An explanation of this would be that the reaction leads to the formation of a high number of relatively short chain-length repeat units. This postulate seems to be verified by the lower melting point observed in this sample, more than 18°C lower than reported values for the melting point of polyamide.

XRD results showed limited inter-layer expansion. Assuming that the premise about the shorted chain-lengths was correct, these chains might not be sufficient in length to promote inter-layer expansion. Another possibility is that the layers were not sufficiently expanded to promote polymerisation between the layers; rather it occurred outside of these layers the net result being their compression.

The most interesting result was from TGA, in the range from 475°C to 850°C the NCH only undergoes a weight loss 14%, compared with approximately 50% for the remainder of the Cast series. The paper from which the experiment was replicated reports that the material demonstrated increased heat resistant properties, so perhaps this result correlates to that particular observation.

The NCH material contained more clay than the cast series, 5wt% and 4wt% respectively. With this increased clay content the optimisation of the process may be even more critical, which as the writers of the paper achieved success is quite possibly the case.

4.7

Reaction Extruded System

All the data has shown that crystalline morphology of the polyamide-6 matrix material is sensitive to processing conditions. The effects of extrusion, compression moulding, and injection moulding have all influenced the structure of the polymeric material.

An interesting observation is the effect of clay addition on the crystalline morphology of polyamide-6. Annealing and fast cooling under load of a polyamide melt will generally produce α -phase crystalline morphology, for example compression moulding of samples. Where as injection moulding of the samples produced the opposite effect to compression moulding conferring a predominantly γ -phase morphology.

The processability of the samples varied dramatically. The J-PA6 series of samples were more difficult to process than the two commercially available products (UBE and B-PA6). This phenomenon has been attributed to poor drying of the JAL series of samples prior to moulding; as a result the drying temperature was raised from 60°C to 110°C.

The DSC data analysis revealed that commercially available materials contain more crystallites that have undergone growth. Suggesting that there are differences in percentage crystallinity and crystalline sizes, which is verified by the very different structures observed using microscopy.

Therefore, it may be stated that SEM, TGA and XRD data has shown that UBE's commercially available hybrid material can be classed as a nanocomposite and, that Toyota's research has been successful in producing a "polyamide resin that contains a dispersed layered silicate therein." It has been concluded that the UBE has better clay dispersion than the JAL series and that this could be due to the latter being an intercalated hybrid and the former being a delaminate (exfoliated) hybrid nanocomposite.

The most important fact that needs to be reiterated is that the J-PA6 series of materials all operated just above or just below their glass-transition temperatures while the commercially available materials both operated well below theirs. The difference in mechanical properties of the B-PA6 and J-PA6, show that the different polymerisation routes produce very different materials. Evidence suggests that the polymerisation or even processing technique was not conducive to the production of a commercially desirable material. An increase in the glass-transition may allow the J-PA6 series to operate at more comparable levels to materials already available. The differences in mechanical properties have been attributed to crystalline morphology, porosity levels and, plasticisers. Using a framework it should be possible to tailor make the composite, which will necessitate compromise. Increased fire retardance and toughness, for example, may be gained by increasing the level of clay addition, but at the expense of a reduction in stiffness, tensile properties and barrier properties.

CHAPTER FIVE

CONCLUSIONS

5.1

Cast System

The following summarises the conclusions reached through this study and subsequent trends observed in reaction cast nanocomposites:

- Between 4.1-6.8% residual ϵ -caprolactam is present within the cast nanocomposites. This is comparable with 8.7% residual ϵ -caprolactam for the C-PA6.
- The molecular weight of the cast nanocomposites shows a general increase compared to that of C-PA6 and comparable with that of B-PA6.
- TGA results give a crude indication that the addition of clay increases thermal stability.
- DSC results point towards a mixture of α and γ crystals being present.
- An increase in the basal spacing of the clay is visible on XRD, further to the treatment of the natural montmorillonite.
- Polymerisation appears to occur between layers, irrespective of any prior treatment of the clay, as here too an increase basal spacing is seen using XRD.
- SEM reveals porosity probably from air trapped during the mixing process.
- Using DMTA the nanocomposites display increased low temperature properties compared with C-PA6 and industrial B-PA6. But these properties decrease dramatically as approach -10°C .

5.2

Reaction Extruded System

The following summarises the tentative conclusions reached through this study and subsequent trends observed in reaction cast nanocomposites:

- J-PA6 contains 14.6% residual ϵ -caprolactam, which appears to reduce with addition of untreated and treated clay to 6.7 and 7.0% respectively.
- Addition of untreated and treated clay increases the residual monomer content of the B-PA6, so the polyamide is actually depolymerised.
- The molecular weight increases of the nanocomposites displays an increase when compared to B-PA6.
- TGA results give a crude indication that the addition of clay increases thermal stability.
- DSC results point towards a mixture of α and γ crystals being present.
- Polymerisation appears to occur between layers, irrespective of any prior treatment of the clay, as here too an increase basal spacing is seen using XRD.
- An increase in the basal spacing of the clay is visible on XRD, further to the injection moulding of the sample and a decrease further to the compression moulding of the sample.
- SEM reveals a poor sample surface inferring that the process is not optimised.
- The degree and direction of dispersion are affected by the processing, as shown by TEM. Notably injection moulding, which gives an increased dispersion in the direction of the polymer flow.
- TEM also indicates that exfoliation is not at its maximum.
- Impact strength decreases in the series: J-PA6, J-PA6 (U) & J-PA6(T).
- However the B-PA6 series, the strength of the treated clay containing sample is greater than that for the untreated sample.
- Tensile strength decreases in the series: J-PA6, J-PA6 (T) & J-PA6(U), which is mirrored by the B-PA-6 series: B-PA6, B-PA6 (T) & B-PA6(U).
- DMTA results for the JAL series show very little by way of improvement. But the B-PA6 samples containing clay demonstrated low temperature improvements.

5.3

Suggestions For Further Work

The crystallisation results give no indication as to why alpha and gamma crystals would form preferentially. It would be of particular interest to ascertain whether the addition of a layered silicate results in the preferential formation favour one particular spherulite type or if a mixture of spherulite types is observed, as shown in Figure 5.1.

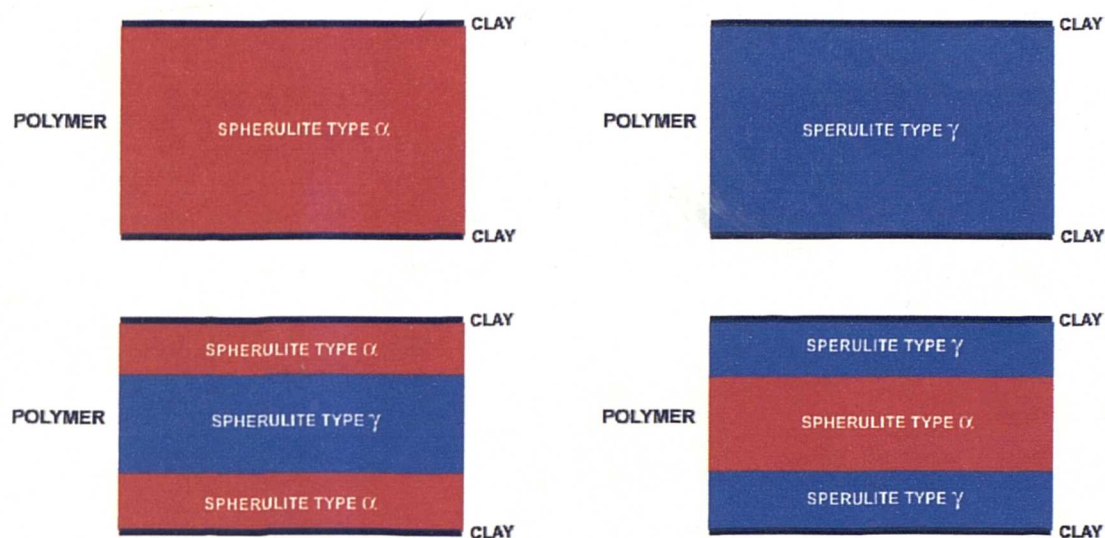


Figure 5.1
Possible spherulite formation

Repetition of the factory trials would establish the reproducibility of this production method, as well as providing a larger pool of samples from which more meaningful averages and result trends could be derived. It would also enable conditions to be optimised.

A technique such as Atomic Force Microscopy (AFM) could be used to gain a quantitative measurement of the layer separation. This increased magnification available through this technique means that it would be possible to visualise the changes occurring within the nano-scale structure. It may even be possible to obtain samples at differing stages through out the reaction. Thus enabling a picture of critical steps and pathways to be established.

Of crucial importance is that the polymerisation reaction itself and the effects that the layered silicates have on these reactions need to be further investigated. A technique such as isotopic labelling could well provide evidence of the reaction pathway. Having established the reaction mechanisms it may well be possible to apply the reactive extrusion process to other layered silicates, notably magnesium hydroxide. The addition of a fire retardant to a system that displays fire retardant properties may result in improved synergies displayed as an increase in thermal stability.

Once the reaction is more completely understood it may well be possible to apply the principles to other layered silicates. Given the inherent fire retardance of nanocomposite systems, of particular interest would be the introduction of an inherent fire retardant, e.g. magnesium hydroxide. Magnesium hydroxide is limited in its applications, owing to the loadings necessary to confer adequate retardancy. It is feasible that lower loading may well be required in such a system.

REFERENCES

- ¹ POWELL,P. *Engineering with polymers*. Chapman & Hall. (1992)
- ² PRITCHARD,G. *Plastics additives*. Chapman & Hall. (1998)
- ³ KATZ,S & MILEWSKI,J.V. (Eds.) *Handbook of fillers and reinforcements for plastics*. Van Nostrand Reinhold Company. (1978)
- ⁴ SEYMOUR,R.B & KIRSHENHAUM,G.S. (Eds.) *High performance polymers: their origins and development*. Elsevier. (1986)
- ⁵ NELSON,W.E. *Polyamide plastics technology*. Newnes-Butterworths. (1976)
- ⁶ KOHAN,M.I. (Ed.) *Nylon plastics handbook*. Hanser. (1995)
- ⁷ DAINTITH,J. (Ed.) *Dictionary of chemistry*. Oxford University Press. (1996)
- ⁸ SIMONDS,H.R & CHURCH,J.M. (Eds.) *The encyclopaedia of basic materials*. Reinhold Publishing Corporation. (1967)
- ⁹ EDWARDS,L & ENDEAN,M. *Manufacturing with materials*. Butterworths. (1990)
- ¹⁰ CRAWFORD,R.J. *Plastics engineering*. Pergamon Press. (1987)
- ¹¹ ASKELAND,D.R. *The science and engineering of materials*. PWS Publishing Company. (1994)
- ¹² ROTHON,R. (Ed.) *Particulate-filled composites*. Longman Scientific & Technical. (1995)
- ¹³ REIMSCHUESSEL,H.K. *Polyamide 6 chemistry and mechanisms*. Journal Of Polymer Science: Macromolecular Reviews. **12** (1977) 65-139
- ¹⁴ YOUNG,R.J & LOVELL,P.A. *Introduction to polymers*. Chapman & Hall. (1991)
- ¹⁵ ACHILLADELIS,B. *A study in technological history. Part I. The manufacture of "Perlon" (polyamide 6) and Caprolactam by IG Farbenindustrie*. Chemistry And Industry. **December** (1970) 1549-1554

- ¹⁶ CAROTHERS, W.H & BERCHET, G.J. *Amides formed from ϵ -aminocaproic acid*. Journal Of The American Chemical Society. **52** (1930) 5289-5291
- ¹⁷ SEBENDA, J & KOURIL, V. *Polymerisation of ϵ -caprolactam in an extruder: process analysis and aspects of industrial applications*. European Polymer Journal. **8** (1972) 437-447
- ¹⁸ TAI, K, TERANISHI, H, ARAI, Y & TAGAWA, T. *The kinetics of hydrolytic polymerisation of ϵ -caprolactam. II. Determination of the kinetic and thermodynamic constants by least squares curve fitting*. Journal Of Applied Polymer Science. **25** (1980) 77-87
- ¹⁹ WICHTERLE, O, SEBENDA, J & KRALICEK, J. *The anionic polymerisation of caprolactam*. Advances In Polymer Science. **2** (1961) 578-595
- ²⁰ NYLACAST. *Technical production of polyamide*.
- ²¹ MENGES, G & BARTILLA, T. *Polymerisation of ϵ -caprolactam in an extruder: process analysis and aspects of industrial applications*. Polymer Engineering And Science. **27** (1987) 1216-1220
- ²² BIENSAN, M & POTIN, P. *American patent: 4067861*. (1978)
- ²³ SEBENDA, J. *Lactam polymerisation*. Journal Of Macromolecular Science, Chemistry. **A6** (1972) 1145-1199
- ²⁴ PARKER, J.P & LINDENMEYER, P.H. *On the crystal structure of Nylon 6*. Journal Of Applied Polymer Science. **21** (1977) 821-837
- ²⁵ FRISCH, K.C. (Ed.) *Cyclic monomers*. Wiley-Interscience. (1972)
- ²⁶ ACHILLADELIS, B. *A study in technological history. Part III. The development of the Snia Viscosa caprolactam process*. Chemistry And Industry. **December** (1970) 1608-1611
- ²⁷ ACHILLADELIS, B. *A study in technological history. Part II. The development of the BASF caprolactam process*. Chemistry And Industry. **December** (1970) 1584-1588
- ²⁸ GUM, W.F, RIESE, W & ULRICH, H. (Ed.) *Reaction polymers*. Hanser Publishers. (1992)
- ²⁹ PETROVIC, Z.S & JAVNI, I. *Polyurethane elastomer with nano-fillers*. ANTEC '98. **2** (1998) 2390-2393
- ³⁰ HORNSBY, P.R & WATSON, C. L. *Interfacial modification of polypropylene filled with magnesium hydroxide*. Journal Of Materials Science. **30** (1995) 5347-5355

- ³¹ TAJIMA,Y & YOKOUCHI,M. *U.S. patent: 522471*. (1993)
- ³² HORNSBY,P.R. *The application of magnesium hydroxide as a fire retardant and smoke-suppressing additive for polymers*. *Fire And Materials*. **18** (1994) 269-276
- ³³ RILEY,A.M, PAYNTER,C.D & MCGENITY,P.M. *Factors affecting the impact properties of mineral filled polypropylene*. *Plastics, Rubber & Composites Processing And Applications*. **14** (1990) 85-93
- ³⁴ LIAUW,C.M, HURST,S.J, LEES,G.C, ROTHON,R.N & ALI,S. *Silane treated magnesium hydroxide for highly filled polypropylene based composites*. *Eurofillers '97*. (1997)
- ³⁵ LONG,Y & SHANKS,R.A. *PP-elastomer-filler hybrids. I. Processing, microstructure & mechanical properties*. *Journal Of Applied Polymer Science*. **61** (1996) 1877-1885
- ³⁶ AKELAH,A & MOET,A. *Polymer-clay nanocomposites: free radical grafting of polystyrene on to organophilic montmorillonite layers*. *Journal Of Materials Science*. **31** (1996) 3589-3596
- ³⁷ SCHOFIELD,W.C.E, HURST,S.J, LEES,G.C, LIAUW,C.M & ROTHON,R.N. *Influence of surface modification of magnesium hydroxide on the processing & mechanical properties of composites of magnesium hydroxide and an ethylene vinyl acetate copolymer*. *Eurofillers '97*. (1997) 255-257
- ³⁸ MATON,D, SUTHERLAND,I & HARRISON,D.L. *Filler surface characterisation and it's relation to mechanical properties of polymer composites*. *Eurofillers '97*. (1997) 163-166
- ³⁹ PLUEDDEMANN,E.P. *Silane coupling agents*. Plenum Press. (1982)
- ⁴⁰ MIYATA,S, IMAHASHI,T & ANABUKI,H. *Fire-retarding polypropylene with magnesium hydroxide*. *Journal Of Applied Polymer Science*. **25** (1980) 415-425
- ⁴¹ WELLS,A.F. *Structural inorganic chemistry*. Oxford University Press. (1975)
- ⁴² WORRALL,W.E. *Clay and ceramic raw materials*. Applied Science Publishers Ltd. (1975)
- ⁴³ GRIM,R.E. *Clay mineralogy*. McGraw-Hill Book Company. (1968)
- ⁴⁴ BAILEY,S.W, BRINDLEY,G.W, JOHNS,W.D, MARTIN,R.T & ROSS,M. *Summary of national and international recommendations on clay mineral nomenclature*. *Clays And Clay Minerals*. **19** (1971) 129-132

- ⁴⁵ WORRALL, W.E. *Clays: their nature, origin and general properties*. MacLaren & Sons. (1968)
- ⁴⁶ VAN OLPHEN, H. *An introduction to colloid chemistry*. Wiley-Interscience. (1977)
- ⁴⁷ SEARLE, A.B & GRIMSHAW, R.W. *The chemistry and physics of clays and other ceramic materials*. Ernest Benn Limited. (1959)
- ⁴⁸ MARTIN, R.T. *Absorbed water on clay: a review*. *Clay And Clay Minerals*. **11** (1962) 28-43
- ⁴⁹ BRADLEY, W.F. *Molecular associations between montmorillonite and some polyfunctional organic liquids*. *Journal Of The American Chemical Society*. **67** (1945) 975-981
- ⁵⁰ HENDRICKS, S.B. *Lattice structure of clay minerals and some properties of clays*. *Journal Of Geology*. **50** (1942) 276-290
- ⁵¹ RYAN, W. *Properties of ceramic raw materials*. Pergamon Press. (1978)
- ⁵² KOMARNENI, S. *Nanocomposites*. *Journal Of Materials Chemistry*. **2**, Number 12 (1992) 1219-1230
- ⁵³ LAPORTE. *An introduction to the chemistry of the laporte range of rheology modifiers*.
- ⁵⁴ BRINDLEY, G.W & HOFFMANN, W. *Orientation and packing of aliphatic chain molecules on montmorillonite*. *Clay And Clay Minerals*. **11** (1962) 546-555
- ⁵⁵ BRINDLEY, G.W & RAY, S. *Complexes of Ca-montmorillonite with primary monohydric alcohols*. *The American Mineralogist*. **49** (1964) 106-115
- ⁵⁶ KATO, C, KURODA, K & MISAWA, M. *Preparation of montmorillonite-nylon complexes and their thermal properties*. *Clay And Clay Minerals*. **27** number 2 (1979) 129-136
- ⁵⁷ THENG, B.K.G. *The chemistry of clay-organic reactions*. Adam Hilger Ltd. (1974)
- ⁵⁸ VAUGHAN, D.E.W, LUSSIER, R.J & MAGEE, J.S. *American patent: 4176090*. (1979)
- ⁵⁹ CRAWFORD, R.J, SMALLEY, M.V & THOMAS, R.K. *The effect of uniaxial stress on the swelling of n-butylammonium vermiculite*. *Advances In Colloid And Interface Science*. **34** (1991) 537-560

- ⁶⁰ BROWN,G. (Ed.) *The X-ray identification and crystal structures of clay minerals*. Mineralogical Society. (1963)
- ⁶¹ HARLAND,C.E. *Ion exchange: theory and practice*. The Royal Society Of Chemistry. (1994)
- ⁶² *Determination of cation exchange capacity and exchangeable cations (including water-soluble) in soils, related materials and sewage sludge*. Her Majesty's Stationary Office. (1979)
- ⁶³ KAHR,G & MADSEN,F.T. *Determination of cation exchange capacity and the surface area of bentonite, illite and kaolinite by methylene blue absorption*. Applied Clay Science. **9** (1995) 327-336
- ⁶⁴ RYAN,W & RADFORD,C. *Whitewares production, testing and quality control*. Institute of Materials. (1997)
- ⁶⁵ BRIGGS,P.J, MCALOON,K & RIDEAL,G.R. *U.S. patent: 4476181*. (1984)
- ⁶⁶ THENG,B.K.G. *Formation and properties of clay-polymer complexes*. Elsevier Scientific Publishing Company. (1979)
- ⁶⁷ KAWASUMI,M, HASEGAWA,N, KATO,M, USUKI,A & OKADA,A. *Preparation and mechanical properties of polypropylene-clay hybrids*. Macromolecules. **30** number 20 (1997) 6333-6338
- ⁶⁸ OKADA,A & USUKI,A. *The chemistry of polymer-clay hybrids*. Materials Science And Engineering. **C3** (1995) 109-115
- ⁶⁹ MARK,J.E. *Ceramic-reinforced polymers and polymer-modified ceramics*. Polymer Engineering And Science. **36**, Number 24 (1996) 2905-2920
- ⁷⁰ ORIAKHI,C. *Nanosandwiches*. Chemistry In Britain. **November** (1998) 59-62
- ⁷¹ WANG,Z, LAN,T, & PINNAVAIA,T. *Hybrid organic-inorganic nanocomposites formed from an epoxy polymer and a layered silicic acid (magdiite)*. Chemistry Of Materials. **8** (1996) 2200-2204
- ⁷² MALLA,P.B & KOMARNENI,S. *Oxide and metal intercalated clay nanocomposites*. Materials Research Society Symposium Proceedings. **286** (1993) 323-334
- ⁷³ VAIA,R.A, ISHII,H & GIANNELIS,E.P. *Synthesis and properties of two-dimensional nanostructures by direct intercalation of polymer melts in layered silicates*. Chemistry Of Materials. **5** number 12 (1993) 1694-1696
- ⁷⁴ MILLER,B. *'Nano' clay particles create new compounds*. Plastics Formulating And Compounding. **May/June** (1997) 30-32

- ⁷⁵ KAMIGAITO,O, FUKUSHIMA,Y, & DOI,H. *U.S. patent: 4472538*. (1984)
- ⁷⁶ WANG,Z, LAN,T, & PINNAVAIA,T. *Mechanisms of clay tactoid exfoliated in epoxy-clay nanocomposites*. *Chemistry Of Materials*. **7** (1995) 2144-2150
- ⁷⁷ MESSERSMITH,P.B & GIANNELIS,E.P. *Synthesis and barrier properties of poly(ϵ -caprolactone)-layered silicate nanocomposite*. *Journal Of Polymer Science: Part A: Polymer Chemistry*. **33** (1995) 1047-1057
- ⁷⁸ GOLDMAN,A.Y, MONTES,J.A, BARAJAS,A & BEALL,G. *Effect of ageing on mineral-filled nanocomposites*. *ANTEC '98*. **2** (1998) 2415-2425
- ⁷⁹ KOJIMA,Y, USUKI,A, KAWASUMI,M, OKADA,A, FUKUSHIMA,Y, KURAUCHI,T & KAMIGAITO,O. *Mechanical properties of nylon 6 clay hybrid*. *Journal Of Materials Research*. **8** (1993) 1185-1189
- ⁸⁰ LAN,T, KAVIRATNA,P & PINNAVAIA,T. *On the nature of polyimide-clay hybrid composites*. *Chemistry Of Materials*. **6** (1994) 573-575
- ⁸¹ OKADA,A, KAWASUMI,M, KOHZAKI,M, FUJIMOTO,M, KOJIMA,Y, KURAUCHI,T & KAMIGAITO,O. *U.S. patent: 4894411*. (1990)
- ⁸² VAIA,R.A, SAUER,B.B, TSE,O.K & GIANNELIS,E.P. *Relaxations of confined chains in polymer nanocomposites: glass transition properties of poly(ethylene oxide) intercalated in montmorillonite*. *Journal Of Polymer Science: Part B: Polymer Physics*. **35** (1997) 59-67
- ⁸³ KRISHNAMOORTI,R, & GIANNELIS,E.P. *Rheology of end-tethered polymer layered silicate nanocomposites*. *Macromolecules*. **30** number 14 (1997) 4097-4102
- ⁸⁴ USUKI,A, MIZUTANI,T, FUKUSHIMA,Y, FUJIMOTO,M, FUKUMORI,K, KOJIMA,Y, SATO,N, KURAUCHI,T & KAMIGAITO,O. *U.S. patent: 4889885*. (1989)
- ⁸⁵ KAWASUMI,M, KOHZAKI,M, KOJIMA,Y, OKADA,A & KAMIGAITO,O. *U.S. patent: 4810734*. (1989)
- ⁸⁶ GONSALVES,K, CHEN,X & BARTON,M. *Mechanistic investigation of the preparation of polymer/ceramic nanocomposites*. *Nanostuctured Materials*. **9** (1997) 181-184
- ⁸⁷ PORTER,D, METCALFE,E & THOMAS,M.J.K. *Nanocomposite fire retardants – a review*. *Fire And Materials*. **24** (2000) 45-52
- ⁸⁸ CALIISTER, Jr.W. *Material science and engineering: an introduction*. John Wiley & Sons. (1994)

- ⁸⁹ OKADA,A, KAWASUMI,M, TAJIMA,I, KURAUCHI,T & KAMIGAITO,O. *A solid state NMR study of crystalline forms of nylon-6*. Journal of Applied Polymer Sciences. **37** (1989) 1363-1371
- ⁹⁰ RTP. *Melt processed polymer-silicate nanocomposites: properties and commercial opportunities*. Press release (1999)
- ⁹¹ VAIA,R.A & GIANNELIS,E.P. *Polymer melt intercalation in organically-modified layered silicates: model predictions and experiment*. Macromolecules. **30** (1997) 8000-8009
- ⁹² LAN,T, & PINNAVAIA,T. *Clay-reinforced epoxy nanocomposites*. Chemistry Of Materials. **6** (1994) 2216-2219
- ⁹³ GIANNELIS,E.P. *Polymer layered silicate nanocomposites*. Advanced Materials. **8** (1996) 29-35
- ⁹⁴ WANG,Z & PINNAVAIA,T. *Hybrid organic-inorganic nanocomposites: exfoliation of magdiite nanolayers in an elastomeric epoxy polymer*. Chemistry Of Materials. **10** (1998) 1820-1826
- ⁹⁵ GILMAN,J.W, MORGAN,A, GIANNELIS,E.P, WUTHENOW,M & MANIAS,E. *Flammability and thermal stability studies of polymer layered-silicate nanocomposites - II*.
- ⁹⁶ CARRADO,K.A & XU,L. *In situ synthesis of polymer-clay nanocomposites from silicate gels*. Chemistry Of Materials. **10** (1998) 1440-1445
- ⁹⁷ ANTON,A. *A direct infrared estimation of cyclic oligomers in water extract of nylon-6*. Journal of Applied Polymer Science. **7** (1963) 1629-1634
- ⁹⁸ VAIA,R.A, JANDT,K.D, KRAMER,E.J & GIANNELIS,E.P. *Kinetics of polymer melt intercalation*. Macromolecules. **28** number 24 (1995) 8080-8085
- ⁹⁹ MESSERSMITH,P,B & STUPP,S.I. *High-temperature chemical and microstructural transformations of a nanocomposites organoceramic*. Chemistry Of Materials. **7** (1995) 454-460
- ¹⁰⁰ JEON,H.G, JUNG,H.-T, LEE,S.W & HUDSON,S.D *Morphology of polymer/silicate nanocomposites*. Polymer Bulletin. **47** (1998) 107-113
- ¹⁰¹ MESSERSMITH,P,B & GIANNELIS,E.P. *Polymer-layered silicatenanocomposites: in-situ intercalative polymerisation of ϵ -caprolactone in layered silicates*. Chemistry Of Materials. **5** (1993) 1064-1066
- ¹⁰² PINNAVAIA GROUP. *Polymer nanocomposites*. <http://slater.cem.msu.edu:80/~pinnweb/nanocomposites.html>

- ¹⁰³ FRIEDLANDER,H,Z & FRINK,C,R. *Organised polymerisation III. Monomers intercalated in montmorillonite*. Journal Of Polymer Science, Part B, Polymer Letters. **2** (1964) 475-479
- ¹⁰⁴ USUKI,A, KATO,M, OKADA,A & KURAUCHI,T. *Synthesis of polypropylene-clay hybrid*. Journal Of Applied Polymer Science. **63** (1997) 137-139
- ¹⁰⁵ KRISHNAMOORTI,R, VAIA,R.A & GIANNELIS,E.P. *Structure and dynamics of polymer-layered silicate nanocomposites*. Chemistry Of Materials. **8** number 8 (1996) 1728-1734
- ¹⁰⁶ SOLC,J, NICHOLS,K, GALBARDES,M & GIANNELIS,E.P. *Thermoplastic-layered silicate nanocomposites*. ANTEC '97. **2** (1997) 1931-1935
- ¹⁰⁷ USUKI,A, KAWASUMI,M, KOJIMA,Y, OKADA,A, KURAUCHI,T & KAMIGAITO,O. *Swelling behaviour of montmorillonite cation exchanged for ω -amino acids by ϵ -caprolactam*. Journal Of Materials Research. **8** (1993) 1174-1178
- ¹⁰⁸ KRESSLER,J & THOMANN,R. *Nanocomposites based on a synthetic layer silicate and polyamide-12*. ANTEC '98. Conference 56 **2** (1998) 2400-2404
- ¹⁰⁹ WHITTINGHAM,M,S & JACOBSON,A,J. *Intercalation chemistry*. Academic Press Inc. (1982)
- ¹¹⁰ BEALL,G.W, TSIPSURSKY,S, SOROKIN,A & GOLDMAN,A. *U.S. patent: 5552469*. (1996)
- ¹¹¹ VAIA,R.A & GIANNELIS,E.P. *Polymer melt intercalation of organically-modified layered silicates: model predictions and experiment*. Macromolecules. **30** number 25 (1997) 8000-8009
- ¹¹² VAIA,R.A & GIANNELIS,E.P. *Lattice model of polymer melt intercalation in organically-modified layered silicates*. Macromolecules. **30** number 25 (1997) 7990-7999
- ¹¹³ FUKUSHIMA,Y, OKADA,A, KAWASUMI,M, KURAUCHI,T & KAMIGAITO,O. *Swelling behaviour of montmorillonite by poly-6-amide*. Clay Minerals. **23** (1988) 27-34
- ¹¹⁴ GIANNELIS,E.P. *Fire-resistant nanocomposites*. ANTEC '96. **3** (1996) 2998-3003

-
- ¹¹⁵ GILMAN,J.W, KASHIWAGI,T & LICHTENHAN,J.D. *Nanocomposites: a revolutionary new flame retardant approach*. SAMPE Journal. **33** number 4 (1997) 40-46
- ¹¹⁶ NYDEN,M.R & GILMAN,J.W. *Molecular dynamics simulations of the thermal degradation of nano-confined polypropylene*. Computational Theoretical Polymer Science. **7** (1997) 191-198
- ¹¹⁷ GILMAN,J.W, KASHIWAGI,T, GIANNELIS,E.P, MANIAS,E, LOMAKIN,S, LICHTENHAN,J.D & JONES,P. *Nanocomposites: radiative gasification and vinyl polymer flammability*. Additives '98. (1998) 204-221
- ¹¹⁸ BARTILLA,T, KIRCH,D, NORDMEIER,J, PROMPER,E & STRAUCH,T. *Physical and chemical changes during the extrusion process*. Advances In Polymer Technology. **6** (1986) 339-387
- ¹¹⁹ WERNER,J.C. *Reactive extrusion of blends with interfacial reactions*. ANTEC '97. **2** (1997) 1838
- ¹²⁰ MALLICK & NEWMAN. (Eds.) *Composite materials technology: processes and properties*. Hanser Publications. (1990)
- ¹²¹ RAUWENDAAL,C. (Ed.) *Mixing in polymer processing*. Marcel Dekker, Inc. (1991)
- ¹²² RAUWENDAAL,C. *Polymer extrusion*. Marcel Dekker. (1991)
- ¹²³ ASKLAND,D.R. *The science and engineering of materials*. PWS Publishing Company. (1994)
- ¹²⁴ BERGHAUS,U & MICHAELI,W. *Reactive extrusion of nylon 6 - aspects of industrial use*. ANTEC '90. (1990) 1929-1930
- ¹²⁵ KROSCWITZ,J. (Ed.) *Reactive extrusion*. Encyclopaedia Of Polymer Science And Engineering. **14** (1988) 169-189
- ¹²⁶ TAJIMA,Y & YOKOUCHI,M. *U.S. patent: 5225471*. (1993)
- ¹²⁷ XANTHOS,M. (Ed.) *Reactive extrusion: principles and practice*. Hanser Publications. (1992)
- ¹²⁸ HORNSBY,P.R & TUNG,J. F . *Characterisation of polyamide 6 made by reactive extrusion. II. Analysis of microstructure*. Journal Of Applied Polymer Science. **54** (1994) 899-907
- ¹²⁹ CHEMOPETROL. *GB patent: 2096155*.

- ¹³⁰ LEE,J, TAKEKOSHI,T & GIANNELIS,E.P. *Fire retardent polyetherimide nanocomposites*. Materials Research Society Symposium Proceedings. **457** (1997) 513-518
- ¹³¹ ONGEMACH,G.G, DORMAN-SMITH,V.A & BEIER,W.E. *Determination of extractables content of nylon 6 by differential refractometry and determination of caprolactam monomer content in nylon 6 extractables by infrared spectrophotometry*. Analytical Chemistry. **38** (1966) 123-125
- ¹³² ROTHON,R.N, McCALLUM,D & ELSNER,D. *The development of a new route to flame retardant filler quality magnesium hydroxide*. Eurofillers '97. (1997) 19-23
- ¹³³ ONGEMACH,G.G & MOODY,A.C. *Determination of caprolactam monomer content in nylon 6 extractables by gas chromatography*. Analytical Chemistry. **39** (1967) 1005-1006
- ¹³⁴ KOJIMA,Y, USUKI,A, KAWASUMI,M, OKADA,A, KURAUCHI,T, KAMIGAITO,O & KAJI,K. *Fine structure of nylon-6-hybrid*. Journal of Polymer Science: Part B: Polymer Physics. **32** (1994) 625-630
- ¹³⁵ GILMAN,J.W. *Flammability and thermal stability studies of polymer layered-silicate (clay) composites*. Applied Clay Science. **15** (1999) 31-49
- ¹³⁶ HORNSBY,P.R. *Development in the use of magnesium hydroxide {PRIVE} as a fire retardent filler for thermoplastics*. Fire Retardancy of Polymeric Materials, Sixth Conference (1997) 60-61
- ¹³⁷ WILLARD,H.H, MERRITT,L.L, DEAN,J.A & SETTLE,F.A. *Instrumental methods of analysis*. Wadsworth Publishing Company. (1988)
- ¹³⁸ TUNG,J.F. *Thesis: Synthesis and characterisation of polyamide-6 blends made by reactive extrusion*. (1993)
- ¹³⁹ HOLDING,S. *Gel permeation chromatography. Outsourcing of molecular weight analysis*. RAPRA Technology Ltd. (2000)
- ¹⁴⁰ WOODISSE,S. *Private communication*. Brunel University. (2000)
- ¹⁴¹ KAMPF,G. *Characterisation of plastic by physical methods*. Hanser Publishers. (1986)
- ¹⁴² BULPELT,R & REYNOLDS, A. *SEM preparation and basic operation*. Experimental Techniques Centre, Brunel University. (1997)
- ¹⁴³ GOODHEW,P.J & HUMPHREYS,F.J. *Electron microscopy and analysis*. Taylor & Francis. (1992)

- ¹⁴⁴ AMELINCKX,S, VAN DYCK,D, VAN LANDUYT,J & VAN TENDELOO,G. (Eds.) *Electron microscopy principles and fundamentals*. VCH Verlagsgesellschaft mdH. (1997)
- ¹⁴⁵ BULPELT,R & REYNOLDS, A. *TEM preparation and basic operation*. Experimental Techniques Centre, Brunel University. (1998)
- ¹⁴⁶ SLAYTER,E.M & SLAYTER, H.S. *Light & electron microscopy*. Cambridge University Press (1994)
- ¹⁴⁷ ASTM D 256
- ¹⁴⁸ WETTON,R. *Dynamic mechanical thermal analysis of polymers and related system*.
- ¹⁴⁹ RHEOMETRIC SCIENTIFIC. *Solids analyser RSA-II, owner's manual*. (1991)
- ¹⁵⁰ MURAYAMA,T. *Dynamic mechanical analysis of polymeric material*. Elsevier. (1978)
- ¹⁵¹ Betol Laboratory Equipment, Luton, England. *Information booklet*
- ¹⁵² British Plastics training Association. *Injection moulding condition setting*. (2000)
- ¹⁵³ USUKI,A, KOJIMA,Y, KAWASUMI,M, OKADA,A, FUKUSHIMA,Y, KURAUCHI,T & KAMIGAITO,O. *Synthesis of nylon 6-clay hybrid*. Journal of Materials Research. **8** (1993) 1179-1184.
- ¹⁵⁴ MATHERS,A.C, WEED,S.B & COLEMAN,N.T. *The effect of acid and heat treatment on montmorillonoids*. Clay And Clay Minerals. **395** (1955) 403-412
- ¹⁵⁵ MESSERSMITH,P.B & GIANNELIS,E. *Synthesis & barrier properties of poly(ϵ -caprolactone)-layered silicates nanocomposites*. Journal of Polymer Science: Part A: Polymer Chemistry. **33** (1995) 1047-1057
- ¹⁵⁶ HYBRID PLASTICS. POSS Technology
<http://www.hybridplastics.com/NanotechComp.htm>
- ¹⁵⁷ USUKI,A, KOIWAI,A, KOJIMA,Y, KAWASUMI,M, OKADA,M, KURAUCHI,T & KMIGAITO,O. *Interaction of nylon-6 surface and mechanical properties of nylon-6 hybrid*. Journal of Applied Polymer Science. **55** (1995) 119-123
- ¹⁵⁸ MURTHY,S. *Metastable crystalline phases in nylon 6*. Polymer Communications **32** (1991) 301 -305
- ¹⁵⁹ CALLISTER,W.D. *Materials science and engineering: an introduction*. John Wiley & Sons Inc. (1994)
- ¹⁶⁰ RONCA,G. *Thesis: Heterogeneous nucleation in polymer crystallisation*. (1985)

-
- ¹⁶¹ TODOKI,M & KAWAGUCHI,T. *The origin of double melting peaks in drawn nylon6 yarns*. Journal of Polymer Science: polymer Physics Edition. **15** (1977) 1067-1075
- ¹⁶² KURAUCHI,T, OKADA,A, NOMURA,T, NISHIO,T, SAEGUSA,S & DEGUCHI,R. *Nylon 6-clay – synthesis, properties and application to automotive timing belt cover*. SAE Technical Paper Series. International Congress and Exposition. (1991)
- ¹⁶³ HORNSBY,P, TUNG,J, TARVERDI,K. *Characterisation of polyamide 6 made by reactive extrusion. I. Synthesis and characterisation of properties*. Journal of Applied Polymer Science. **53** (1994) 891-897
- ¹⁶⁴ SEBENDA,J. *Recent progress in the polymerisation of lactams*. Progress in Polymer Science. **6** (1978) 123-168
- ¹⁶⁵ GIANNELIS, E, JANDT,K, KRAMER,E & VAIA,R. *Microstructural evolution of melt intercalated polymer-organically modified layered silicate nanocomposites*. Chemistry of Materials. **8**, number 11 (1996) 2628-2635
- ¹⁶⁶ GILMAN,G.W & KASHIWAGI,T. *Nanocomposites: a revolutionary new flame retardant approach*. 42nd International Symposium. (1997)
- ¹⁶⁷ SHI,H, LAN,T & PINNAVAIA,T. *Interfacial effects on the reinforcement properties of polymer-organoclay nanocomposites*. Chemistry of materials. **8** (1996) 1584-1587
- ¹⁶⁸ LEBARON,P.C, WANG,Z & PINNAVAIA,T.J. *Polymer-layered silicate nanocomposites: an overview*. Applied Clay Science. **15** (1999) 11-29


APPENDIX I

Table Of Materials

Material	Supplied
6-aminocaproic acid	Sigma-Aldrich Ltd.
12-aminododecanoic acid (12-aminolauric acid)	Sigma-Aldrich Ltd.
Activator B (Bruggolen® C20)	L. Brüggemann KG.
Catalyst B (Bruggolen® C320)	L. Brüggemann KG.
Cloisite® 15A	Laporte Industries Ltd.
Cloisite® 25A	Laporte Industries Ltd.
Cloisite® 30B	Laporte Industries Ltd.
Concentrated hydrochloric acid	Sigma-Aldrich Ltd.
Dilute hydrochloric acid	Sigma-Aldrich Ltd.
ϵ -caprolactam	Bayer Plc.
Polyamide-6 (Ultramid B25)	BASF Plc.
Sodium chloride	Sigma-Aldrich Ltd.
Sodium-montmorillonite	Laporte Industries Ltd.
UBE Nylon-6	UBE Industries Ltd.

APPENDIX II

Process Scheme for Screening Tests

 Research and Development																	
INCORPORATING: NYLONTECHNICS, NYWNCHEM, RESEARCH & DEVELOPMENT, MONOMER CASTING AND MANUFACTURING DIVISIONS																	
P-SCRN1 Process scheme for screening tests																	
1.	Switch oven on at 170c																
2.	Use 125cc glass bottles with bakelite caps (e.g. BDH/ASL p. 4-106, 215/0350/15 @ £16.85 per 40, caps 215/0353/07 @ £9.80 per 100 caps).																
3.	Use 100mm x 24/25mm specimen tubes soda glass flat bottom (e.g. Richardsons pl16, V2730 @ £12.20 per 100)																
4.	Select 12 sets of glass bottles and vials, put in oven in oven. (Put vials on a flat surface).																
5.	Add 50g capro flake to each glass bottle																
6.	Wait to melt capro- generally by the time all the glass bottles have been prepared, the capro in the first one will have melted.																
7.	Label each glass jar as H/Sxxx is added to the following scheme;																
	<table style="margin-left: 40px;"> <tr> <td>Organic dye or pigment;</td> <td style="text-align: right;">0.05g</td> </tr> <tr> <td>Seeding agent</td> <td style="text-align: right;">0.1g</td> </tr> <tr> <td>Inorganic pigment</td> <td style="text-align: right;">0.1g</td> </tr> <tr> <td>Thixiotrope</td> <td style="text-align: right;">0.5g</td> </tr> <tr> <td>Antioxidant</td> <td style="text-align: right;">0.5g</td> </tr> <tr> <td>Surfactant</td> <td style="text-align: right;">0.5g</td> </tr> <tr> <td>Flame retardant</td> <td style="text-align: right;">2g</td> </tr> <tr> <td>Lubricant</td> <td style="text-align: right;">2g</td> </tr> </table>	Organic dye or pigment;	0.05g	Seeding agent	0.1g	Inorganic pigment	0.1g	Thixiotrope	0.5g	Antioxidant	0.5g	Surfactant	0.5g	Flame retardant	2g	Lubricant	2g
Organic dye or pigment;	0.05g																
Seeding agent	0.1g																
Inorganic pigment	0.1g																
Thixiotrope	0.5g																
Antioxidant	0.5g																
Surfactant	0.5g																
Flame retardant	2g																
Lubricant	2g																
8.	Add 1g of Cat D (CR005) and stir, return glass jar to oven																
9.	Add 0.5g of Act B (CR007) and stir. Immediately pour contents into glass vial. Label glass vial and return to oven in a stable, upright position.																
10.	Fill in form P-Screen and transfer this data to Report RC016																
F:\Richard\nylonchem\process\P-scrn1																	

APPENDIX III

DMTA Raw Data

DMTA	E'			E'			E'				
	°C	°C	Pa	°C	°C	Pa	°C	°C	Pa		
	-100	-99.8	3.83E+09	-100	-99.8	3.79E+09	-100	-99.9	3.95E+09		
	-40	-40	3.60E+09	-40	-39.9	3.53E+09	-40	-39.7	3.76E+09		
C-PA6	25	23.3	2.81E+09	C-PA6, 2	25	23.3	2.60E+09	C-PA6, 3	25	23.3	2.80E+09
	120	119.3	6.53E+08		120	119.1	5.72E+08		120	119.2	6.43E+08
	220	219.4	2.94E+08		220	219.3	2.77E+08		220	219.4	2.88E+08
	-100	-100.2	4.18E+09		-100	-100	3.37E+09		-100	-99.9	3.32E+09
B-PA6 IJM, 1	-40	-39.7	3.03E+09		-40	-39.9	2.73E+09		-40	-39.9	2.61E+09
	25	23	2.17E+09	B-PA6 IJM, 2	25	23.3	1.99E+09	B-PA6 IJM, 3	25	23.4	2.28E+09
	120	119.2	3.69E+08		120	119.2	3.29E+08		120	119.1	3.54E+08
	220	183.4	2.47E+08		220	219.1	7.46E+07		220	219.5	7.89E+07
	-100	-99.8	4.45E+09		-100	-99.8	4.11E+09		-100	-99.6	3.91E+09
B-PA6(U) IJM, 1	-40	-39.8	4.17E+09		-40	-40.1	3.87E+09		-40	-40	3.65E+09
	25	23	3.16E+09	B-PA6(U) IJM, 2	25	23.2	2.78E+09	B-PA6(U) IJM, 3	25	23.1	2.67E+09
	120	119.2	6.86E+08		120	119.1	6.05E+08		120	119.2	5.85E+08
	220	219.2	5.38E+07		220	215.3	8.15E+07		220	215.2	8.05E+07
	-100	-100	4.58E+09		-100	-99.7	4.54E+09		-100	-100.2	4.26E+09
B-PA6(T) IJM, 1	-40	-39.8	4.38E+09		-40	-39.9	4.24E+09		-40	-39.8	3.89E+09
	25	23.3	2.15E+09	B-PA6(T) IJM, 2	25	23.1	2.18E+09	B-PA6(T) IJM, 3	25	23.1	1.88E+09
	120	119.2	5.20E+08		120	119.1	5.42E+08		120	119.2	4.59E+08
	220	211.3	7.66E+07		220	219.2	3.05E+07		220	219.2	1.94E+07
	-100	-99.8	5.58E+09		-100	-99.8	4.44E+09				
J-PA6 IJM, 1	-40	-40	4.38E+09		-40	-39.7	3.59E+09				
	25	22.1	1.58E+09	J-PA6 IJM, 2	25	23.2	1.02E+09				
	120	118.2	3.60E+08		120	119.2	3.58E+08				
	220	219.9	1.28E+08		220	219.4	5.73E+08				
	-100	-99.9	3.91E+09		-100	-99.6	3.97E+09		-100	-100.1	3.71E+09
J-PA6(U) IJM, 1	-40	-40	3.40E+09		-40	-39.8	3.39E+09		-40	-39.9	3.16E+09
	25	23.5	9.84E+08	J-PA6(U) IJM, 2	25	23.5	9.51E+08	J-PA6(U) IJM, 3	25	23.3	9.08E+08
	120	119.2	3.60E+08		120	119.2	3.12E+08		120	119.1	3.31E+08
	220	215.1	2.44E+07		220	211.3	3.42E+07		220	215.2	2.66E+08
	-100	-99.6	4.23E+09		-100	-99.8	4.12E+09		-100	-99.8	3.85E+09
J-PA6(T) IJM, 1	-40	-40	3.67E+09		-40	-40	3.68E+09		-40	-40.2	3.25E+09
	25	23.3	9.76E+08	J-PA6(T) IJM, 2	25	23.4	9.79E+08	J-PA6(T) IJM, 2	25	22.1	1.68E+09
	120	119.3	2.99E+08		120	119.2	2.71E+08		120	118	5.04E+08
	220	215.3	4.10E+08		220	203.3	2.96E+07		220	205.1	7.33E+07
	-100	-99.8	4.11E+09		-100	-99.6	3.50E+09		-100	-99.9	3.89E+09
	-40	-39.9	3.76E+09		-40	-39.8	3.38E+09		-40	-39.9	3.50E+09
UBE IJM, 1	25	23.5	2.98E+09	UBE IJM, 2	25	23.2	2.74E+09	UBE IJM, 2	25	23.3	2.80E+09
	120	118.1	8.39E+08		120	119.1	8.69E+08		120	119.2	8.30E+08
	220	218.3	6.90E+07		220	219.2	7.12E+07		220	219.2	7.04E+07

APPENDIX IV

XRD Raw Data

Sample	Angle (°)	d-spacing (nm)	Relative intensity
Montmorillonite	6.045	1.461	93
	6.507	1.357	100
	19.758	0.449	65
	21.816	0.407	39
	28.935	0.308	33
	32.085	0.279	23
C-PA6	20.115	0.441	100
	21.564	0.412	55
	23.790	0.374	100
C020	4.360	2.025	100
	20.080	0.442	74
	23.900	0.372	76
C021	4.280	2.063	99
	20.060	0.442	58
	23.980	0.371	75
C022	4.320	2.044	68
	19.980	0.444	63
	23.700	0.375	100
C029	4.722	1.870	26
	19.044	0.466	17
	21.123	0.420	100
	23.412	0.380	17
NCH	19.952	0.445	95
	21.569	0.412	45
	23.942	0.371	100
B-PA6 AR	20.199	0.439	66
	21.333	0.416	100
	23.223	0.383	43
B-PA6 CM	20.283	0.438	95
	23.664	0.376	100
B-PA6 IM	21.165	0.419	100
B-PA6(U) AR	4.428	1.994	9
	21.396	0.415	100
B-PA6(U) CM	4.218	2.093	14
	21.375	0.415	100
	23.685	0.375	32
B-PA6(U) IM	21.102	0.421	100
B-PA6(T) AR	4.974	1.775	12
	18.960	0.468	29
	19.800	0.448	34
	21.396	0.415	100
B-PA6(T) CM	4.932	1.790	16
	19.044	0.466	32
	20.304	0.437	48
	21.396	0.415	100
	23.832	0.373	44
B-PA6(T) IM	6.213	1.421	10
	18.666	0.475	17
	21.186	0.419	100
UBE AR	3.00	2.943	13
	21.375	0.415	100
UBE CM	3.084	2.863	12
	21.480	0.413	100
UBE IM	3.042	2.902	23
	21.228	0.418	99

Sample	Angle (°)	d-spacing (nm)	Relative intensity
J-PA6 AR	21.157	0.440	100
	21.438	0.414	64
	23.685	0.375	97
J-PA6 CM	20.178	0.440	90
	21.543	0.412	50
	23.853	0.373	100
J-PA6 IM	21.207	0.419	100
J-PA6(U) AR	4.932	1.790	16
	20.157	0.440	39
	21.291	0.417	100
	23.517	0.378	32
J-PA6(U) CM	4.302	2.052	15
	20.094	0.442	54
	21.291	0.417	42
	23.874	0.372	100
J-PA6(U) IM	3.630	2.432	20
	21.207	0.419	100
J-PA6(T) AR	4.701	1.878	12
	21.312	0.417	100
J-PA6(T) CM	4.827	1.829	9
	20.115	0.441	64
	21.417	0.415	100
	23.748	0.374	62
J-PA6(T) IM	4.029	2.191	16
	21.186	0.419	100